AMMRC TR 82-12

PROPERTIES AND RESIDUAL STRESSES IN ANGLE-PLY POLYMER MATRIX COMPOSITES

March 1982

ABDEL A. FAHMY,, HARVEY A. WEST, and MARK A. ELKINS
North Carolina State University
P.O. Box 5356
Raleigh, North Carolina 27607

FINAL REPORT Contract No. DAAG46-79-C-0021

Prepared for

ARMY MATERIALS AND MECHANICS RESEARCH CENTER
Watertown, Massachusetts 02172

The findings in this report are not to be construed as an official Department of the Army position, unless so designated by other authorized documents.

Mention of any trade names or manufacturers in this report shall not be construed as advertising nor as an official indorsement or approval of such products or companies by the United States Government.

DISPOSITION INSTRUCTIONS

Destroy this report when it is no longer needed.
Do not return it to the originator.

UNCLASSIFIED

SECURITY CLASSIFICATION OF THIS PAGE (When Data Entered)

REPORT DOCUMENTATION PAGE		READ INSTRUCTIONS BEFORE COMPLETING FORM
1. REPORT NUMBER AMMRC TR 82-12	2. GOVT ACCESSION NO.	3. RECIPIENT'S CATALOG NUMBER
4. TITLE (and Subtitle) PROPERTIES AND RESIDUAL STRESSES IN ANGLE-PLY POLYMER MATRIX COMPOSITES		5. TYPE OF REPORT & PERIOD COVERED Final Report 20 Mar 79 to 20 Dec 79
		6. PERFORMING ORG. REPORT NUMBER
7. AUTHOR(s) Abdel A. Fahmy, Harvey A. West, and Mark A. Elkins		8. CONTRACT OR GRANT NUMBER(s) DAAG46-79-C-0021
9. PERFORMING ORGANIZATION NAME AND ADDRESS Army Materials and Mechanics Research Center ATTN: DRXMR-K Watertown, Massachusetts 02172		10. PROGRAM ELEMENT, PROJECT, TASK AREA & WORK UNIT NUMBERS
11. CONTROLLING OFFICE NAME AND ADDRESS North Carolina State University P.O. Box 5356 Raleigh, NC 27607		12. REPORT DATE March 1982 13. NUMBER OF PAGES
14. MONITORING AGENCY NAME & ADDRESS(if different from Controlling Office)		15. SECURITY CLASS. (of this report) Unclassified 15a. DECLASSIFICATION/DOWNGRADING SCHEDULE

16. DISTRIBUTION STATEMENT (of this Report)

Approved for public release; distribution unlimited.

17. DISTRIBUTION STATEMENT (of the abstract entered in Block 20, if different from Report)

18. SUPPLEMENTARY NOTES

19. KEY WORDS (Continue on reverse side if necessary and identify by block number)

Composites	Thermal expansion	Epoxy laminates
Residual stress	Glass fibers	Aramid fibers
Mechanical properties	Carbon fibers	Thickness

20. ABSTRACT (Continue on reverse side if necessary and identify by block number)

(SEE REVERSE SIDE)

DD FORM 1 JAN 73 1473 EDITION OF 1 NOV 65 IS OBSOLETE

UNCLASSIFIED

SECURITY CLASSIFICATION OF THIS PAGE (When Data Entered)

Block No. 20

ABSTRACT

A series of samples of graphite/epoxy, glass/epoxy, and Kevlar epoxy were prepared. In addition, hybrids of glass epoxy and Kevlar epoxy were laid up in various configurations. The samples were subjected to hygro-thermal cycling and properties in the through-the-thickness direction were measured as a function of cycling. Thermal expansion and residual stress measurements were made and the effect of ply orientation was determined on both the hybrid and standard composites.

TABLE OF CONTENTS

LIST OF FIGURES

LIST OF TABLES

INTRODUCTION

During the past fifteen to twenty years a great deal of progress has been achieved in the manufacture and application of fiber reinforced composite materials, particularly those with polymer matrices. Helicopter components such as rotor blades and fuselage panels, rocket launch tubes and missile motor cases are only a few examples of army applications of such advanced composites. The precise characterization of these materials is of course essential to their proper utilization. The useful properties of the composite materials depend upon the properties of the reinforcing fibers, the resin system, the volume fraction of fiber and the spatial distribution of fibers in the resin. Of particular interest are laminated fiber composites consisting of layers or plies. In each ply the fibers are aligned but the orientation of such alignment is different from one ply to the other according to the "design" of the laminate. The stress and strain distribution in the laminate coupled with the proper failure criteria determine the load carrying ability of the laminate. The stresss distribution, which is obtained by laminate analysis under any given loading condition, may differ significantly from the actual stress distribution. The difference is caused by stresses that may develop in the laminate during manufacture or due to exposure to the environment; these residual stresses must be taken into account.

SCOPE OF WORK

This is an investigation of the residual stresses in fiber reinforced composites, particularly polymer-matrix composites. Three systems: graphite-epoxy, glass-epoxy and kevlar-epoxy as well as hybrids of the latter two were investigated. In each system unidirectional and symmetric angle-ply laminates were tested, in addition to kevlar-glass-epoxy interply hybrids of several configurations. This investigation may be divided broadly into the following sections:

I - Materials and Laminate Preparation

II - Characterization and Testing

III - Experiments, Results and Discussions

- A. Effect of Hygrothermal Cycling on Elastic Properties
- B. Thermal Expansion Experiments
- C. Strength and Failure Modes on Angle-Ply Laminates
- D. Properties Along Thickness Direction of Laminates

IV - Residual Stresses

- A. Background and Experiments
- B. Results and Discussion
- C. Residual Stresses in Hybrid Laminates

V - Summary and Conclusions

BRIEF REVIEW

It has been realized for some time now that a pattern of residual stresses exists between the fiber and matrix of a unidirectional fiber reinforced composite as a result of thermal expansion mismatch, since stiffer fiber generally has a lower coefficient of thermal expansion than the resin matrix. In addition, residual stresses are also known to exist between plies of a laminated composite since the principal in-plane thermal expansion directions in one ply do not coincide with those in another ply due to fiber orientation differences between plies. The former was demonstrated in the early sixties in boron aluminum composites using x-ray diffraction to monitor the strains - and hence the stresses - both in the aluminum matrix as well as in the boron fibers. Lamination residual stresses have been thoroughly analyzed by Chamis (1-2) assuming linear elastic response. These stresses were shown to reach - under normal curing conditions of resin in resin-base composites - an extent that would result in transverse cracking as has been frequently observed experimentally. Interlaminar separation may also result from these stresses. The build-up of stress as a result of temperature variation has been analyzed in the case of thick filament wound polymer base tubes and the effect of these stresses on the net thermal expansion of the tube were both analyzed and experimentally measured (3-4). The effect of cycling these thermally induced stresses on the microstructure and integrity of laminated composites has also been examined (5).

An understanding of the intensity and distribution of these residual stresses and their effects on mechanical properties and thermal expansion can only be studied if the material system is thoroughly characterized as far as elastic properties, strength properties, and thermal expansion behavior of the individual ply are concerned. Hence, a large portion of this work has been devoted to such characterization.

I. MATERIALS AND LAMINATE PREPARATION

Laminated panels were prepared from three types of pre-preg tape obtained from Narmco Materials, Inc. in Costa Mesa, California. The types were T-300 graphite in Rigidite 5209 resin, Kevlar 49C in Rigidite 5216 resin and E-glass in Rigidite 5216 resin. All resins are thermosetting, therefore, the tapes had to be kept at $0^{o}F$ in a chest freezer.

Balanced angle-ply composite laminates of varying ply angles were required for this investigation. The mold used produced panels 6" x 6" from which tensile coupons and thermal expansion samples could be cut. All panels were sixteen ply thick. Each ply was cut from the pre-preg tape at the proper angle. The plies were properly stacked and placed into the mold. The mold was made of tool steel and, for each use, was sprayed with Frekote 33 to aid in release. Also, 6" x 6" pieces of 2 mil teflon were placed on both sides of the uncured composite to futher eliminate sticking.

The mold was then placed for the curing cycle in one of our two heated platen, temperature and pressure controlled presses, a Pasadena Hydraulic and a Vickers Press. First, the composite was heated to $79^{o}C$ without any pressure and held there for 30 minutes. Then the temperature was raised to $130^{o}C$ and pressure was applied for 90 minutes. The kevlar and glass composites were subjected to 50 psi pressure and the graphite subjected to a pressure of 100 psi during this final heating stage. After 90 minutes under pressure at $130^{o}C$, the mold was cooled in one of two fashions. In slow cooling, the platen heaters were turned off and allowed to air cool. The mold, still under pressure, cooled to room temperature.

in about two and a half hours. In fast cooling, water was circulated through the platens after the heaters were turned off. While still under pressure, the mold cooled in ten minutes. For each composite type and ply angle, two panels were prepared, one slow cooled and one fast cooled. During curing, a slight loss of resin by bleeding occurred. However, the volume fraction of fibers was determined on the finished panel and no appreciable difference existed between laminates of the same system.

After cooling, the panels were removed from the mold. They were cut into 5 1/2" x 3/4" coupons and 2" x 1/2" thermal expansion samples. This was accomplished by employing a Felker-Dresser cabinet mounted cut-off machine with an 8" diameter, 0.040" thick DIAIR diamond cut-off blade. Before cutting out samples, 1/8" was cut from each side of the plates to minmize errors due to edge defects caused by slight discrepancies in the size of each ply as cut out of the pre-preg tape. In this manner we produced three tension coupons and four thermal expansion samples each, of kevlar-, glass-, and graphite-reinforced laminates with the following ply angles: 0^{o}, 15^{o}, 30^{o}, 45^{o}, 60^{o}, 75^{o}, 90^{o}, and crossply $0^{o}/90^{o}$ (which is actually a ±45 panel with the panel edges parallel and perpendicular to the fibers rather than bisecting the angles between them). Also, two types of hybrids were prepared from kevlar and glass pre-pregs since they both contained Rigidite 5216 as a matrix resin. In type I the eight inside plies were of one fiber-resin system and the eight outside plies (four on each side) were of the other i.e., glass/kevlar/glass or kevlar/glass/kevlar. In the other, type II, $\pm\theta$ ply pairs of one system alternated with $\pm\theta$ ply pairs of the other but keeping the laminate symmetric with respect to the

mid-plane e.g. $(+\theta_G, -\theta_G, +\theta_K, -\theta_K, +\theta_G, -\theta_G, +\theta_K, -\theta_K, -\theta_K, +\theta_K, -\theta_G, +\theta_G, -\theta_K, +\theta_K, -\theta_G, +\theta_G)$ so that the type II systems were more finely interdispersed. Two ply angles, 15^o and 45^o, were tried with each hybrid system. Tensile coupons and thermal expansion samples were again prepared.

II. CHARACTERIZATION AND TESTING

Three tensile coupons approximately 5 1/2" x 3/4" x 1/10" were prepared from each composite panel. Of these three, two were cycled in a temperature and humidity controlled environmental chamber and, periodically, Young's modulus E, and Poisson's ratio υ_{LT} were determined. The other was loaded to failure for determination of the fracture strength σ_f.

Before cycling, strain gages were glued to each sample and coated, for protection during humidity cycling. For each composite, one coupon was tested using a single gage, Micro-Measurements EA-06-125AD-120, for measuring E. The other coupon was tested using a 0/90 double gage rosette, Micro-Measurements EA-06-125TM-120, for determining E and υ_{LT}. Each gage was applied as outlined in Micro-Measurements Instruction Bulletin using M-bond 600 two-part epoxy. The glue lines were cured at 100°C for two hours with a postcure at 130°C for two hours. The entire strain gage and terminal installation was then covered with Dow Corning 3145 RTV silicon protective coating.

Tension testing was performed on an Instron floor model TTC-Ml testing machine with a crosshead speed of 0.05 inches per minute. The chart was driven by the longitudinal strain gage output coupled with the Instron X-Y chart drive amplifier and strain gage preamplifier. On the samples with rosettes, the transverse gage was monitored with a Vishay VE-20A digital strain indicator. Each sample was pulled longitudinally to a strain of approximately 1000 $\mu\varepsilon$ and the corresponding transverse strain was recorded.

Humidity and temperature cycling was performed in a "3-PC climate lab" environmental chamber made by American Instrument Company. The samples were initially tested then placed in the chamber for 12 1/2 days. They experienced 50 cycles from 40°F with 85% RH to 160°F with 100% RH. After testing they were again exposed to 50 more cycles, tested, exposed again, then finally tested after a total of 150 cyles.

Thermal expansion coefficients were determined using an Orton automatic recording dilatometer, a push rod type instrument, in which the linear displacement was measured by means of a sensitive transducer. The temperature was monitored with a chromel-alumel thermocouple. The instrument was modified to increase its sensitivity for both temperature and expansion measurement. The samples which were 2" long and approximately 1/4" wide were cut from the as-fabricated panels. They were heated at the rate of approximately $1^{o}C$/minute for room temperature until past $130^{o}C$ then allowed to cool back to room temperature by cutting off the heating current to the dilaometer furnace. The coefficient was calculated from the cooling curve since the heating curve was affected by desorption of moisture.

1. Elastic Strength and Thermal Expansion Properties of Unidirectional Composites as Fabricated

Fiber	Elastic Modulus E_L (msi)	
	Manufacturer*	Present Work
Graphite	21.4	17.8
Kevlar	11.0	10.5
Glass	5.7	6.2

Fiber	Tensile Strength (σ_{xx}) (ksi)	
	Manufacturer*	Present Work
Graphite	260	206
Kevlar	170	189
Glass	143	212

Fiber	Poisson's Ratio	Coefficient of Thermal Expansion ($^oC^{-1} \times 10^{-6}$)	
	Present Work	Present Work	
		Longitudinal	Transverse
Graphite	0.36	0.3	62.8
Kevlar	0.43	-4.2	89.5
Glass	0.33	6.9	47.8

*Graphite and Glass data obtained from Narmco Materials, Inc. Kevlar data obtained from DuPont, Inc.

2. Fiber Volume Fraction Determination

Although the manufacturers provided data on the percent volume of fibers in the three fiber-resin systems, it was thought advisable to determine these values experimentally on the cured unidirectional

composites to take care of any resin bleeding during the preparation process. This was accomplished by using the "point counting" method on micrographs of polished sections of the composites. Averages of fifteen determinations were taken, although in the case of Glass/Epoxy fourty-five determinations were made and the result was within 1% of the fifteen determination average.

Fiber volume fractions were as follows:

in Graphite/Epoxy	73.8%
in Kevlar/Epoxy	71.8%
in Glass/Epoxy	69.4%

RESULTS OF MECHANICAL TESTING

The elastic properties, namely Young's modulus E_1 along the line bisecting the angle between the fibers of the symmetric angle-ply laminates and along the 0 direction in the 0-90 (cross-ply laminates) were determined. Two samples of the fast cooled laminates and two of the slow cooled were tested. This was done on the as-fabricated panels, Fig. (1 to 3) and on the hygrothermally cycled panels Fig. (3 to 36) and tables of the same numbers. Results shown are the two-sample averages. Inspection of these results indicate that the rate of cooling after curing had little - if any - effect on the modulus. The major Poisson's ratio was determined in one sample of each of the fast and slow cooled laminates. The results for the as-fabricated panels are shown on Fig. 37 to 39 and for the cycled samples on Fig. 40 to 72. Here again, the cooling rate did not seem to be of appreciable effect.

III. EXPERIMENTAL, RESULTS AND DISCUSSION

A. EFFECT OF HYGROTHERMAL CYCLING ON ELASTIC PROPERTIES

The effect of hygrothermal cycling on elastic properties are shown in Figs. (1-72) and may be summarized as follows:

1. Tensile Modulus

   a. Graphite

      0^{o} - Small reduction at 50 and 100 cycles but increased to initial value at 150 cycles.

      15^{o} - No appreciable effect.

      30^{o} - Steadily declining except for increase above initial at high cycles for slow cooled samples.

      45^{o} - Two samples, one fast cooled and the other slow cooled, showed no marked effect. One slow cooled behaved erratically but one fast cooled showed a decrease then an increase above the initial modulus.

      60^{o} - All showed decreased trend but two, one slow and one fast cooled showed slightly increased modulus at 150 cycles.

      $0/90^{o}$ - Most showed erratic behavior.

   b. Kevlar

      0^{o} - Samples F1 and S1 show a steady, slight decrease, F2 and S2 stayed fairly constant.

      15^{o} - Fluctuating values.

      30^{o} - Most gave slight reductions except at 150 cycles where the modulus rose to initial value.

      45^{o} - Fluctuating values.

      60^{o} - Slight reduction trend followed by increase at 150 cycles.

      $0/90^{o}$ - No appreciable effect.

c. Glass

0^{o} - Averages for fast and slow cooled samples show steady, slight decrease. Some increase in 150 cycles values.

15^{o} - Two samples, one fast and one slow cooled showed steady decrease. The second fast cooled samples showed no change and the second slow cooled behaved erratically.

30^{o} - All showed steady decrease.

45^{o} - Two samples, one slow and one fast cooled showed decreasing trend while the others stayed almost unchanged.

60^{o} - The fast cooled samples showed large initial drop then steady values. The slow cooled showed steady decrease with one showing slight increase at 150 cycles.

$0/90^{o}$ - Fairly consistent readings for all samples.

d. Hybrids

15T1KGK - Steady decrease except for increase at 150 cycles for the slow cooled samples.

15T1GKG - Steady decrease except for increase in all samples at 150 cycles.

45T1KGK - All showed steady decrease.

45T1GKG - All consistent readings after slight initial drop after 50 cycles.

15T2 - Steady decreasing trend in all samples except for rise in the slow cooled samples at 150 cycles.

45T2 - All show steady decrease except for slight rise after 150 cycles.

Many readings after 150 cycles were above the 100 cycle values. This was first thought to be caused by the fact that testing after 150 cycles was not

carried out as promptly as the testing after 50 and 100 cycles and that the moisture content and distribution may have affected the results. However, two samples of unidirectional graphite-epoxy, one fast and one slow cooled, were placed in water for four days, and tested immediately after removal from the water. The values obtained showed no significant change from "control" samples. Thus, any moisture left over from cycling could not have significantly lowered the 50 and 100 cycle values.

2. Poisson's Ratio (υ_{12})

   a. Graphite

      0^{o} - Steady decrease, the slight rise at 150 cycles.

      15^{o} - Appreciable steady decrease.

      30^{o} - Steady decrease, slight rise at 150 cycles.

      45^{o} - Decreasing trend with some erratic behavior.

      60^{o} - Steady decrease except for exceptionally low initial value for slow cooled sample.

      $0/90^{o}$ - Steady decrease.

   b. Kevlar

      0^{o} - Steady decrease, slight rise at 150 cycles.

      15^{o} - Slight decreasing trend, much erratic behavior, especially after 150 cycles.

      30^{o} - Erratic behavior.

      45^{o} - Steady decrease in slow cool, erratic behavior in fast cool.

      60^{o} - Steady decrease in fast cool, erratic behavior in slow cool.

      $0/90^{o}$ - Steady decrease.

   c. Glass

      0^{o} - Steady decrease, slight rise after 150 cycles.

15^{o} - Erratic behavior.

30^{o} - Appreciable decrease, but slight rise after 150 cycles.

45^{o} - Steady decrease, slight rise after 150 cycles.

60^{o} - Erratic behavior.

$0/90^{o}$ - Steady decrease, rise after 150 cycles.

d. Hybrids

15T1KGK - Decreasing trend.

15T1GKG - Decreasing trend.

45T1KGK - Decreasing trend.

45T1GKG - Decreasing trend.

15T2 - Decreasing trend.

45T2 - Appreciable steady decrease.

In summary it can be said that the effect of hygrothermal cycling had very little effect on Young's modulus. This effect is generally a slight decrease after a small number of cycles with no further changes or in some cases even an increase after a larger number. However, the effect on the major Poisson's ratio was quite evident and was generally, and more consistently, an appreciable decrease.

B. THERMAL EXPANSION EXPERIMENTS

Results of the thermal expansion experiments are shown on Fig. 79 and Table 80 for the graphite/epoxy laminates, Fig. 80 and Table 81 for the kevlar/epoxy laminates and Fig. 81 and Table 82 for the glass/epoxy laminates. The thermal expansion behavior of the laminates varied widely from one fiber-resin system to another, apart from a strong dependence on ply angle.

The unidirectional laminates and the cross-ply laminates (or identically the $\pm 45^{o}$ laminates which are plane isotropic in their thermal expansion behavior) showed fairly smooth expansion curves, with the slope changing very gently over the temperature range considered (30^{o}-130^{o}C). Laminates of ply angles of 30^{o} (and to a lesser extent those of 15^{o} ply angle) had coefficients of expansions that decreased substantially upon heating. The transverse expansion coefficients of these laminates (or the longitudinal coefficients of laminates of complimentary angle, namely 60^{o} and 75^{o} respectively) increased substantially upon heating. These effects were in some cases quite drastic. For example the $\pm 30^{o}$ glass-epoxy laminates started from room temperature with a positive coefficient which decreased to around zero to 80^{o}C with little or no change until 100^{o}C. Beyond this temperature the coefficient became strongly negative. Correspondingly, the $\pm 60^{o}$ glass-epoxy laminate exhibited two expansion regimes, in both of which the coefficient was positive but its magnitude in the higher temperature range was more than three times as much as it was at lower temperatures.

C. STRENGTH AND FAILURE MODES OF ANGLE-PLY LAMINATES

Laminated composites have distinctively different modes of failure depending on their ply angle. By analyzing these failure modes, a better understanding of their strengths can be achieved.

The three major modes of failure are fiber separation (FS), fiber breakage (FB) and ply delamination (PD). Total failure of an angle ply laminate can occur by a combination of these three modes, again, depending on the ply angle. The extreme cases of an angle ply composite, $\pm 0^{0}$ and $\pm 90^{0}$, exhibit a single, but different mode of failure. The ±0 composite fails by FB only while the ±90 fails by FS. All other laminates fail by some combination of these three modes.

When a laminate is pulled in uniaxial tension, three major stresses of interest are produced; the normal stress σ_x, the in plane shearing stress τ_{yx}, and the interlaminar shearing stress τ_{zx}. (See Fig. 1). The normal stress is constant throughout the width of the laminate except for a slight decrease in magnitude at the edge. The in plane shear stress is also constant throughout the width except for a decrease to zero at the edge. The interlaminar shear stress is constantly zero throughout most of the width of the laminate, however, it begins building up at some point within the laminate and sometimes reaches extremely high values at the edge. This stress arises due to the fact that one ply with an orientation of $+\theta$ wants to rotate in one direction, while the adjacent ply of $-\theta$ wants to rotate in the opposite direction. The net result is a shearing stress between the two plys. This is an important stress that ultimately leads to the failure of many intermediate angle-ply laminates by the PD mode.

Interlaminar shear in a laminate depends on three factors; the ply angle, the ply thickness, and the elastic properties of the material used. The actual

magnitudes of the interlaminar shear are difficult to measure directly; however, a good representation of its magnitude with respect to the ply angle can be determined by calculating the Shear Distortion Coefficient. The Shear Distortion Coefficient is given by the equation

$$m_1 = \sin 2\theta[\upsilon_{LT} + \frac{E_L}{E_T} - \frac{1}{2}\frac{E_L}{G_{LT}} - \cos^2\theta(1+2\upsilon_{LT} + \frac{E_L}{E_T} - \frac{E_L}{G_{LT}})]$$

Graphs of this coefficient are given in Fig. 76 for all: T300 Graphite, kevlar 49 and E-glass, epoxy systems. As can be seen by these graphs, the interlaminar shear is zero at ±0, builds up to a maximum around ±30, decreases to zero and increases negatively between ±50 and ±80 depending on the system, and returns zero at ±90. Where the interlaminar shearing stress is zero or very low, no ply delamination will occur. Likewise, where the interlaminar shear is high, ply delamination will be the major mode of failure. So by changing the ply-angle in a laminate, the amount of the PD mode found in a failure will vary.

Another factor which affects the magnitude of the interlaminar shear is the thickness of the ply in the laminate. The thicker the ply, the higher the interlaminar shear stress since greater loads have to be transmitted to the thicker ply through the same interfacial area. Delamination of the plies always beginsat the edge of the laminate due, again, to the high interlaminar shearing stress. This edge effect was shown to exist by Pipes et al (6) by the use of Moire fringe patterns. This delamination will propagate inwards, usually working with the FS mode. Many times the FS mode will begin the failure, followed by PD. This will continue through the thickness of the laminate until only a partial failure has occurred across only a portion of the width of the laminate. After this partial failure, the ply angle will dictate the

failure of the remaining unfailed laminate. At low ply angles (±15) most of the applied load will be transmitted to the fiber direction leading to the FB mode. At slightly higher ply angles (e.g. ±30), less stress is transmitted in the fiber direction and more in the transverse direction. Also, the interlaminar shear stress is about at its highest level. Both of these effects lead to a failure that is a combination of FS and PD with sometimes a small amount of FB. At still higher angles, ($\pm 45^{o}$), the applied stress is equally transmitted to both the fiber and the transverse directions, with still a relatively high interlaminar shear stress resulting in a FS, PD mode of failure. (This combination of stress; $\sigma_L = \sigma_T$, $\tau_{zx} >>> o$ could lead to the high strain at failure noted in the ±45 composites.) When the ply angle is around the $\pm 60^{o}$, $\pm 75^{o}$ range, most of the applied stress is transmitted to the transverse direction and the interlaminar shearing stress is very low, leading primarily to a matrix failure. In this type of failure the $+\theta$ ply will fail by the FS mode and the $-\theta$ plies will have a fiber "kinking" effect. Depending on the elasticity of the fiber, this "kinking" effect may lead to the actual fracture of the fiber by a combination of bending and shearing stresses.

All laminates in the three systems, T300 Graphite/5209 Epoxy, Kevlar 49C/5216 Epoxy and E-Glass/5216 Epoxy, obeyed the above reasoning. In the case of the $\pm 0^{o}$, or unidirectional laminates, all three failed by the FB mode.

The $\pm 15^{o}$ laminates all failed by a combination of all three modes. In each case, the beginning of the failure consisted of the PD and FS modes due to the increase in interlaminar shear (edge effect). Once these modes had propagated across a portion of the width of the sample, the redistribution of stresses led to much higher stresses in the fiber direction resulting in FB.

As the ply angle increased to $\pm 30^{o}$, all three systems exhibited primarily failure by the PD, FS modes. This is due to the extremely high interlaminar

shearing stress found in $\pm 30^{0}$ laminates. However, some FB was also noted due to the redistribution of stresses in the fiber direction.

The ±45 laminates in all three systems failed totally by the PD, FS modes. At this ply-angle, the interlaminar shear is high enough to cause total failure before enough stress can be transmitted to the fiber direction to cause FB. It is also noted that ±45 laminates are the only ones to fail in a ductile manner.

The ±60 laminates failed by FS, along with fiber kinking, and a very small amount of PD. The kinking resulted in some fiber failure in the E-Glass and total fiber failure in the T300 Graphite laminates. It was also noted that in the case of the E-Glass $\pm 60^{0}$ laminates, more PD occurred than in either T300 Graphite or Kevlar 49. This behavior is due to the fact that the ply thickness of the E-Glass is appreciably larger than the T300 Graphite or the Kevlar 49 plies. As noted earlier, as ply thickness increases, the interlaminar shear increases leading to a greater possibility of the occurrance of PD. This phenomenon was further experimentally proven by making a $\pm 60^{0}$ T300 Graphite Epoxy laminate with twice the ply thickness as usual and pulling to failure. As expected, this thick ply laminate exhibited an appreciably greater amount of PD than did the laminate of the same material with the regular ply thickness.

The $\pm 75^{0}$ laminates of all three sytems exhibited the FS mode along with the "kinking" effect and very little or no delamination present. Again the kinking of the fibers in the T300 Graphite laminate led to breakage of the fiber due to the bending and shear stresses caused by the kinking.

An attempt was made to ascertain whether the failure of the composites tested fit the modified Tsai-Hill failure criterion for anisotropic materials. The Tsai-Hill equation in its reduced form is as follows:

$$\frac{\cos^4\theta}{x^2} + \left(\frac{1}{S^2} - \frac{1}{X^2}\right)\cos^2\theta\sin^2\theta + \frac{\sin^4\theta}{Y^2} = \frac{1}{\sigma_x^2}$$

where θ = off axis angle

X = strength in fiber direction

Y = strength in transverse direction

S = shear strength

σ_x = stress at failure

This criterion is for unidirectional laminates pulled at any off axis angle θ. In its application to the angle-ply laminates it must be assumed that at least the onset of failure is coincident with the failure of the first ply. However, as seen by the test results, the Tsai-Hill criterion greatly underestimates the failure strengths of the laminates. The Tsai-Hill predictions and the test results are plotted against ply angle on graphs. This is not surprising since the loads are transmitted to the ply in a different manner from the way a unidirectional composite is loaded.

A better understanding of the fracture strengths can be obtained if a comparison of the material strengths; longitudinal, transverse, and shear, to the resolved stresses applied to the laminate; σ_L, σ_T, τ_{LT}, can be made keeping in mind the failure mode in which the laminate actually failed. (Table 79)

Beginning with the graphite laminates, the unidirectional samples failed at a stress level of 206,300 psi. The resolved stress in the fiber direction and the material longitudinal strength are of course identical, and the laminate failed by fiber breakage. In the case of the $\pm 15^o$ laminate, the fracture strength was 129,040 psi, which resolves in the transverse direction to a stress of -7,131 psi, exceeding the material transverse strength of 6,500 psi. So the material would be expected to experience transverse cracking, or fiber

separation, which was indeed the initial mode of failure. Before this initial failure occurred, the resolved shear stress reached a value of -4,937 psi, however, after the initial fiber separation, redistribution of stress would increase this shear stress past the material shear strength of 9,000 psi resulting in the ply delamination mode. In turn, after this failure mode had occurred, the redistribution of stresses, with the bending and shearing stresses experienced by the fibers, fiber breakage takes place, completing the failure process. This was indeed what occurred experimentally. The $\pm 30^{o}$ laminate, at the time of failure, had both the resolved transverse stress and shearing stress exceeding the material transverse and shear strengths respectively resulting in gross transverse cracking (fiber separation) and ply delamination. Again after the onset of initial failure, the redistribution of stresses caused fiber breakage to complete the failure process as was seen experimentally. The $\pm 45^{o}$ sample, was experiencing at failure, a very high resolved shearing stress which exceeded the material shear strength resulting in gross delamination. This large amount of delamination could do nothing but cause fiber separation, completing the failure as was observed. Both the $\pm 60^{o}$ and the $\pm 75^{o}$ samples experienced very high resolved transverse stresses, higher than the material transverse strength, resulting primarily in transverse cracking as the mode of failure.

The glass and kevlar samples followed the same patterns. So, by comparing the applied resolved stresses to the material strengths, one may readily see why the laminates failed in the modes in which they did.

D. PROPERTIES ALONG THICKNESS DIRECTIONS OF LAMINATES

Extra thick laminates were prepared of each of the three fiber-resin systems with ply angles of $\pm 22.5^{o}$ and $\pm 45^{o}$. These were 300 plies thick and measured 1 inch x 2 inches in plane and 2 to 2.5 inch thick. They were cured in a small pressure vessel which was heated in an electric furnace. The ply orientation alternated all the way through the thickness. The samples were instrumented with one strain gage transversely oriented and a $0\text{-}90^{o}$ two-element gage mounted on the adjacent face with one element oriented along the loading direction. Young's modulus E_3 and Poisson's ratios υ_{32} and υ_{31} were determined for each and the results are given below.

$\pm 22.5^{o}$ Laminates

	E_3	υ_{31}	υ_{32}
Graphite/Epoxy	1.175	-.0403	.4031
Kevlar/Epoxy	0.404	-.0586	.3561
Glass/Epoxy	1.666	-.0434	.406

$\pm 45^{o}$ Laminates

	E_3	υ_{31}	υ_{32}
Graphite/Epoxy	.9313	.0719	.0569
Kevlar/Epoxy	.6472	-.0387	.0824
Glass/Epoxy	1.905	.1415	.2075

Previous work here has shown that a negative Poisson's ratio involving the thickness is indeed expected. In the $\pm 45^{o}$ laminates, the values of the Poisson's ratio are very small as previous work has suggested, but the values for the kevlar/epoxy obviously lack accuracy since they should have been ideally equal.

IV. RESIDUAL STRESSES

A. BACKGROUND & EXPERIMENTS

1. Thermal Expansion Method:

This is based on measurements of the thermal expansion coefficients of the unidirectional material representing the ply properties and of the angle ply laminate in which the plies undergo "restrained" expansion. This method can yield the residual stresses developed if the temperature is known below which no stress relief takes place upon cooling from the curing temperature of the resin.

The residual strain in a ply is the difference between the "restrained" and "unrestrained" thermal strain of the ply, i.e. the difference between the thermal expansion of the laminate and the thermal expansion of the ply, had it not been laminated. The unrestrained thermal strain is calculated from the thermal expansion coefficients of the unidirectional composite α_L and α_T along the longitudinal and transverse directions respectively. These are measured directly on the dilatometer. The restrained expansions of the ply are those of the whole laminate and may again be measured experimentally, or calculated using the experimentally determined values of the elastic constants and expansion coefficients of the unidirectional material. The thermal expansion of the unidirectional composite may be calculated in terms of fiber and matrix properties and volume fraction of fibers. The calculations have been found to give an accurate estimate of the longitudinal but not of the transverse coefficient. This is not only due to the sensitivity of the latter to fiber distribution but more importantly to lack of reliable information on the transverse properties of fibers. It was decided, however, to use in our analysis the experimental values of α_L and α_T for the three fiber-resin systems.

2. Embedded Strain Gage Method:

In this method a three-element electrical strain gage rosette is embedded in the laminate during the lay-up of the pre-preg tape at the location at which it is desired to determine the residual stress. The embedded gage is thus exposed to the entire cure cycle and its output as well as temperature is monitored. It was decided to placed the gages between two plies of the same orientation, and hence they were placed on the midplane of the laminate where directly above and directly below were similar plies. The strain gage output was corrected by subtracting the gage thermal output which is due to temperature changes in resistivity and the gage thermal dilatation. One advantage of this method is that it can continuously monitor the build-up of stress. Here again the strain gage is effectively used to determine the laminate thermal strain which is the restrained strain of any ply; and by knowledge of the unrestrained strain it is possible to calculate the residual stress.

3. A Deflection Method for Investigating Residual Stresses in Laminates:

In this method a laminate of only two plies of $+\theta$ and $-\theta$ orientations are prepared and cured in the same way as the thicker and balanced angle ply laminates are prepared for the rest of this work. These thin two-ply laminates do not possess midplane symmetry and if residual lamination stresses develop in them they would distort and warp upon completion of the cycle and removal from the press. The extent of distortion and warp may be used to calculate the residual stress. Alternatively, a tiny strain gage rosette may be attached, the output of which depends upon the residual stress. This method is now being developed here to yield complete information on the stress state. However, the degree of warp gives a relative indication of the intensity of the stress and

by simply heating the thin laminates the warp gradually diminishes until it disappears completely at the "stress free" temperature. It is thus possible to make qualitative comparisons of residual stress levels in different laminates and to determine the temperature below which stresses build up upon cooling.

4. An X-Ray Diffraction Method Using a Crystalline Filler:

The residual stresses as determined by thermal expansion, strain gages or deflection are ply stresses or macrostresses which are in fact averaged over the fiber and matrix with the fibers being naturally more highly stressed than the matrix. The stress and strain of each of the two constituents of the composite or rather the microstress and microstrain distribution are of interest and may influence the initiation of failure of the composite. X-ray diffraction was used in exploratory experiments to investigate this. In this method a very small amount of a fine crystalline powder is incorporated between two plies of a laminate while the pre-preg tape is being laid up. A diffraction pattern of the loose crystalline powder is obtained and a strong line in the back reflection region is elected and carefully scanned to give the line profile. The same powder incorporated in the composite is x-rayed, using an attachment which allows the positioning of the composite so that the powder plane normal passes through the diffractometer axis and bisects the angle between the incident and diffracted beams. The shift in the peak position observed is used to calculate the strain in the powder and hence the matrix. The powder selected after experimentally screening five possible candidates was tungsten and the diffraction line was the (321) line occurring at 131.2^{o} with copper K_{α} radiation. This method was used with unidirectional kevlar-epoxy laminates.

B. RESULTS AND DISCUSSION

Although all four techniques mentioned above were attempted, only the first, namely the thermal expansion method was used extensively throughout this investigation as will be detailed later. The embedded strain gage method was used only with kevlar/epoxy laminates and only with two ply angles namely 22 1/2^{o} and 45^{o}. The gages were Micromeasurement's rosettes type WA-06-030Wy-120. In both cases by use of a strain Mohr circle the principal strain-directions almost coincided with the 0^{o} and 90^{o} of the sample, and an analysis of the stress state gave the following stress values at room temperature referred to the longitudinal and transverse directions of the individaul +θ ply. (The -θ ply has a reversed sign on its shear stress.)

for $\pm 22.5^{o}$ laminate

σ_L = -1343 psi

σ_T = +1181 psi

τ_{LT}= -1010 psi

and for $\pm 45^{o}$ laminate

σ_L = -3262 psi

σ_T = +4030 psi

τ_{LT}= 235 psi

Conditions of symmetry and equilibrium necessitate that for the $\pm 45^{o}$ laminate the shear stress be zero and the two normal stresses to be equal and opposite. The $\pm 22.5^{o}$ would be expected to experience a high level of shear stress and less intense normal stresses than the $\pm 45^{o}$ laminate. The above results show this trend although obviously the numerical values must be subject to appreciable experimental error. At their face values, however, and by comparison to the thermal expansion computations it would appear that the stress level

is lower than one would expect had they been building up over the entire temperature range from the curing to room temperature.

The deflection method was used on all three fiber resin systems. The two-ply coupons had ply angles of $\pm 15^{o}$, $\pm 30^{o}$, $\pm 45^{o}$, $\pm 60^{o}$, and $\pm 75^{o}$. Obviously, the $\pm 15^{o}$ and $\pm 75^{o}$ are identical in lay-up and so are the $\pm 30^{o}$ and $\pm 60^{o}$; however, the coupons were 1" by 4 1/2" rectangles and the long axis pointed in the zero direction in each case and this duplication served as a check in any case.

The experiments which were carried out in a circulating air, plexiglass door oven gave the following temperatures as the stress free temperature for laminates.

Graphite/Epoxy

Ply Angle	Temperature
$\pm 15^{o}$, $\pm 75^{o}$	127
$\pm 30^{o}$, $\pm 60^{o}$	126
$\pm 45^{o}$	150

Kevlar/Epoxy

Ply Angle	Temperature
$\pm 15^{o}$, $\pm 75^{o}$	51
$\pm 30^{o}$, $\pm 60^{o}$	70
$\pm 45^{o}$	118

Glass/Epoxy

Ply Angle	Temperature
$\pm 15^{o}$, $\pm 75^{o}$	89
$\pm 30^{o}$, $\pm 60^{o}$	129
$\pm 45^{o}$	156

The x-ray method gave a shift in the (321) line peak of $+\Delta 2\theta = .031^{o}$ or 5.37×10^{-4} when the fiber direction was in the diffractometer plane. Only an approximate estimate can be made at this time. An assumption has to be made as to whether the powder in the powder-matrix assembly represents an equi-stress or equi-strain situation. The latter is probably more realistic and although it underestimates the stress it was used for the following rough estimate. The sum of the two principal stresses in the powder plane are thus

$$(\sigma_1 + \sigma_2) = \cot\frac{\theta}{2} \cdot \frac{\Delta 2\theta}{2} \cdot \frac{E}{\upsilon}$$

where υ is Poisson's ratio of tungsten, and E is Young's modulus of the epoxy. This gives a stress of an approximate value of only 200 psi but as mentioned earlier this represents a lower bound on the value. Residual stresses computed from thermal expansion data were analyzed for all three fiber resin systems for ±15, ±30 and ±45 ply angles. The thermal expansion coefficients for laminates of the graphite/epoxy, kevlar/epoxy, and glass/epoxy laminates are shown in Fig. (79), (80) and (81). The coefficients were determined experimentally as well as computed from data on the expansion behavior of the single ply and its elastic properties. The agreement on the whole was good and values from the smooth curve were used rather than the individual determinations. The computed residual stresses referred to the principal materials axes, i.e. σ_L, σ_T and τ_{LT} for the three systems are shown in Figs. (82), (83) and (84) for graphite/epoxy, kevlar/epoxy, and glass/epoxy respectively.

It may be noted here that despite the large variation in properties between the three systems, the thermal residual stress, not only shows almost identical trends in all three, but also the numerical values for the same ply angle of the three systems are very close.

The large shear stresses developed in laminates of ±30 (or ±60) may account for the unusual behavior of these upon heating as described elsewhere.

C. RESIDUAL STRESS IN THE HYBRID LAMINATES

The residual stresses were determined for the hybrids from thermal expansion data. The coefficient of expansion and hence the residual stresses were found to be independent of the lay-up sequence but of course not of the orientation of the plies. As described previously three lay-up sequences were used; glass-epoxy skin with kevlar-epoxy core, kevlar-epoxy skin with glass-epoxy core, and glass-epxoy alternating with kevlar-epoxy keeping midplane symmetry. The ply angles used were ±15 and ±45^{o}. The number of plies of each system was equal but the glass-epoxy ply was .00681 inch thick while the kevlar-epoxy ply was only .00545 inch thick, measured after curing.

The average longitudinal and transverse thermal expansion coefficient for the ±15^{o} laminate was taken as -2.24 x $10^{-6}/^{o}C$ and 56.10 x $10^{-6}/^{o}C$ respectively, and the residual stresses generated were as follows:

For the kevlar-epoxy ply:

σ_L = 52.70 psi/^{o}C

σ_T =-20.28 psi/^{o}C

τ_{LT}= 7.73 psi/^{o}C

and for the glass-epoxy ply:

σ_L =-31.01 psi/^{o}C

σ_T = 4.87 psi/^{o}C

τ_{LT}= 13.74 psi/^{o}C

The expansion coefficients for the ±45^{o} were identical and estimated to be 10.32 x $10^{-6}/^{o}C$. The residual stresses developed were:

For the kevlar-epoxy ply:

σ_L = 133.59 psi/^{o}C

σ_T = -42.51 psi/^{o}C

τ_{LT}= 0

and for the glass-epoxy ply:

σ_L = -0.57 psi/^oC

σ_T =-66.40 psi/^oC

τ_{LT}= 0

V. SUMMARY AND CONCLUSIONS

Residual stresses were determined for symmetric angle-ply composites of the Graphite/Epoxy, Kevlar/Epoxy, and Glass/Epoxy systems as well as hybrids of kevlar-glass/epoxies. The methods available for such determinations were reviewed but the thermal expansion as determined by the dilatometer was the one method used extensively, although embedded strain gages, deflection and x-ray diffraction techniques were tried.

The intensity and distribution of residual stress was surprisingly similar in the three systems despite the large differences in their properties. The hybrids, however, showed stress levels and distributions that was markedly different from one ply system to the other and this holds the promise of controlling these stress patterns to suit the properties of the individual ply.

In the process of determining residual stresses it was necessary to study the thermal expansion behavior of the laminates of the three systems and the hybrids. Certain anomalies in the expansion behavior were noted especially at ply angles of ±30 (or $\pm 60^{\circ}$) which may be due to interlaminar shear effects. These deserve further study. This work also suggests that the rate of cooling of the laminates after curing does not affect to any appreciable degree, its strength, stiffness or thermal expansion behavior.

The effect of hygrothermal cycling was studied and was found to have very little effect on Young's modulus but substantially reduced their major Poisson's ratio.

Failure modes and analysis of the stresses at failure were studied and a correlation was found to exist between them.

Properties of the laminates of the three systems along their thickness direction were briefly studied and results, notably the negative Poisson's ratio υ_{31}, confirmed earlier findings. Thickness properties of laminates deserve further study.

BIBLIOGRAPHY

1. Chamis, C. C., "Lamination Residual Stresses in Cross-Plied Fiber Composites." Proceedings of 26th Annual Conference of S.P.I. Paper No. 17-D, February 1971.

2. Chamis, C. C., "Design and Analysis of Fiber Composite Structural Components." NASA Report SP 277, 1970, pg. 217.

3. Fahmy, A. A., Chiang, C. H., and Halpin, B. M., "The Thermal Expansion Behavior of Filament Wound Composite Tubes." Thermal Expansion 6 (1978), Plenum Publishing Corp., New York, 1978.

4. Fahmy, A. A., "Examination of Filament Wound Tubes." Progress Report submitted to AMMRC (Batelle Task No. 75-333) 1975.

5. Fahmy, A. A. and Cunningham, T. G., "Investigation of Thermal Fatigue in Fiber Composite Materials." NASA CR-2641, July 1976.

6. Pipes, R. Byron and Daniel, I. M., "Moire Analysis of the Interlaminar Shear Edge Effect in Laminated Composites," J. Composite Materials, April 1971, pp. 255-259.

TABLE 1. YOUNG'S MODULUS VS. PLY ANGLE WITHOUT CYCLING FOR T300 GRAPHITE/RIGIDITE 5216 EPOXY

PLY ANGLE (DEGREES)	YOUNG'S MODULUS (MSI) FAST	SLOW
0	18.08	17.58
15	16.20	16.03
30	6.13	7.12
45	2.15	2.58
60	1.78	1.83
90	1.02	1.02

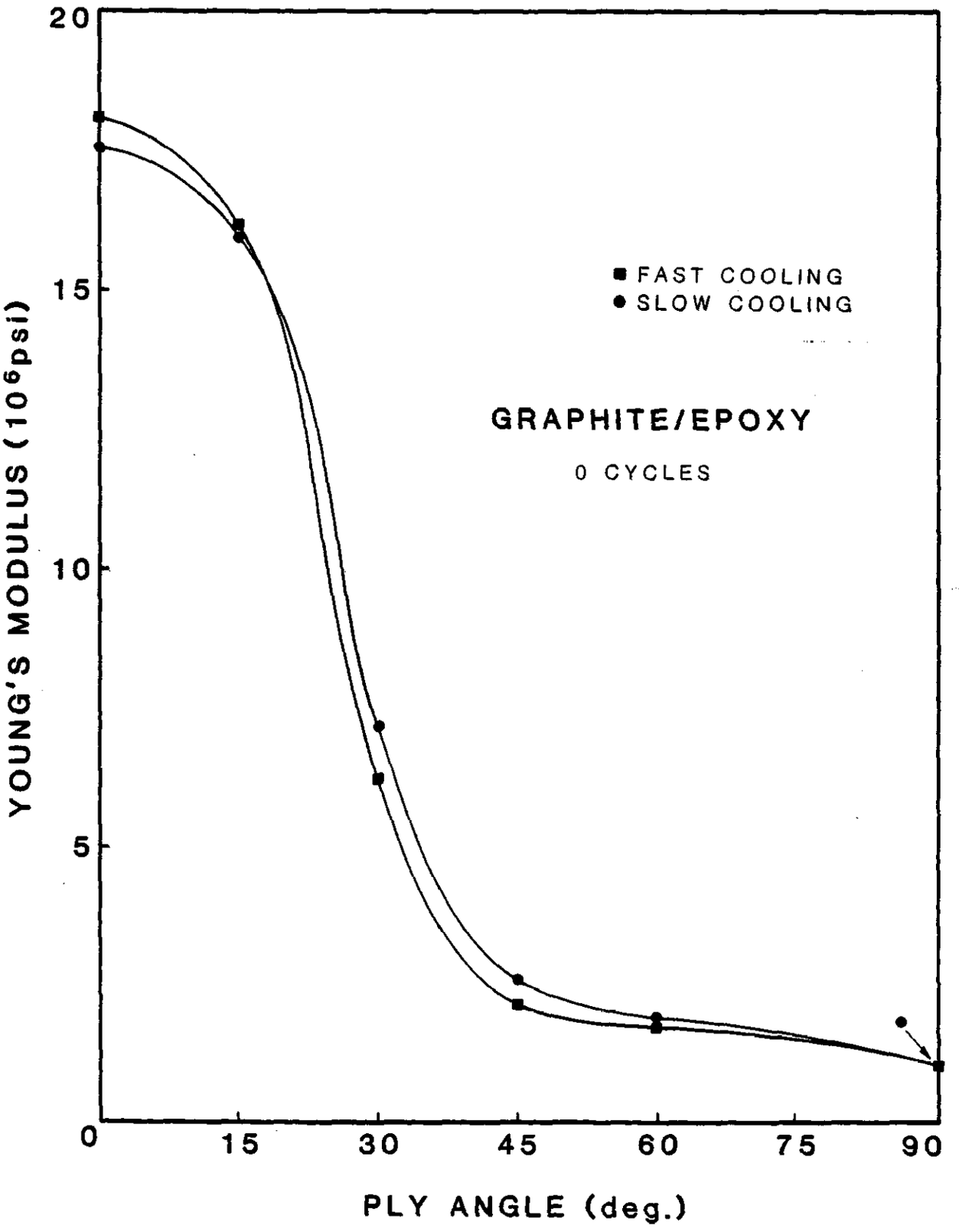

Figure 1. Young's Modulus vs. Ply Angle without cycling for T300 Graphite/Rigidite 5209 Epoxy.

TABLE 2. YOUNG'S MODULUS VS. PLY ANGLE WITHOUT CYCLING FOR KEVLAR 49C/RIGIDITE 5216 EPOXY

PLY ANGLE	YOUNG'S MODULUS (MSI)	
(DEGREES)	FAST	SLOW
0	10.16	10.31
15	8.43	8.23
30	3.27	3.07
45	1.05	1.16
60	0.78	0.77
90	0.65	0.51

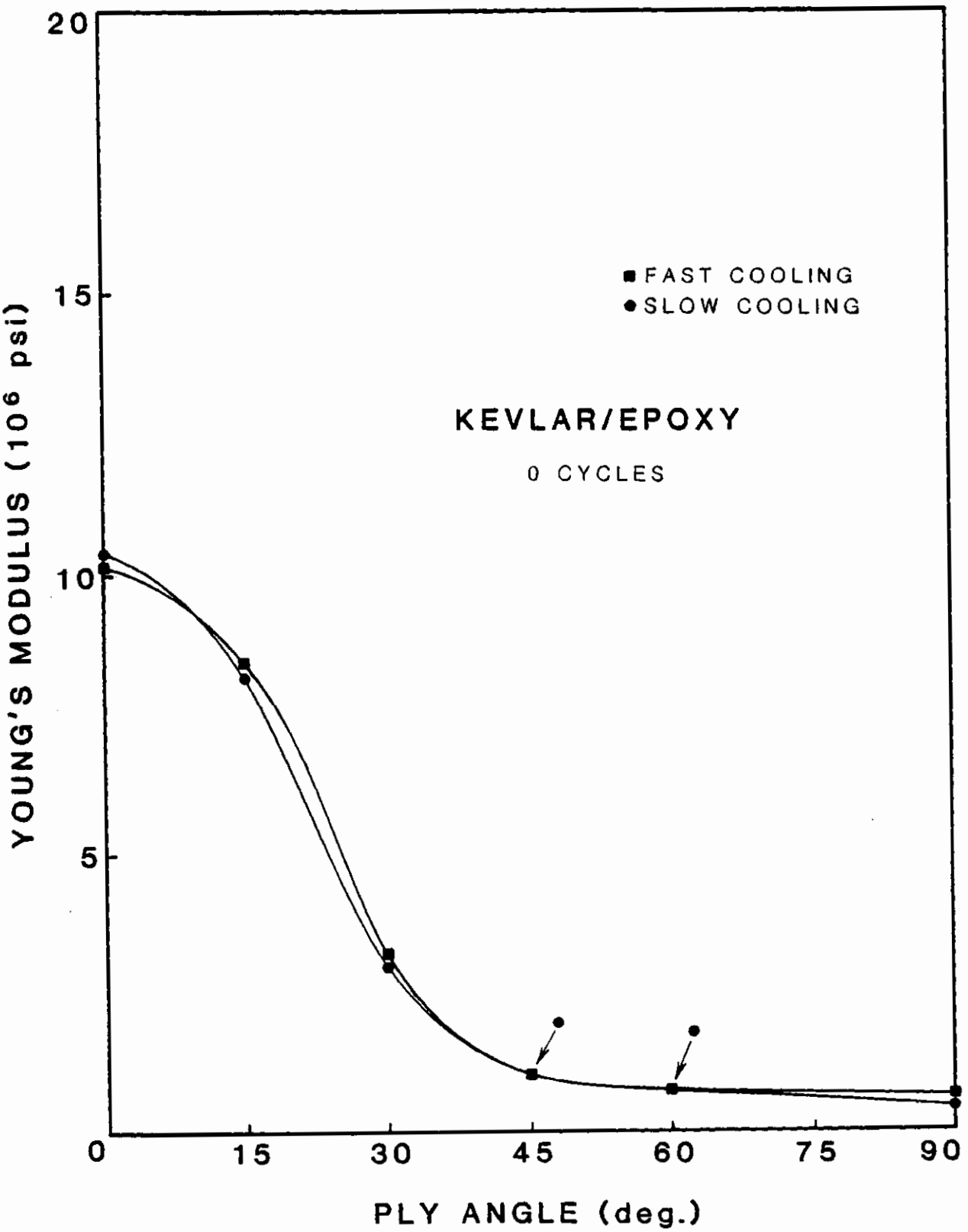

Figure 2. Young's Modulus vs. Ply Angle without cycling for Kevlar 49C/Rigidite 5216 Epoxy.

TABLE 3. YOUNG'S MODULUS VS. PLY ANGLE WITHOUT CYCLING FOR E-GLASS/RIGIDITE 5216 EPOXY

PLY ANGLE (DEGREES)	YOUNG'S MODULUS (MSI) FAST	SLOW
0	6.27	6.20
15	6.45	6.54
30	4.90	4.85
45	2.22	2.35
60	3.20	2.73
90	1.65	1.90

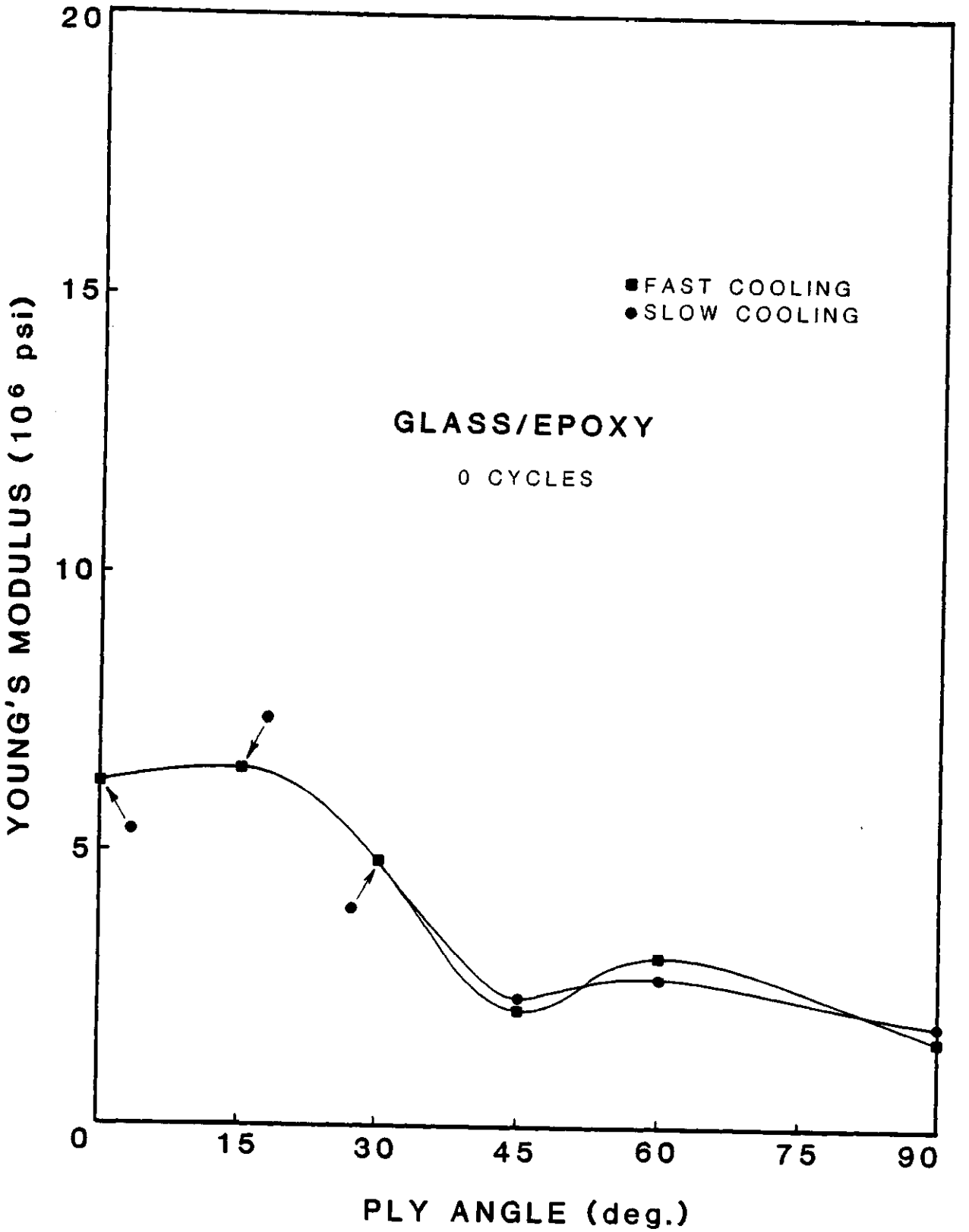

Figure 3. Young's Modulus vs. Ply Angle without cycling for E-Glass/Rigidite 5216 Epoxy.

TABLE 4. YOUNG'S MODULUS VS. PLY ANGLE AFTER 50 CYCLES FOR T300 GRAPHITE/RIGIDITE 5209 EPOXY

PLY ANGLE (DEGREES)	YOUNG'S MODULUS (MSI)	
	FAST	SLOW
0	16.49	17.16
15	16.04	15.29
30	5.75	6.46
45	2.12	2.26
60	1.52	1.31

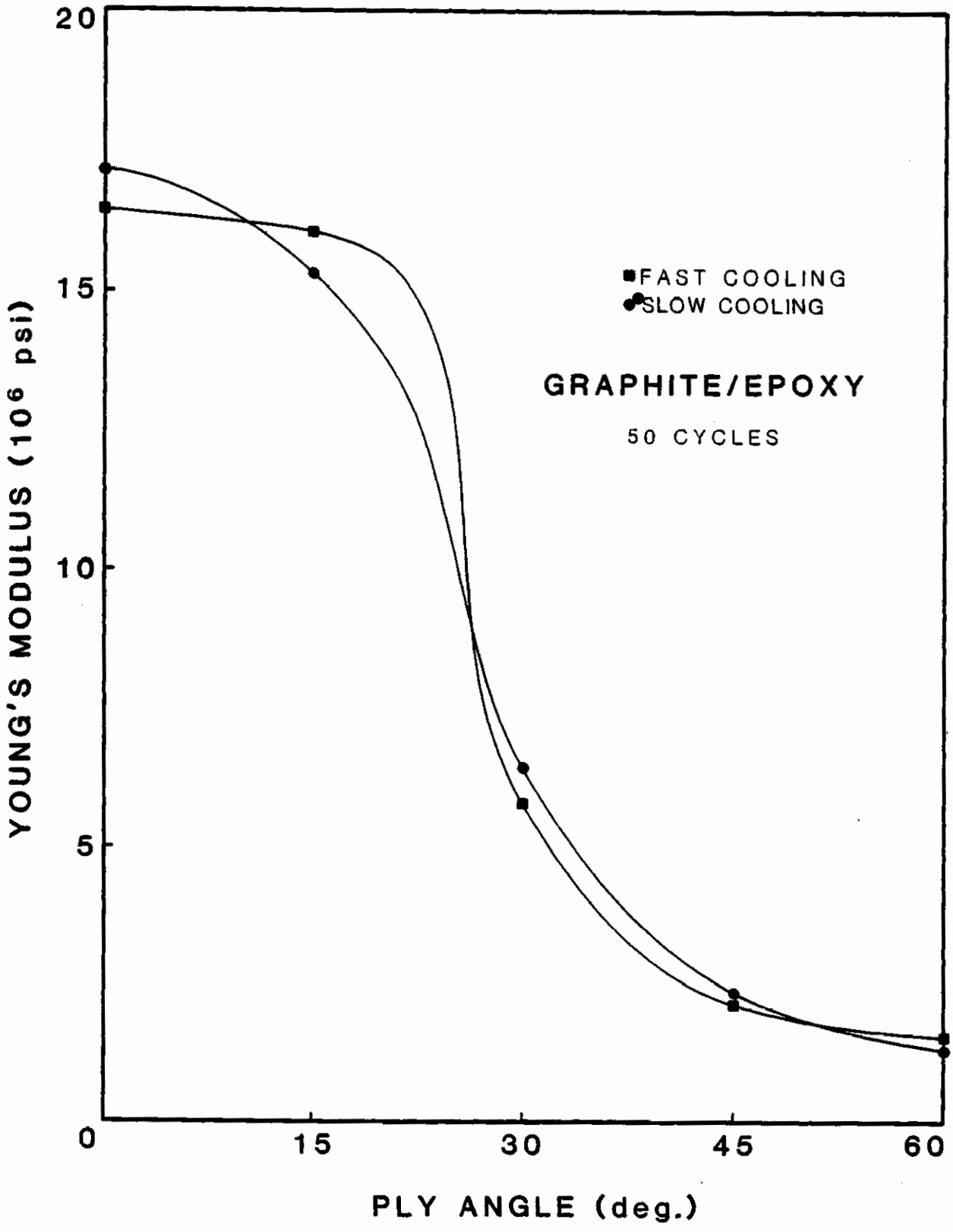

Figure 4. Young's Modulus vs. Ply Angle after 50 cycles for T300 Graphite/Rigidite 5209 Epoxy.

TABLE 5. YOUNG'S MODULUS VS. PLY ANGLE AFTER 50 CYCLES FOR KEVLAR 49C/RIGIDITE 5216 EPOXY

PLY ANGLE	YOUNG'S MODULUS (MSI)	
(DEGREES)	FAST	SLOW
0	10.13	9.80
15	7.94	7.45
30	2.90	2.86
45	0.97	1.00
60	0.68	0.72

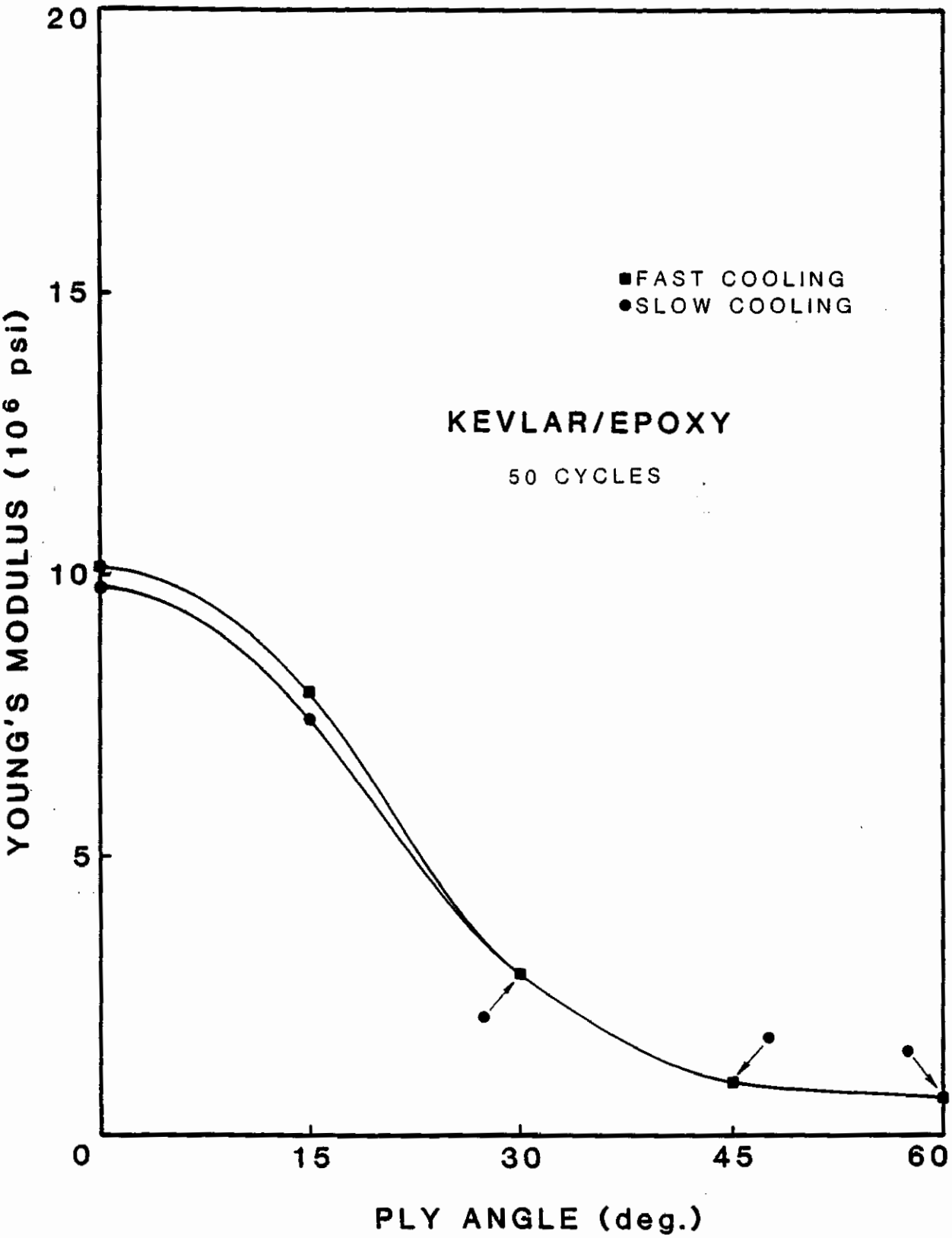

Figure 5. Young's Modulus vs. Ply Angle after 50 cycles for Kevlar 49C/Rigidite 5216 Epoxy.

TABLE 6. YOUNG'S MODULUS VS. PLY ANGLE AFTER 50 CYCLES FOR E-GLASS/RIGIDITE 5216 EPOXY

PLY ANGLE (DEGREES)	YOUNG'S MODULUS (MSI)	
	FAST	SLOW
0	6.22	6.02
15	6.35	6.24
30	4.43	4.63
45	2.06	2.14
60	2.24	2.43

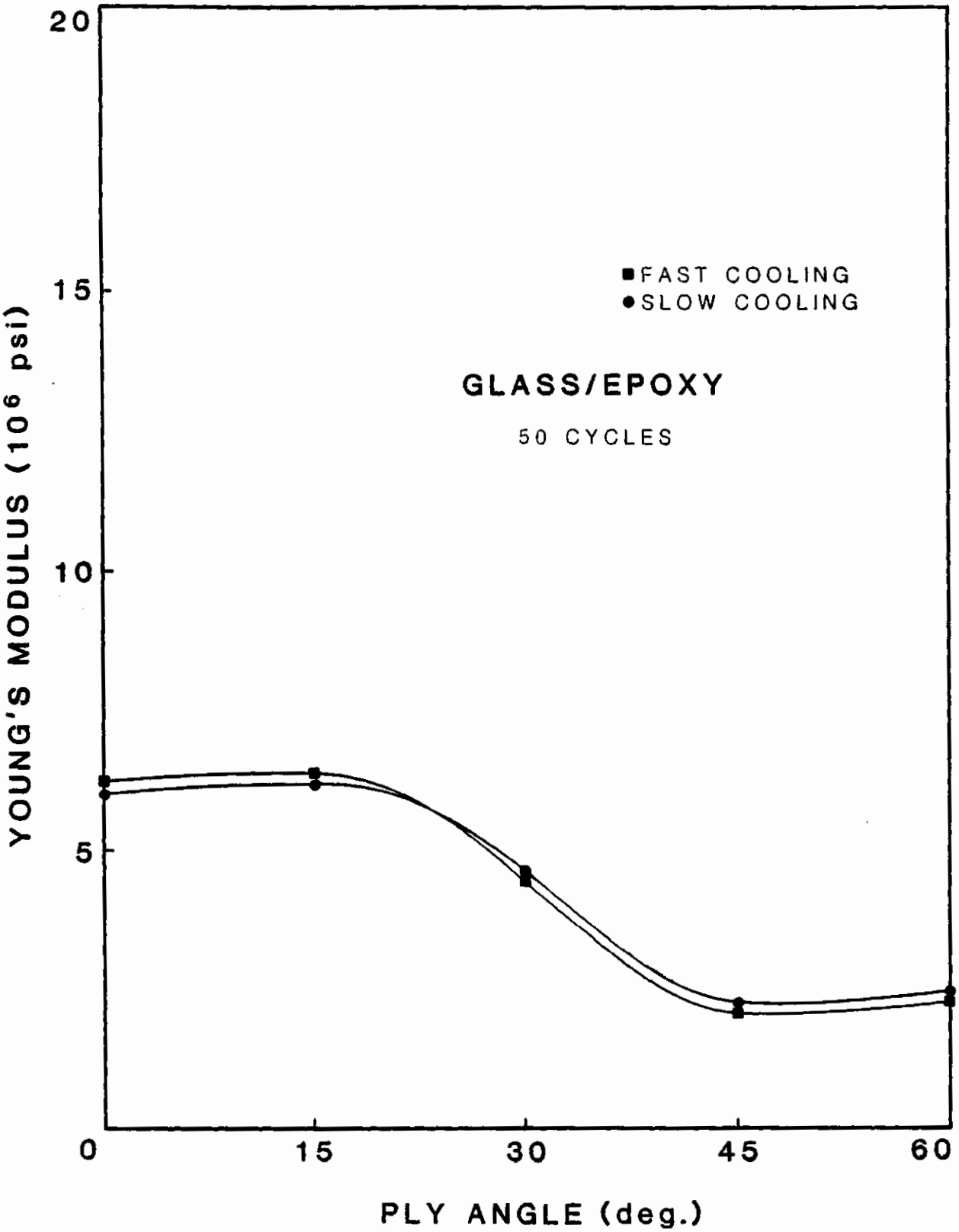

Figure 6. Young's Modulus vs. Ply Angle after 50 cycles for E-Glass/Rigidite 5216 Epoxy.

TABLE 7. YOUNG'S MODULUS VS. PLY ANGLE AFTER 100 CYCLES FOR T300 GRAPHITE/RIGIDITE 5209 EPOXY

PLY ANGLE	YOUNG'S MODULUS (MSI)	
(DEGREES)	FAST	SLOW
0	16.72	17.48
15	17.44	15.18
30	5.49	7.85
45	2.03	2.42
60	1.26	1.47

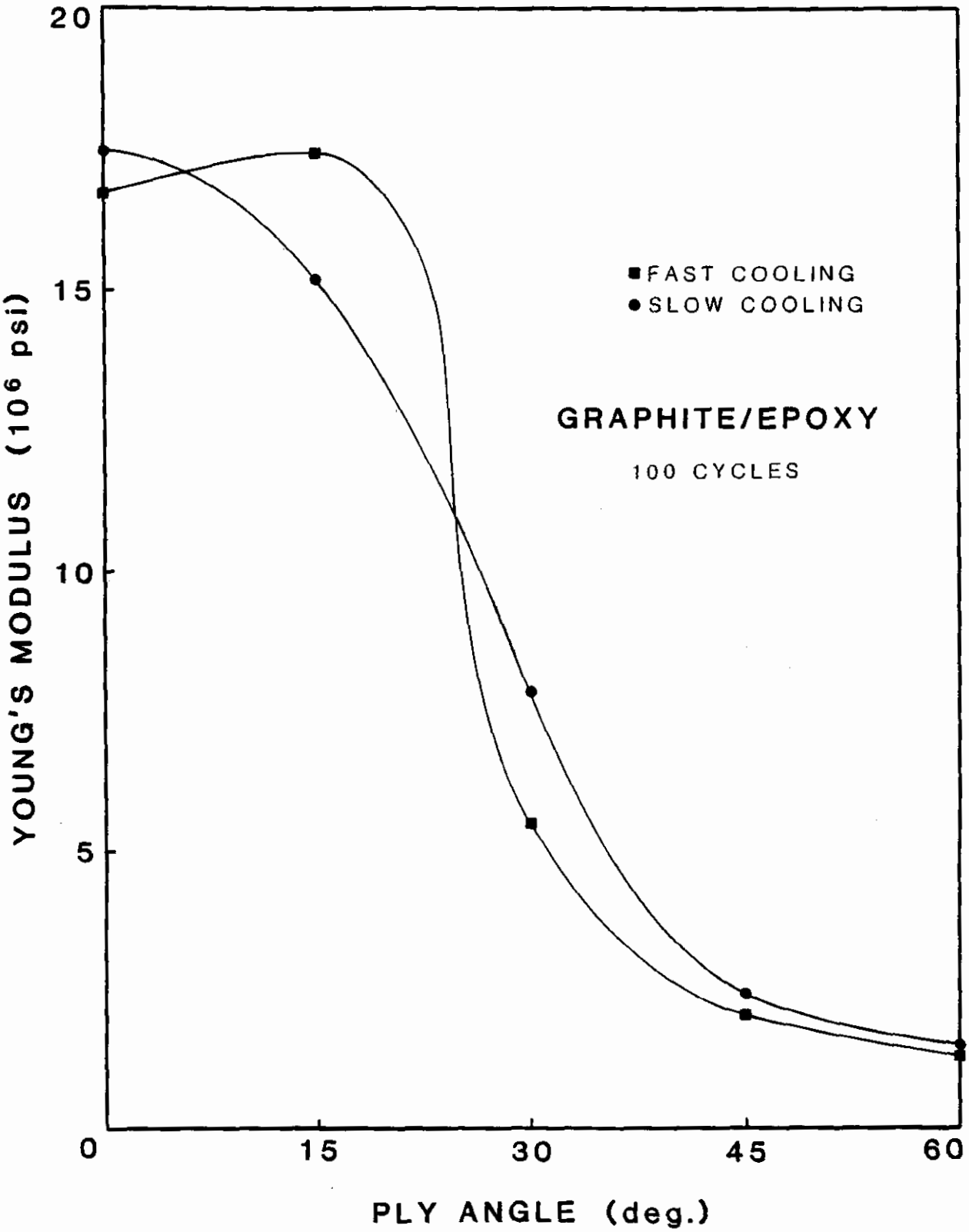

Figure 7. Young's Modulus vs. Ply Angle after 100 cycles for T300 Graphite/Rigidite 5209 Epoxy.

TABLE 8. YOUNG'S MODULUS VS. PLY ANGLE AFTER 100 CYCLES FOR KEVLAR 49C/RIGIDITE 5216 EPOXY

PLY ANGLE	YOUNG'S MODULUS (MSI)	
(DEGREES)	FAST	SLOW
0	10.10	9.46
15	7.85	7.86
30	2.82	3.50
45	0.93	1.04
60	0.66	1.12

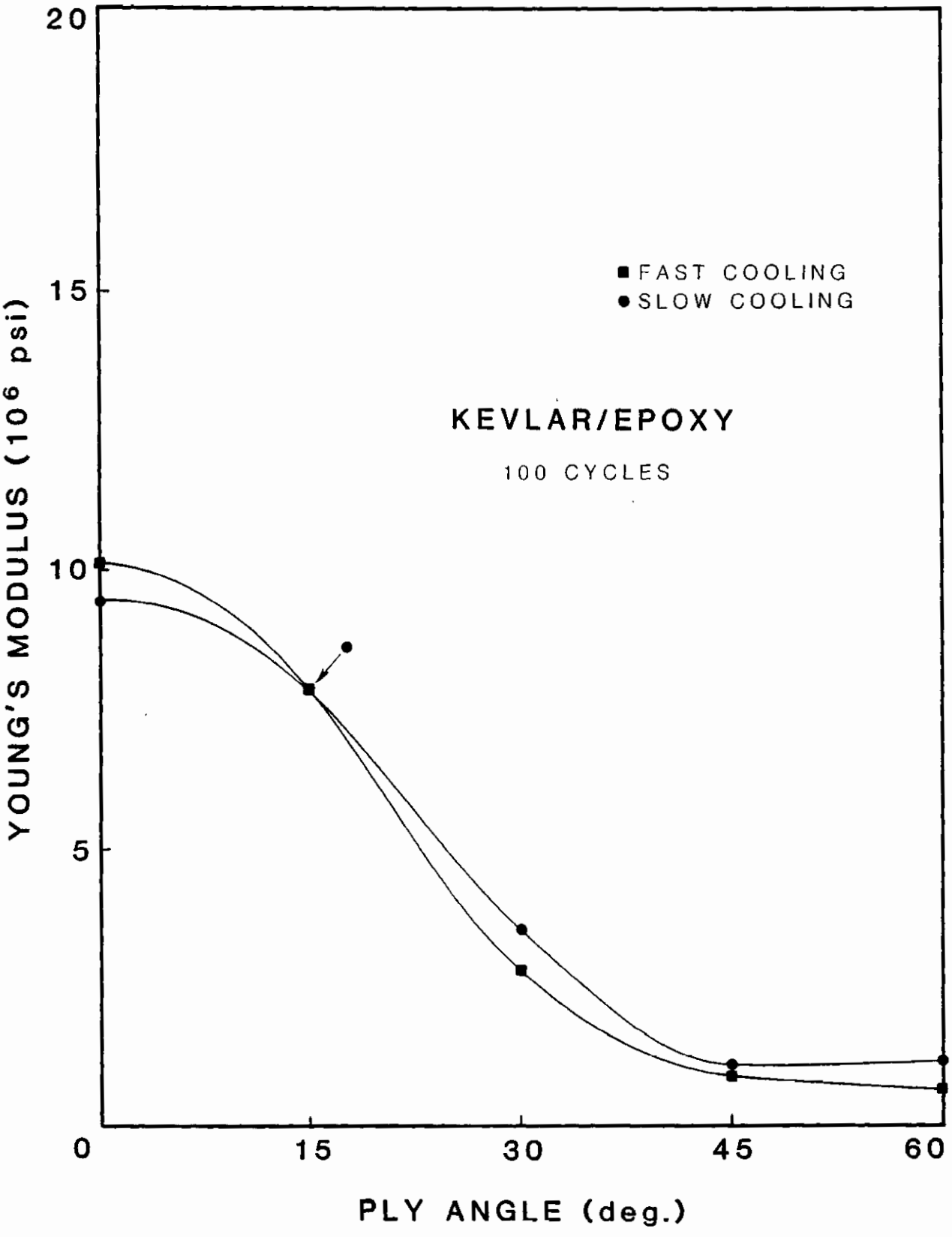

Figure 8. Young's Modulus vs. Ply Angle after 100 cycles for Kevlar 49C/Rigidite 5216 Epoxy.

TABLE 9. YOUNG'S MODULUS VS. PLY ANGLE AFTER 100 CYCLES FOR E-GLASS/RIGIDITE 5216 EPOXY

PLY ANGLE (DEGREES)	YOUNG'S MODULUS (MSI)	
	FAST	SLOW
0	6.05	6.00
15	6.26	6.08
30	4.41	4.36
45	2.08	2.19
60	2.30	2.19

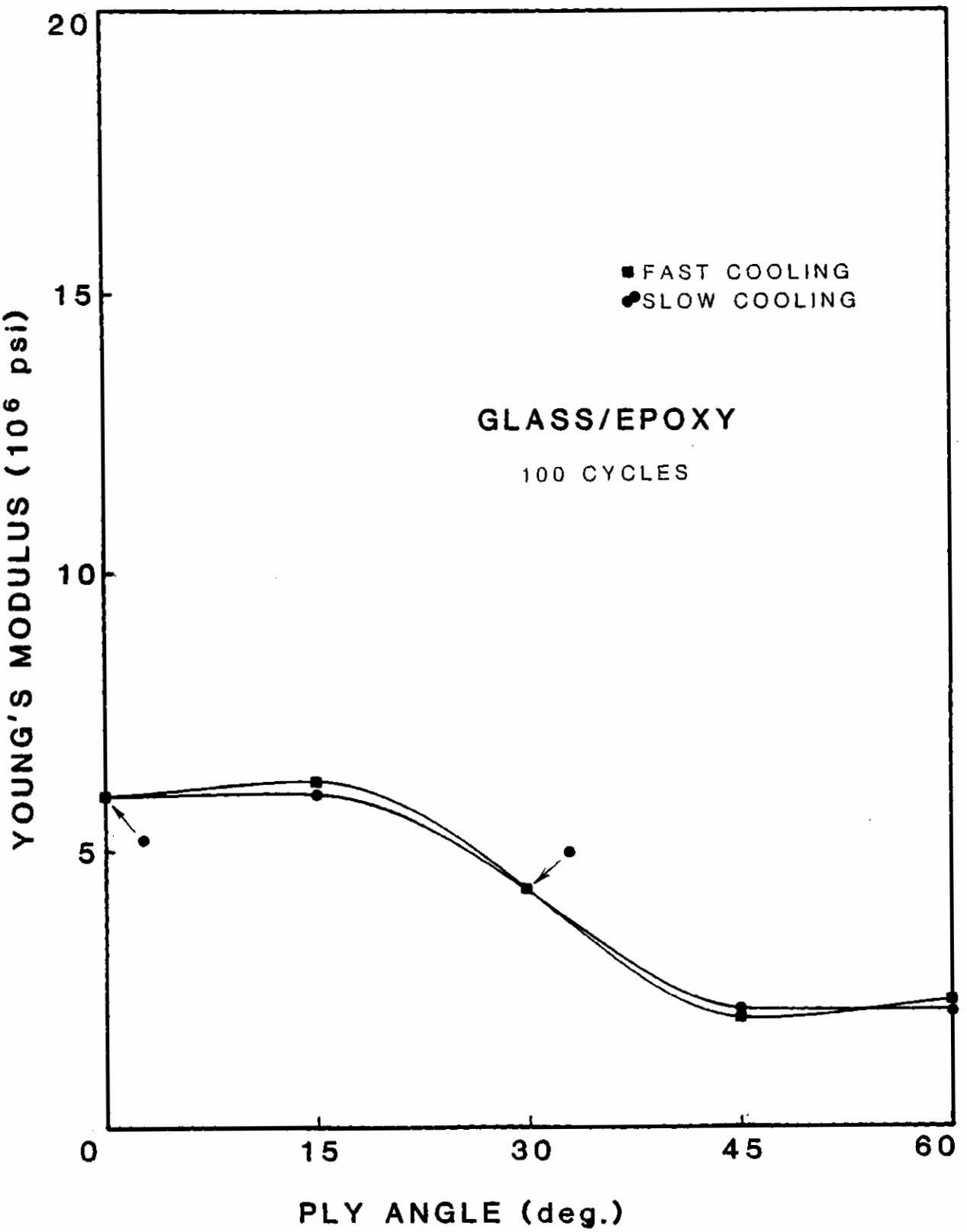

Figure 9. Young's Modulus vs. Ply Angle after 100 cycles for E-Glass/Rigidite 5216 Epoxy.

TABLE 10. YOUNG'S MODULUS VS. PLY ANGLE AFTER 150 CYCLES FOR T300 GRAPHITE/RIGIDITE 5209 EPOXY

PLY ANGLE	YOUNG'S MODULUS (MSI)	
(DEGREES)	FAST	SLOW
0	17.32	18.62
15	15.45	16.77
30	5.53	7.39
45	2.43	2.26
60	1.41	1.83

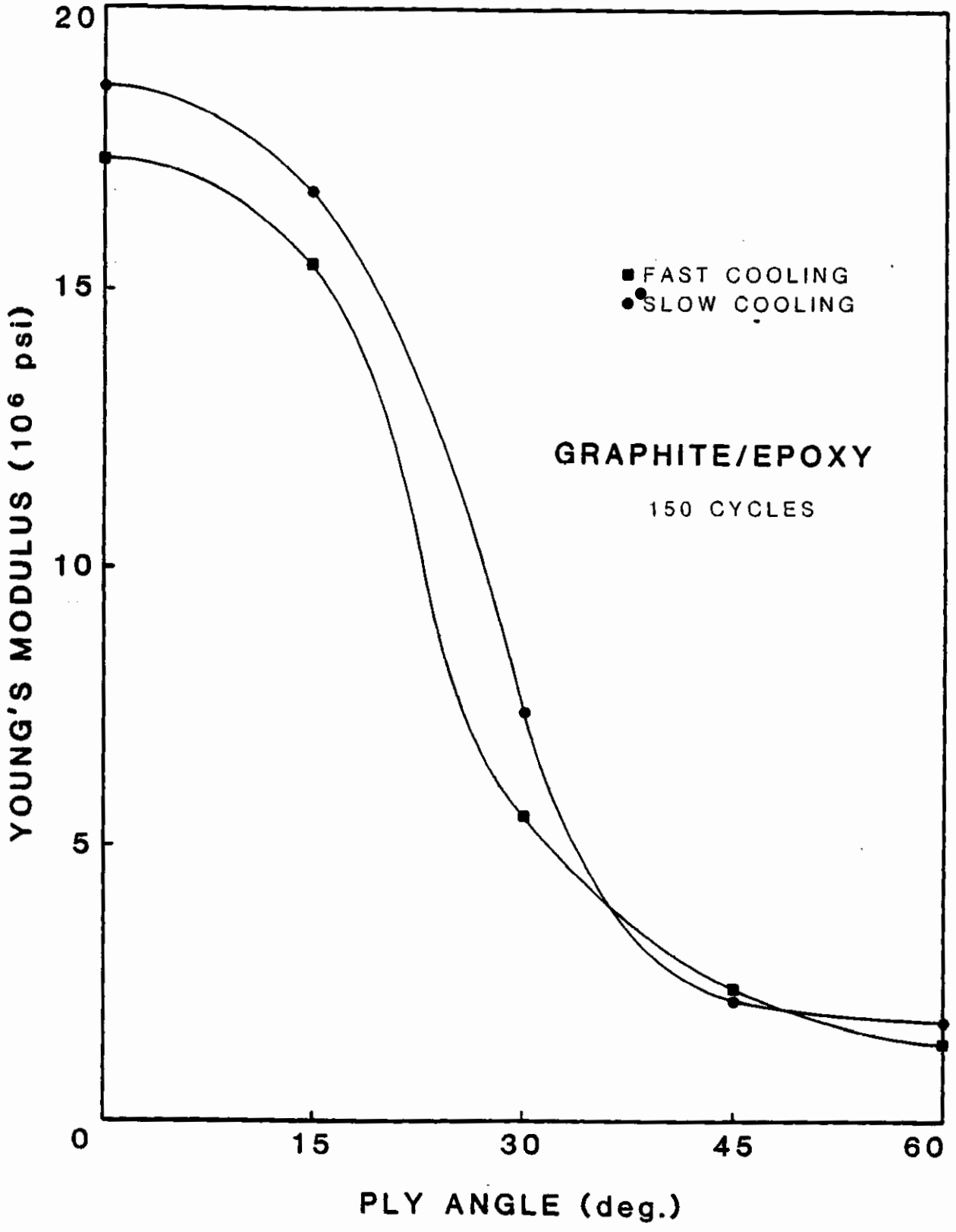

Figure 10. Young's Modulus vs. Ply Angle after 150 cycles for T300 Graphite/Rigidite 5209 Epoxy.

TABLE 11. YOUNG'S MODULUS VS. PLY ANGLE AFTER 150 CYCLES FOR KEVLAR 49C/RIGIDITE 5216 EPOXY

PLY ANGLE	YOUNG'S MODULUS (MSI)	
(DEGREES)	FAST	SLOW
0	10.40	9.45
15	7.99	8.24
30	2.98	3.08
45	0.98	0.90
60	0.67	0.71

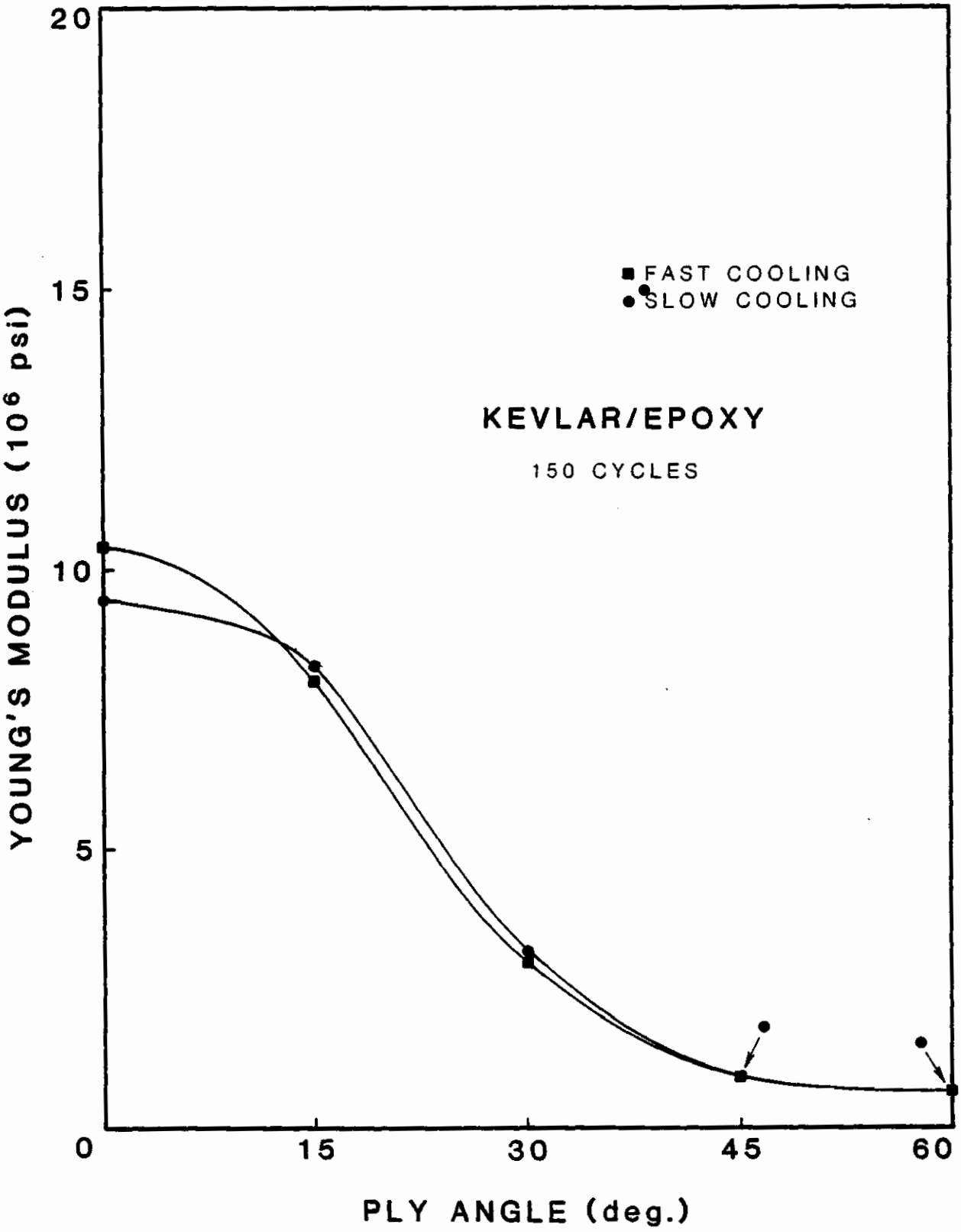

Figure 11. Young's Modulus vs. Ply Angle after 150 cycles for Kevlar 49C/Rigidite 5216 Epoxy.

TABLE 12. YOUNG'S MODULUS VS. PLY ANGLE AFTER 150 CYCLES FOR E-GLASS/RIGIDITE 5216 EPOXY

PLY ANGLE (DEGREES)	YOUNG'S MODULUS (MSI) FAST	SLOW
0	6.00	5.82
15	6.07	6.15
30	4.23	4.78
45	1.94	2.00
60	2.35	2.15

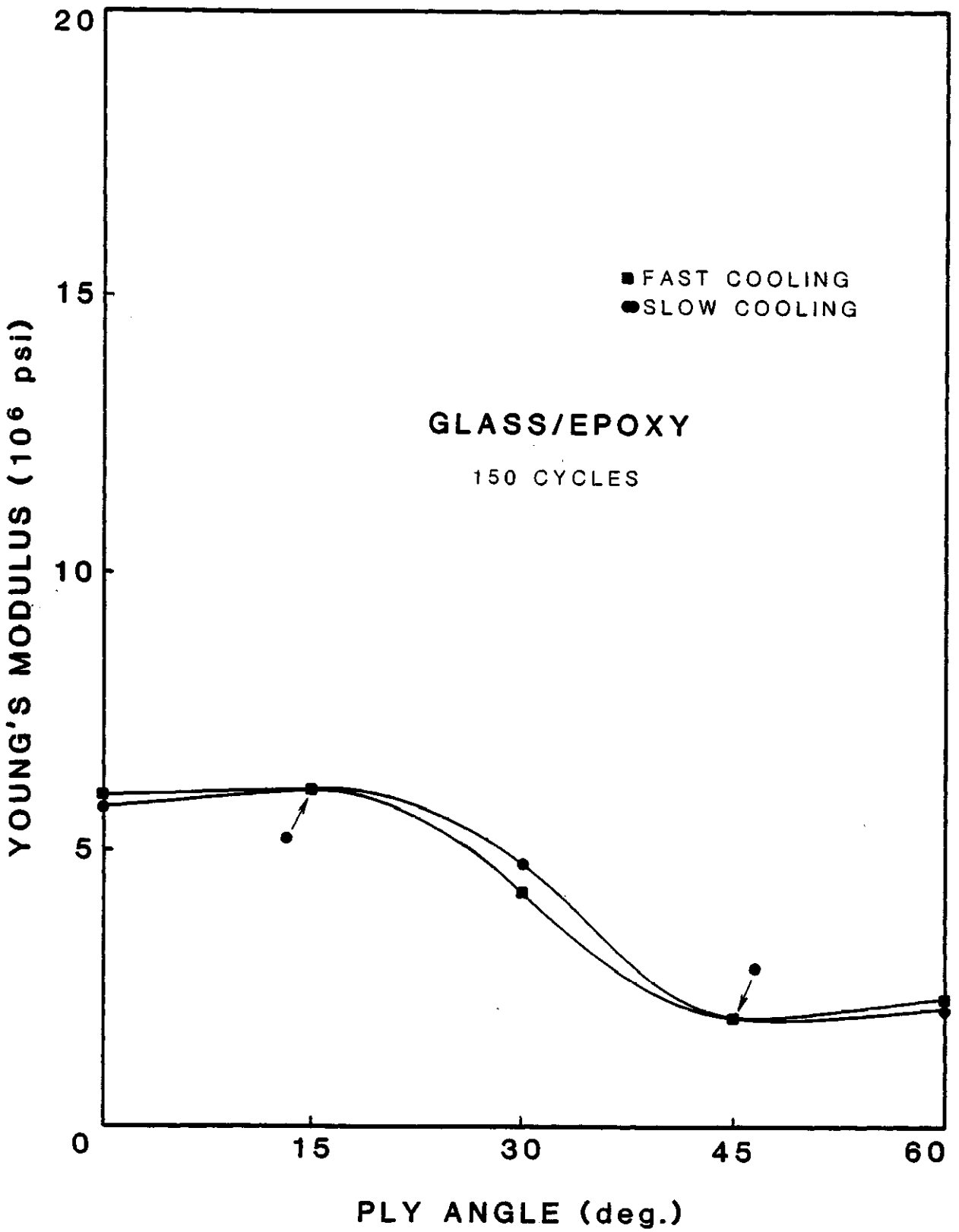

Figure 12. Young's Modulus vs. Ply Angle after 150 cycles for E-Glass/Rigidite 5216 Epoxy.

TABLE 13. YOUNG'S MODULUS VS. NUMBER OF CYCLES FOR UNIDIRECTIONAL T300 GRAPHITE/RIGIDITE 5209 EPOXY

NUMBER OF CYCLES	YOUNG'S MODULUS (MSI) FAST	SLOW
0	18.08	17.58
50	16.49	17.16
100	16.72	17.49
150	17.32	18.62

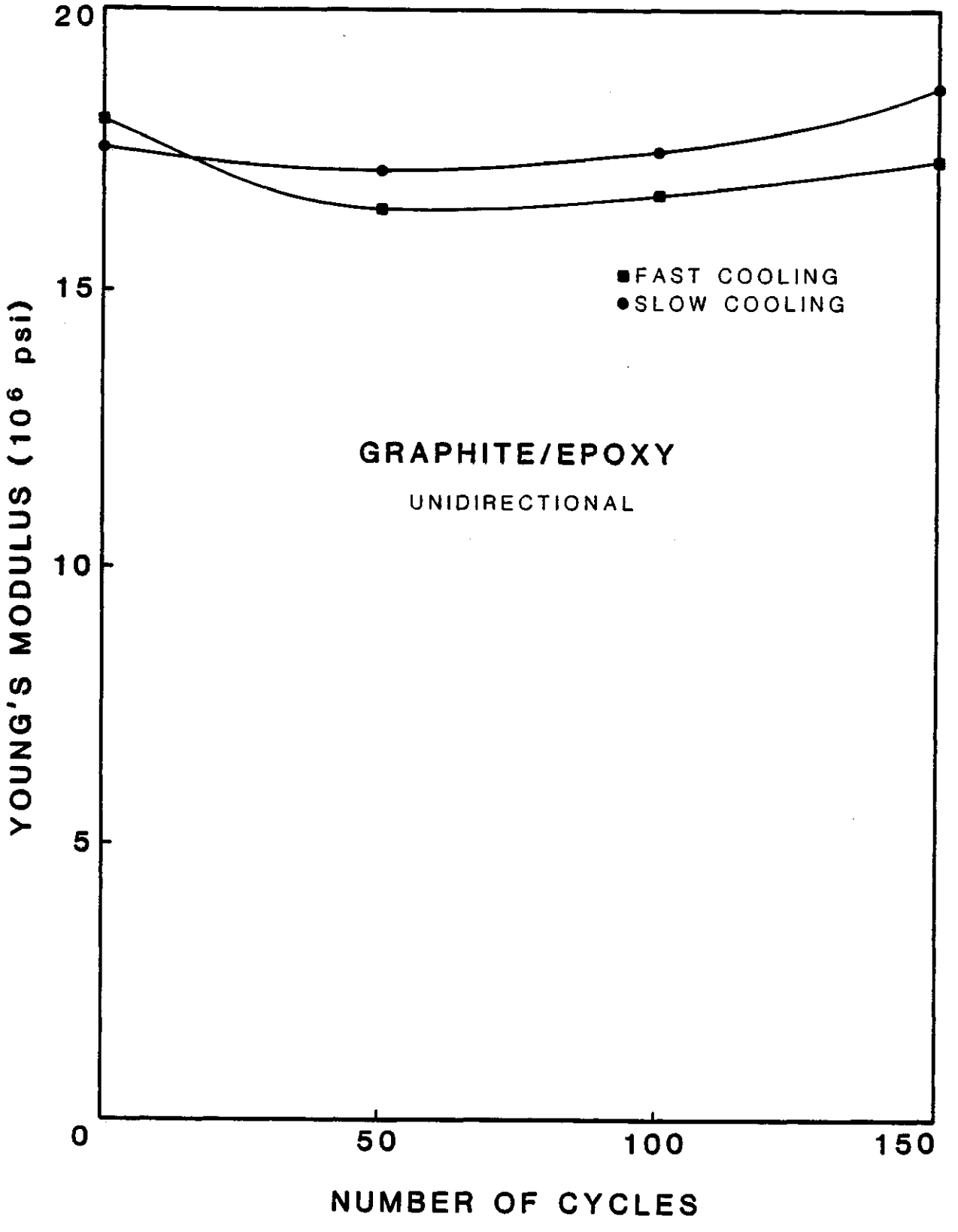

Figure 13. Young's Modulus vs. number of cycles for unidirectional T300 Graphite/Rigidite 5209 Epoxy.

TABLE 14. YOUNG'S MODULUS VS. NUMBER OF CYCLES FOR UNIDIRECTIONAL KEVLAR 49C/RIGIDITE 5216 EPOXY

NUMBER OF CYCLES	YOUNG'S MODULUS (MSI)	
	FAST	SLOW
0	10.16	10.31
50	10.13	9.80
100	10.10	9.46
150	10.40	9.45

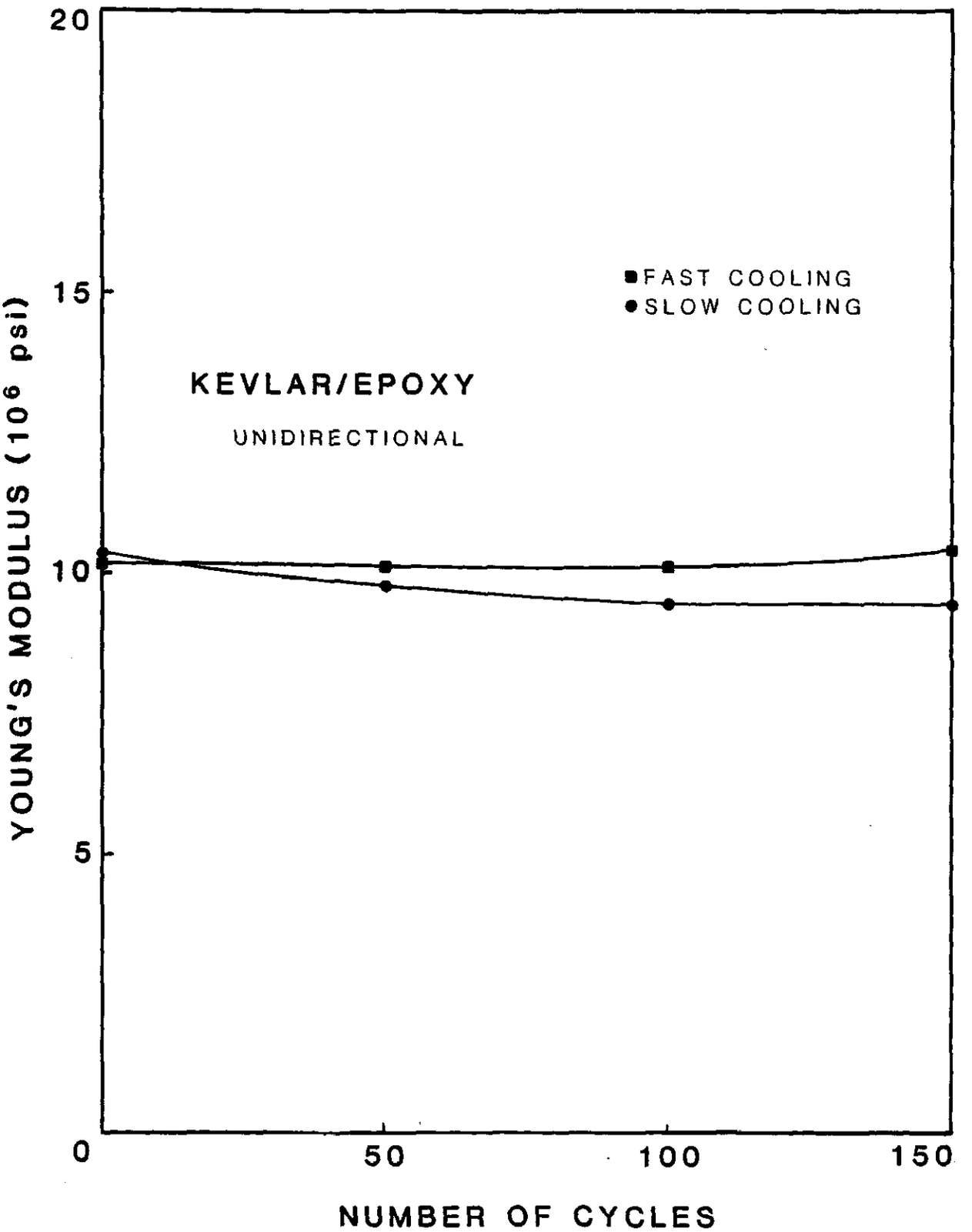

Figure 14. Young's Modulus vs. number of cycles for unidirectional Kevlar 49C/Rigidite 5216 Epoxy.

TABLE 15. YOUNG'S MODULUS VS. NUMBER OF CYCLES FOR UNIDIRECTIONAL E-GLASS/RIGIDITE 5216 EPOXY

NUMBER OF CYCLES	YOUNG'S MODULUS (MSI) FAST	SLOW
0	6.27	6.20
50	6.22	6.02
150	6.00	5.82

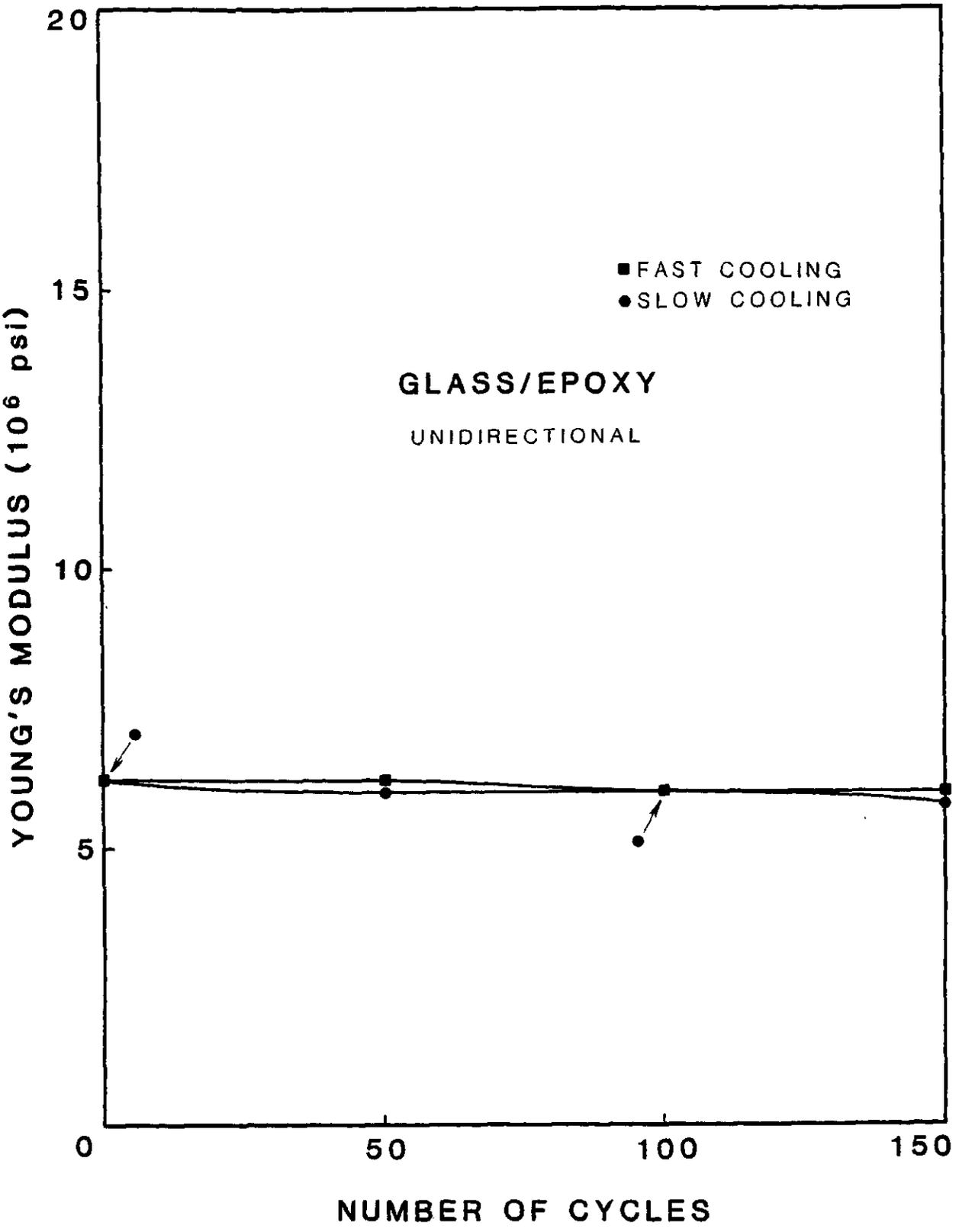

Figure 15. Young's Modulus vs. number of cycles for unidirectional E-Glass/Rigidite 5216 Epoxy.

TABLE 16. YOUNG'S MODULUS VS. NUMBER OF CYCLES FOR CROSS-PLY T300 GRAPHITE/RIGIDITE 5209 EPOXY

NUMBER OF CYCLES	YOUNG'S MODULUS (MSI)	
	FAST	SLOW
0	9.40	8.99
50	8.98	8.61
100	9.15	9.31
150	9.31	8.84

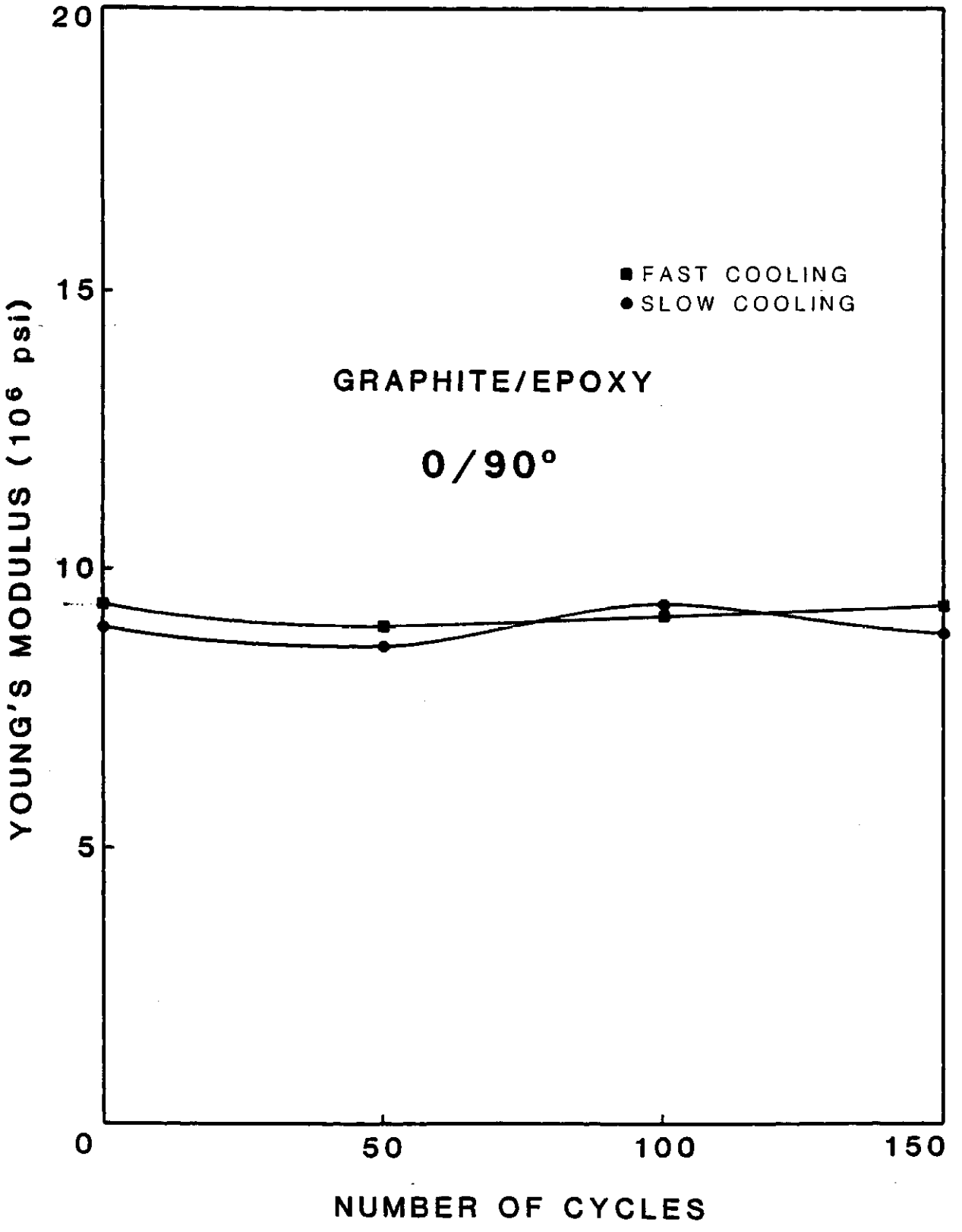

Figure 16. Young's Modulus vs. number of cycles for cross-ply T300 Graphite/Rigidite 5209 Epoxy.

TABLE 17. YOUNG'S MODULUS VS. NUMBER OF CYCLES FOR CROSS-PLY KEVLAR 49C/RIGIDITE 5216 EPOXY

NUMBER OF CYCLES	YOUNG'S MODULUS (MSI) FAST	SLOW
0	5.42	5.03
50	4.99	4.77
100	4.99	4.83
150	5.15	4.64

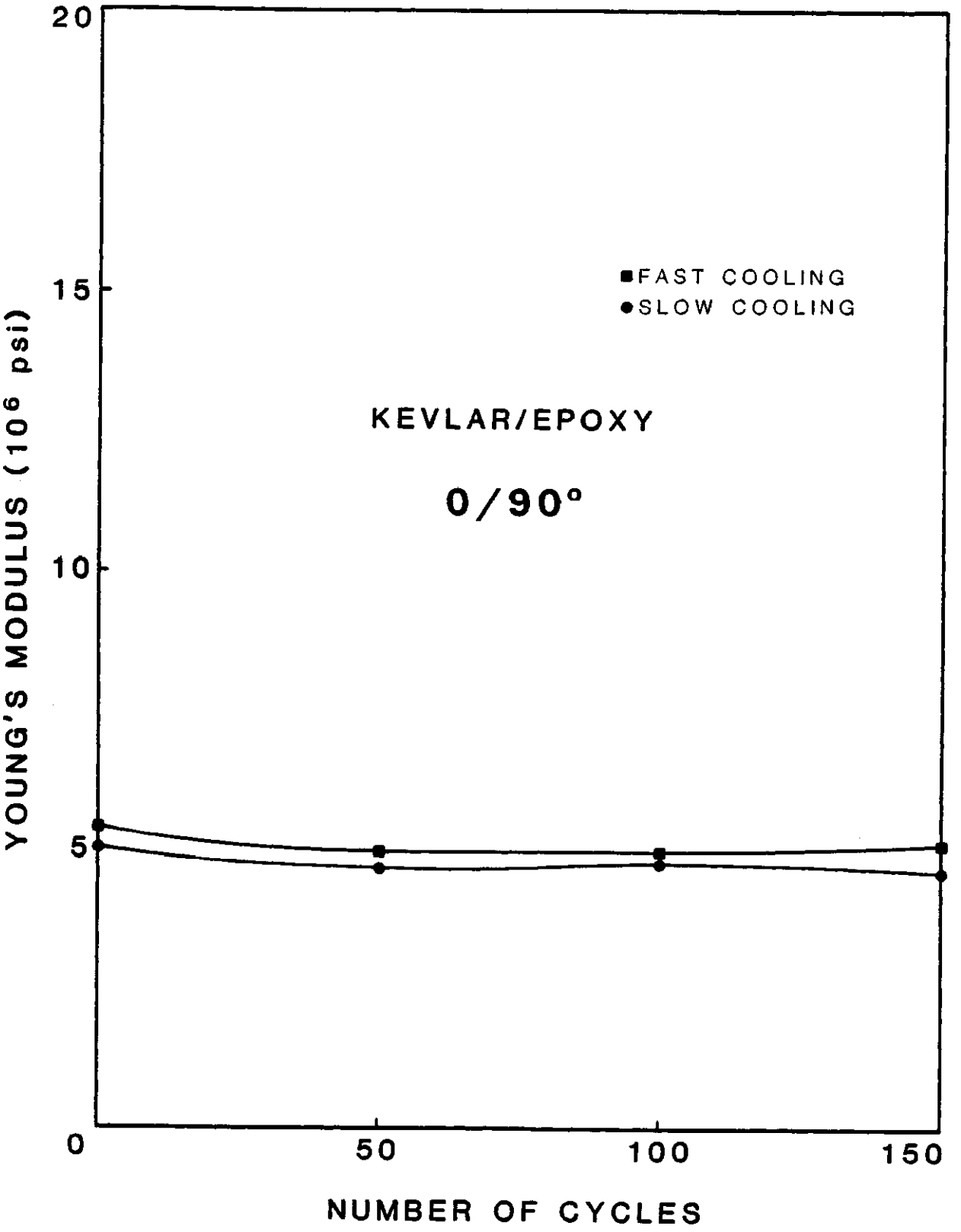

Figure 17. Young's Modulus vs. number of cycles for cross-ply Kevlar 49C/Rigidite 5216 Epoxy.

TABLE 18. YOUNG'S MODULUS VS. NUMBER OF CYCLES FOR CROSS-PLY E-GLASS/RIGIDITE 5216 EPOXY

NUMBER OF CYCLES	YOUNG'S MODULUS (MSI) FAST	SLOW
0	4.30	4.94
50	4.37	4.88
100	4.28	4.80
150	3.75	4.44

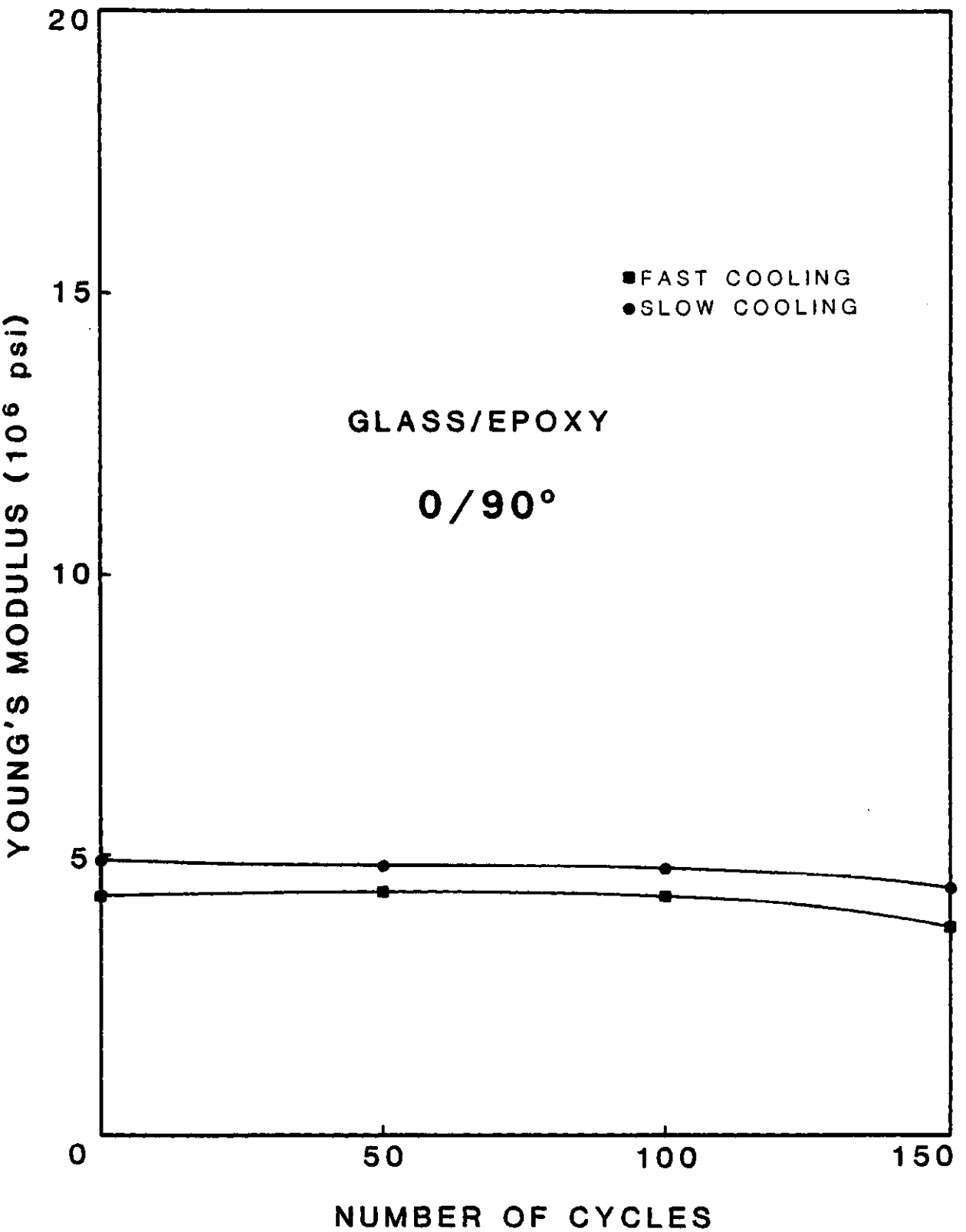

Figure 18. Young's Modulus vs. number of cycles for cross-ply E-Glass/Rigidite 5216 Epoxy.

TABLE 19. YOUNG'S MODULUS VS. NUMBER OF CYCLES FOR 15 DEGREES T300 GRAPHITE/RIGIDITE 5209 EPOXY

NUMBER OF CYCLES	YOUNG'S MODULUS (MSI)	
	FAST	SLOW
0	16.20	16.03
50	16.04	15.29
100	17.44	15.18
150	15.45	16.77

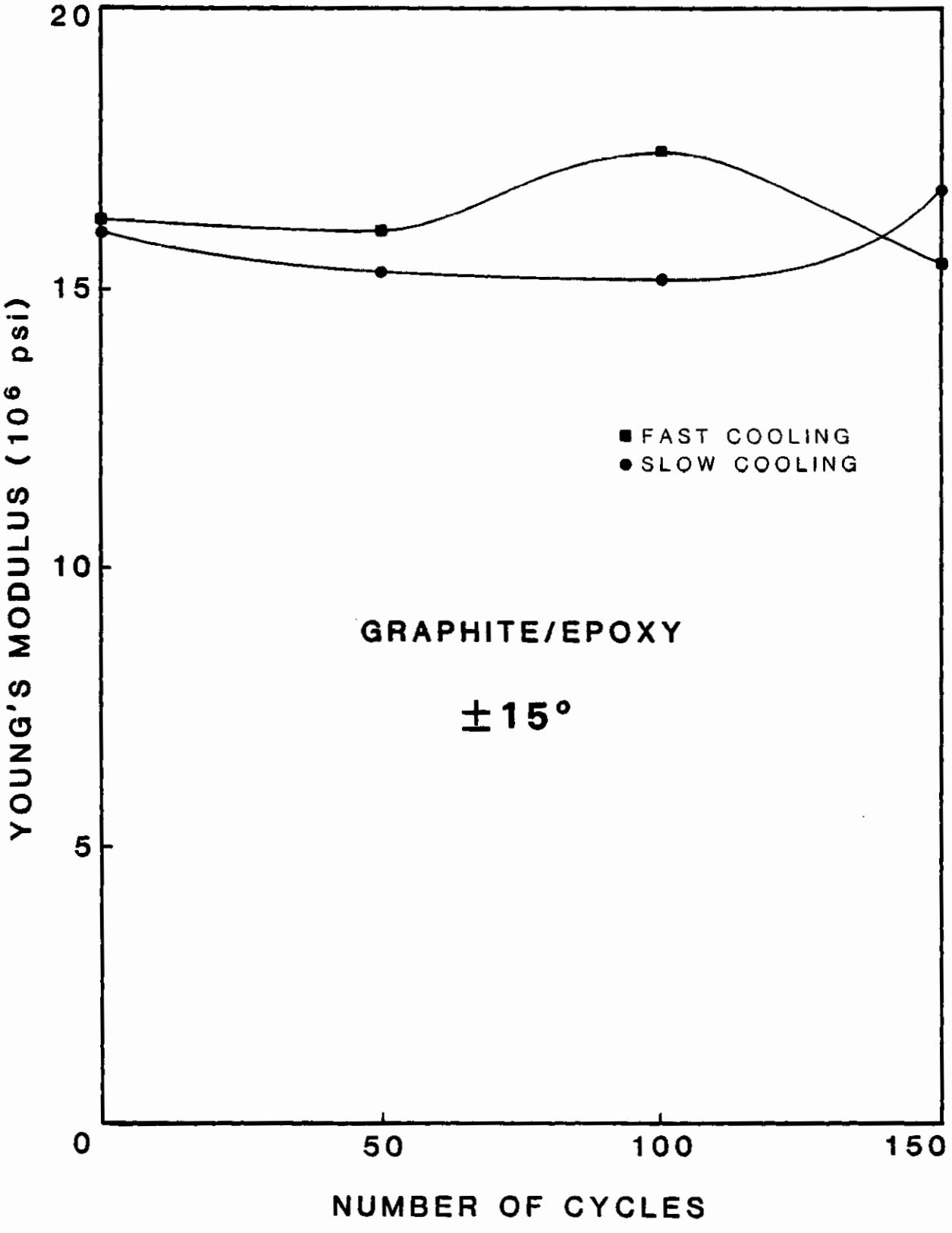

Figure 19. Young's Modulus vs. number of cycles for 15^{o} T300 Graphite/Rigidite 5209 Epoxy.

TABLE 20. YOUNG'S MODULUS VS. NUMBER OF CYCLES FOR 15 DEGREE KEVLAR 49C/RIGIDITE 5216 EPOXY

NUMBER OF CYCLES	YOUNG'S MODULUS (MSI) FAST	SLOW
0	8.43	8.23
50	7.94	7.45
100	7.85	7.86
150	7.99	8.24

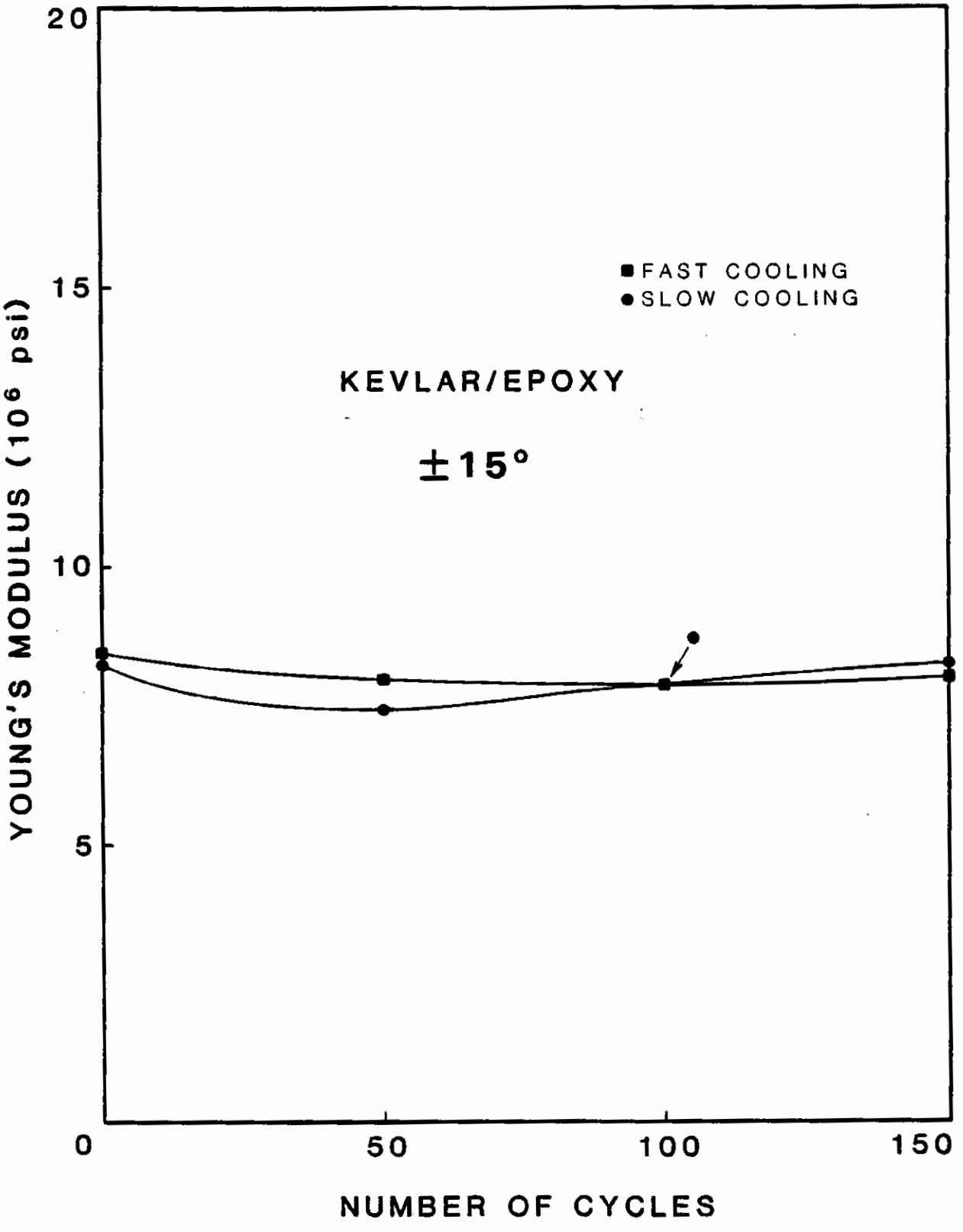

Figure 20. Young's Modulus vs. number of cycles for 15° Kevlar 49C/Rigidite 5216 Epoxy.

TABLE 21. YOUNG'S MODULUS VS. NUMBER OF CYCLES FOR 15 DEGREE E-GLASS/RIGIDITE 5216 EPOXY

NUMBER OF CYCLES	YOUNG'S MODULUS (MSI) FAST	SLOW
0	6.45	6.54
50	6.35	6.24
100	6.26	6.08
150	6.07	6.15

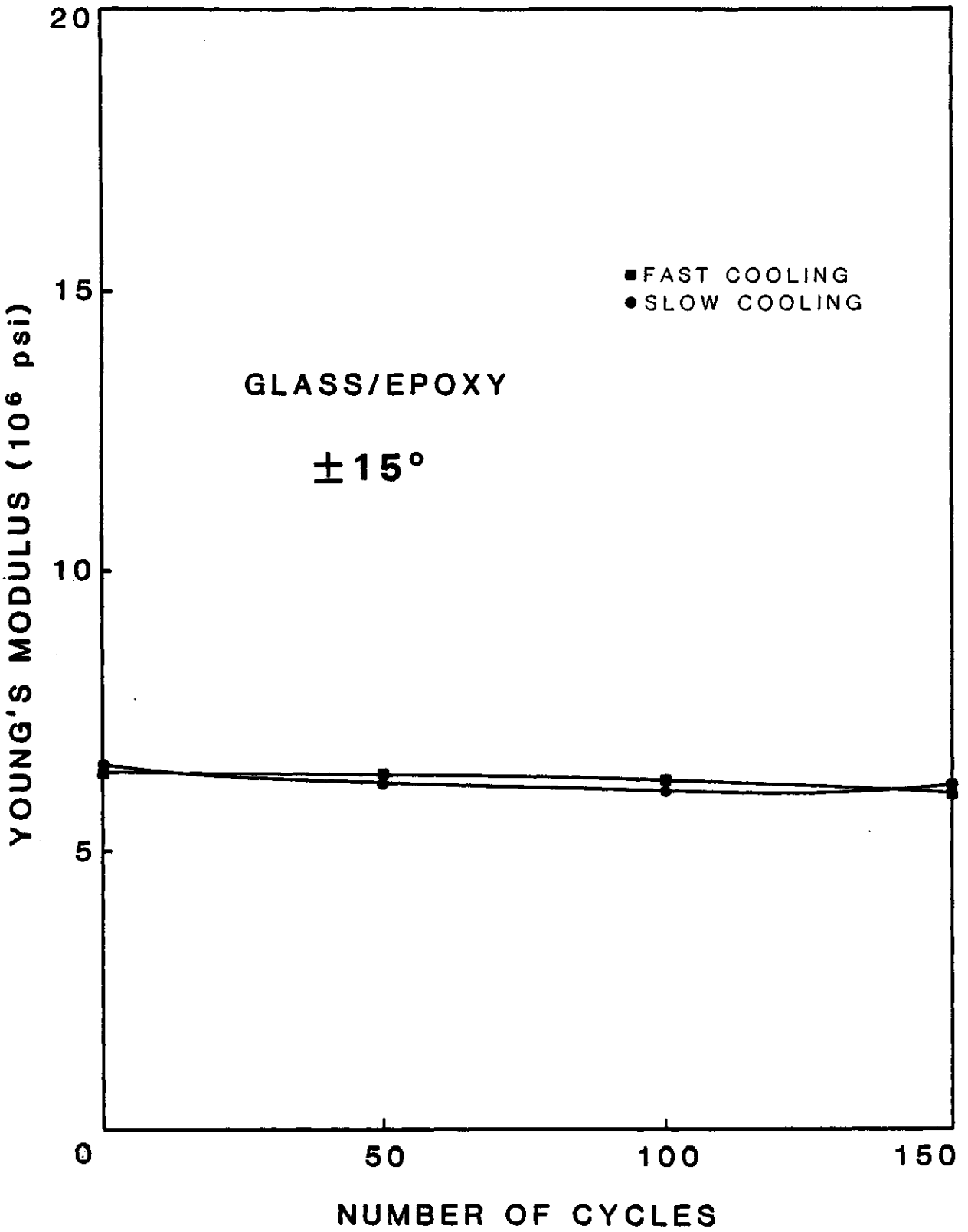

Figure 21. Young's Modulus vs. number of cycles for 15^{0} E-Glass/Rigidite 5216 Epoxy.

TABLE 22. YOUNG'S MODULUS VS. NUMBER OF CYCLES FOR 30 DEGREE T300 GRAPHITE/RIGIDITE 5209 EPOXY

NUMBER OF CYCLES	YOUNG'S MODULUS (MSI)	
	FAST	SLOW
0	6.13	7.12
50	5.75	6.46
100	5.49	7.85
150	5.53	7.39

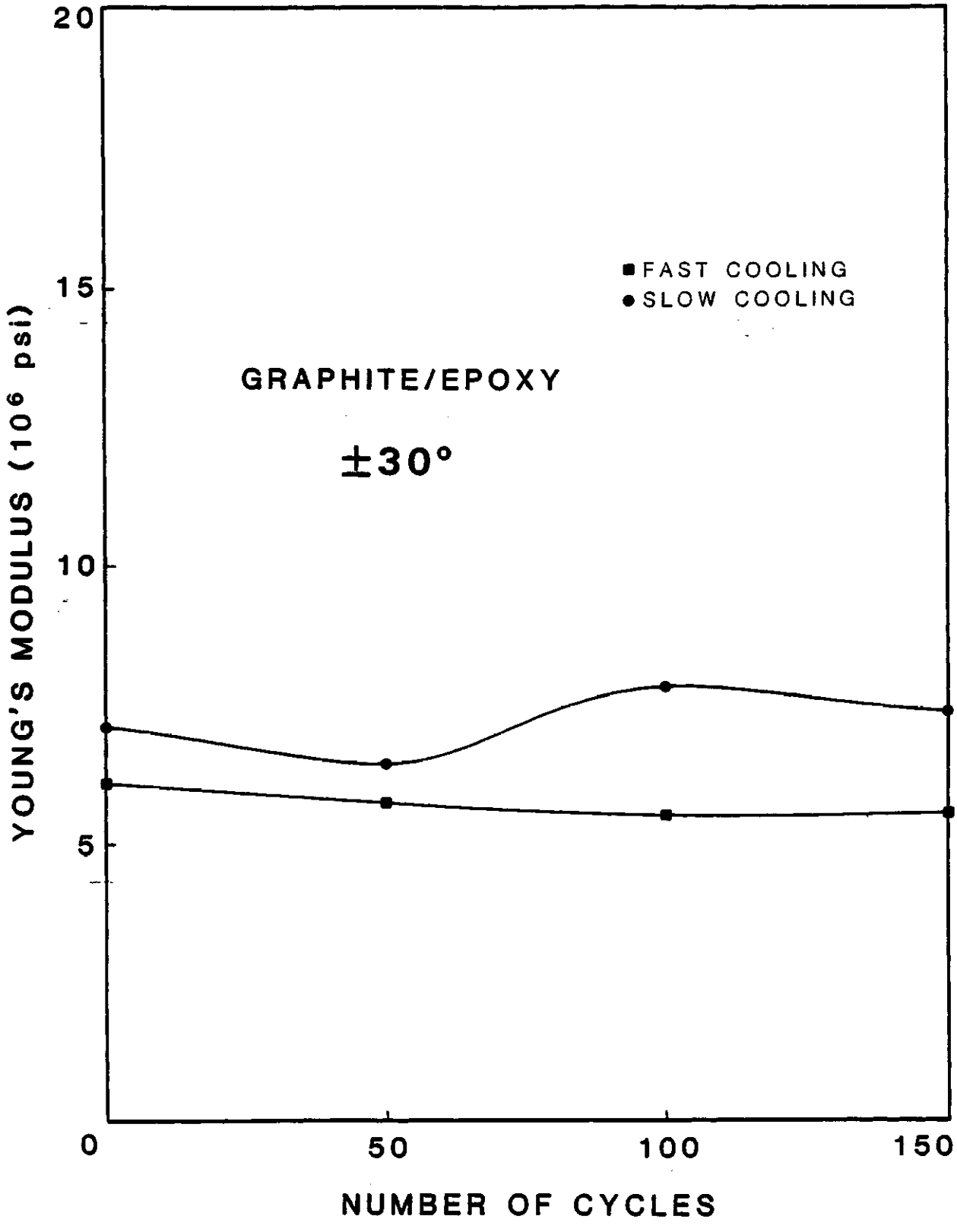

Figure 22. Young's Modulus vs. number of cycles for 30^{o} T300 Graphite/Rigidite 5209 Epoxy.

TABLE 23. YOUNG'S MODULUS VS. NUMBER OF CYCLES FOR 30 DEGREE KEVLAR 49C/RIGIDITE 5216 EPOXY

NUMBER OF CYCLES	YOUNG'S MODULUS (MSI)	
	FAST	SLOW
0	3.27	3.07
50	2.90	2.86
100	2.82	3.50
150	2.98	3.08

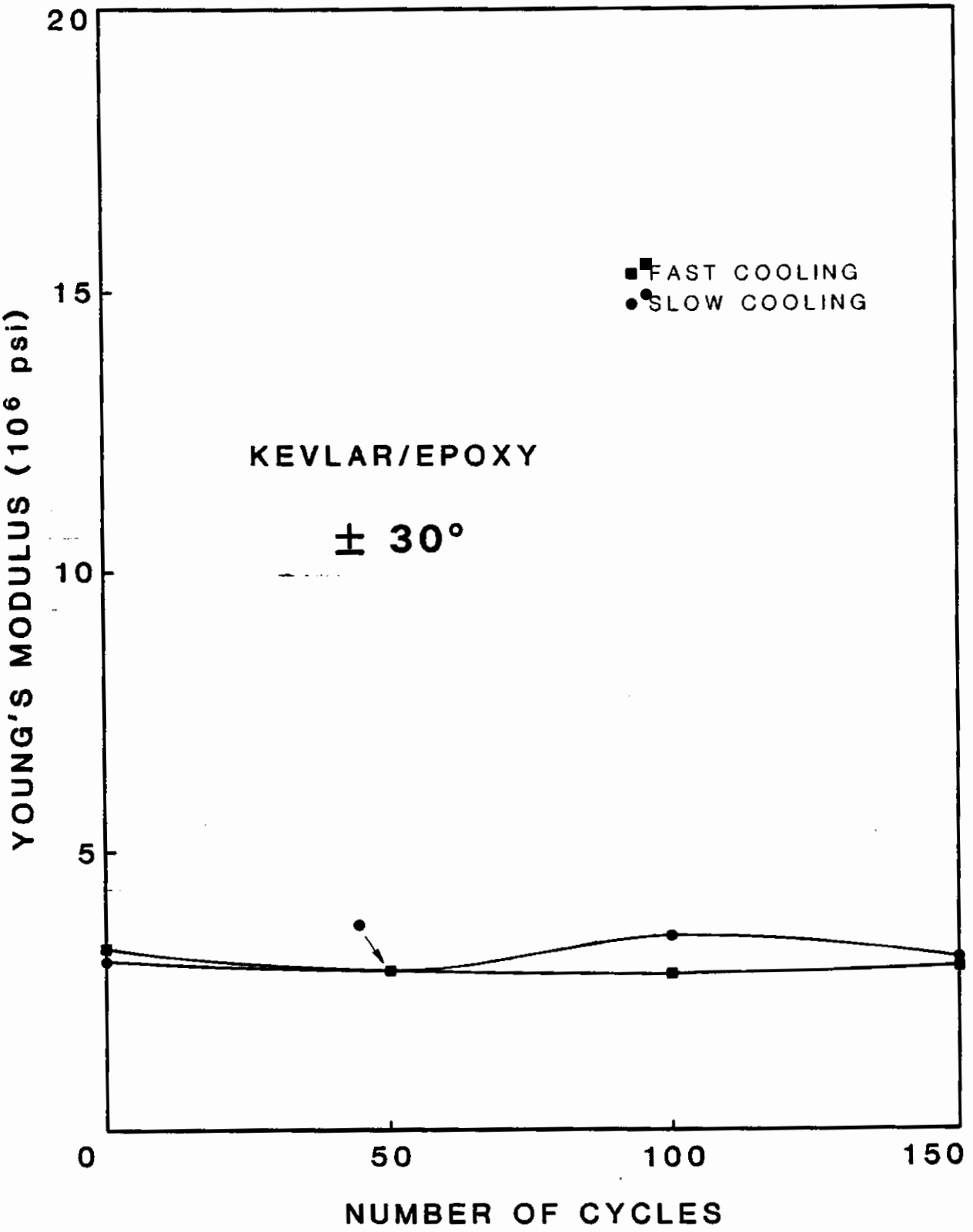

Figure 23. Young's Modulus vs. number of cycles for 30^{o} Kevlar 49C/Rigidite 5216 Epoxy.

TABLE 24. YOUNG'S MODULUS VS. NUMBER OF CYCLES FOR 30 DEGREE E-GLASS/RIGIDITE 5216 EPOXY

NUMBER OF CYCLES	YOUNG'S MODULUS (MSI) FAST	SLOW
0	4.90	4.85
50	4.43	4.63
100	4.41	4.63
150	4.23	**.**

. Invalid data due to malfunctions of measurement devices.

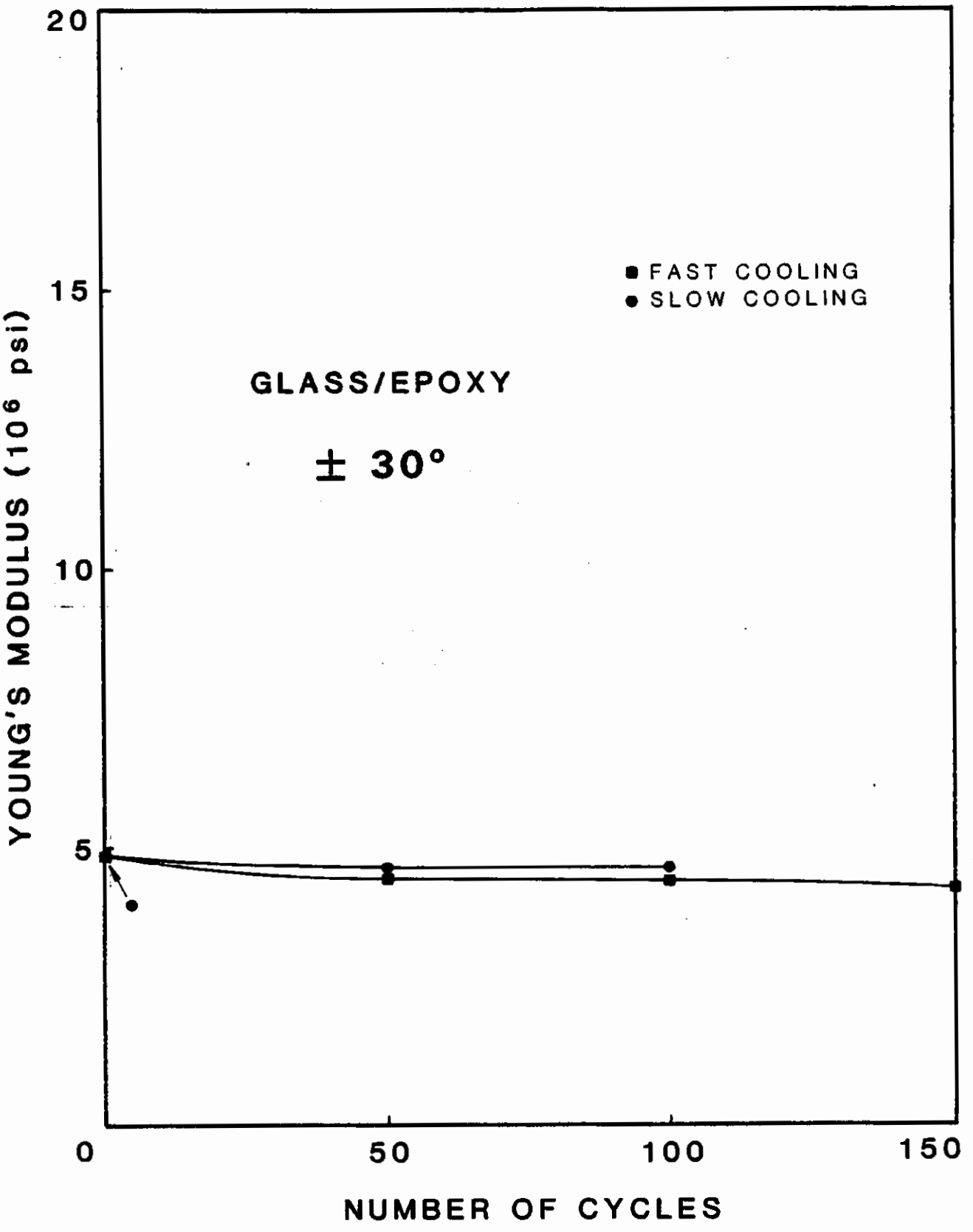

Figure 24. Young's Modulus vs. number of cycles for 30^{o} E-Glass/Rigidite 5216 Epoxy.

TABLE 25. YOUNG'S MODULUS VS. NUMBER OF CYCLES FOR 45 DEGREE T300 GRAPHITE/RIGIDITE 5209 EPOXY

NUMBER OF CYCLES	YOUNG'S MODULUS (MSI) FAST	SLOW
0	2.15	2.58
50	2.12	2.26
100	2.03	2.42
150	2.43	2.26

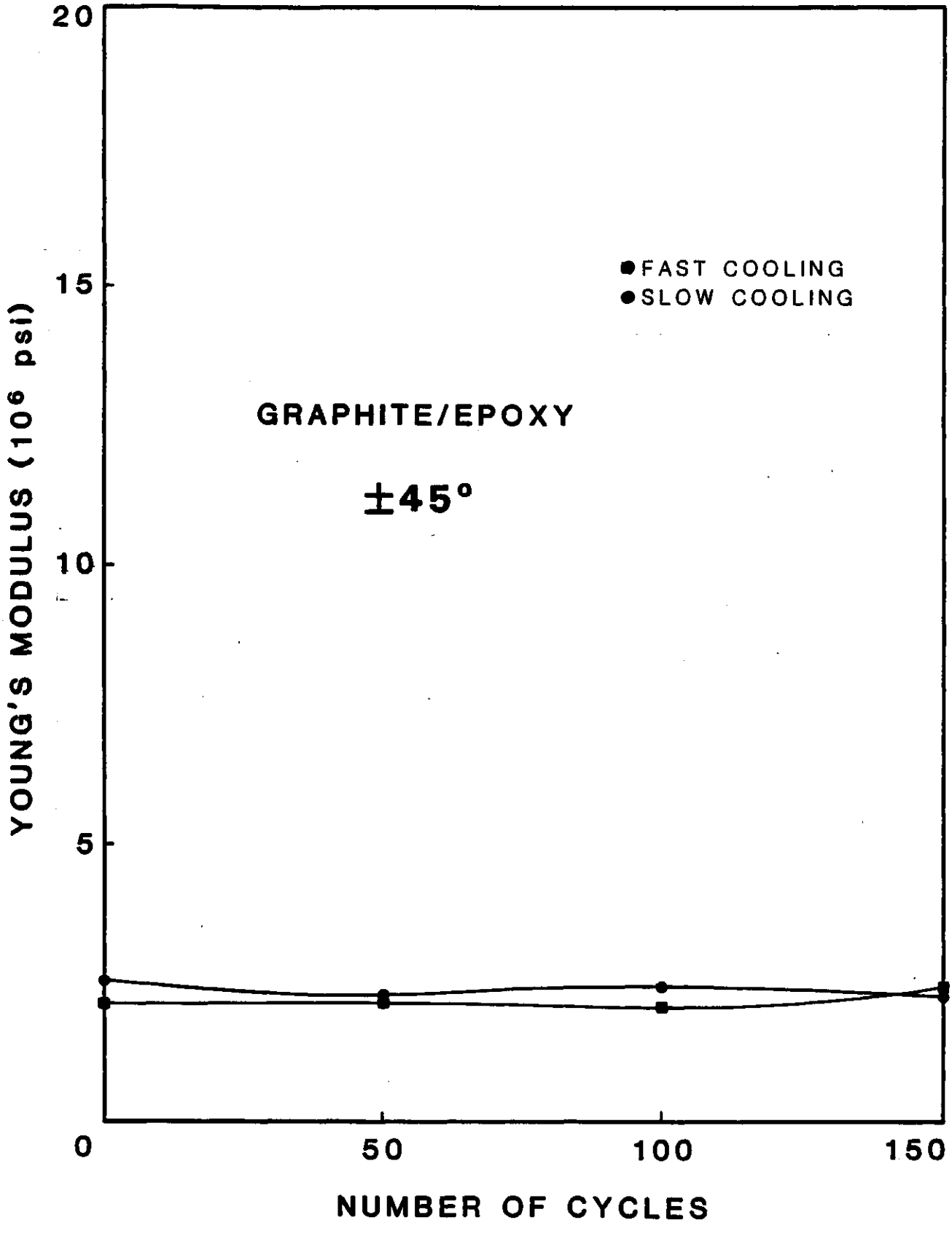

Figure 25. Young's Modulus vs. number of cycles for 45^{o} T300 Graphite/Rigidite 5209 Epoxy.

TABLE 26. YOUNG'S MODULUS VS. NUMBER OF CYCLES FOR 45 DEGREE KEVLAR 49C/RIGIDITE 5216 EPOXY

NUMBER OF CYCLES	YOUNG'S MODULUS (MSI) FAST	SLOW
0	1.05	1.16
50	0.97	1.00
100	0.93	1.04
150	0.98	0.90

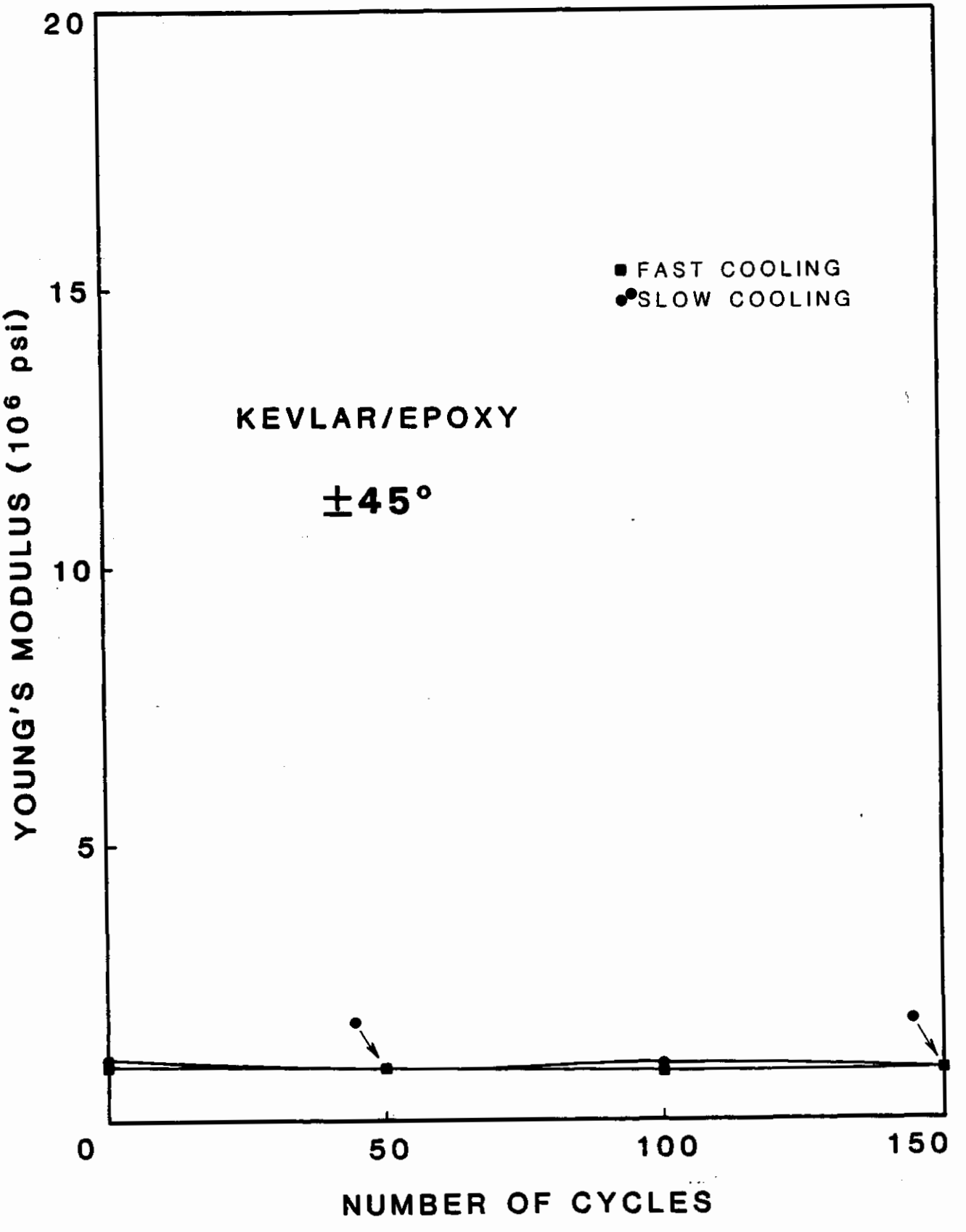

Figure 26. Young's Modulus vs. number of cycles for 45^{o} Kevlar 49C/Rigidite 5216 Epoxy.

TABLE 27. YOUNG'S MODULUS VS. NUMBER OF CYCLES FOR 45 DEGREE E-GLASS/RIGIDITE 5216 EPOXY

NUMBER OF CYCLES	YOUNG'S MODULUS (MSI) FAST	SLOW
0	2.22	2.35
50	2.06	2.14
100	2.08	2.19
10	1.94	2.00

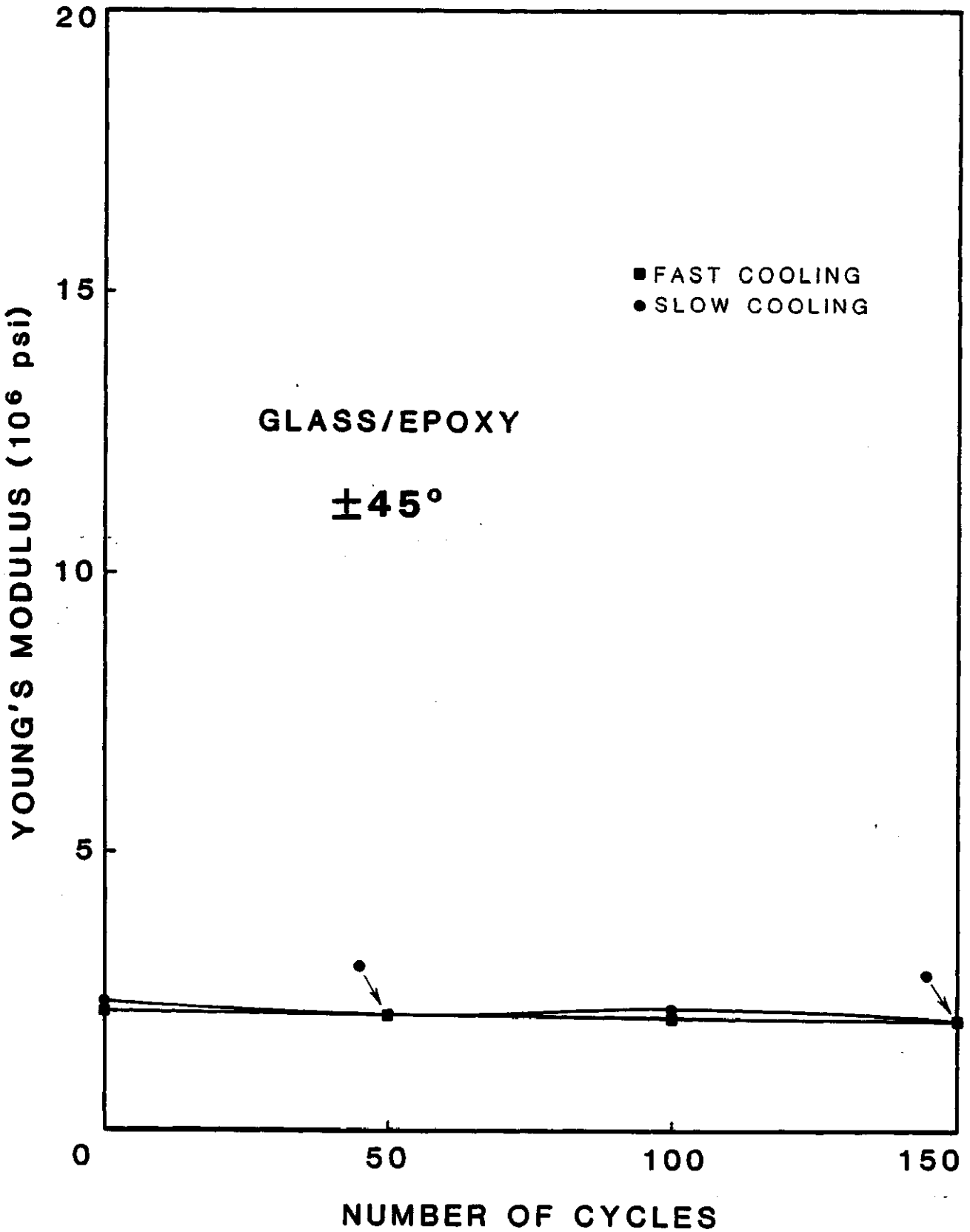

Figure 27. Young's Modulus vs. number of cycles for 45^{o} E-Glass/Rigidite 5216 Epoxy.

TABLE 28. YOUNG'S MODULUS VS. NUMBER OF CYCLES FOR 60 DEGREE T300 GRAPHITE/RIGIDITE 5209 EPOXY

NUMBER OF CYCLES	YOUNG'S MODULUS (MSI) FAST	SLOW
0	1.78	1.83
50	1.52	1.31
100	1.26	1.47
150	1.41	1.83

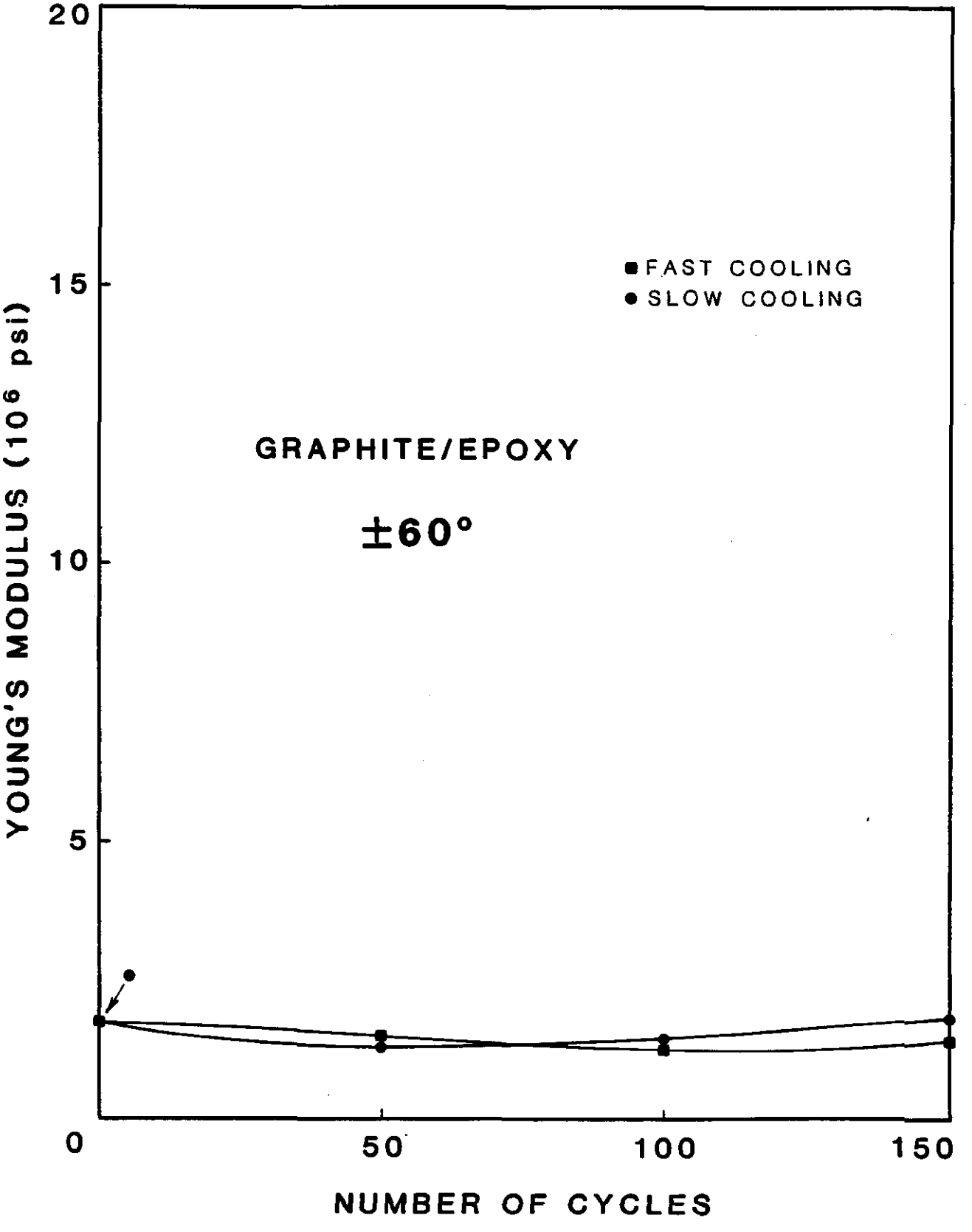

Figure 28. Young's Modulus vs. number of cycles for 60^{o} T300 Graphite/Rigidite 5209 Epoxy.

TABLE 29. YOUNG'S MODULUS VS. NUMBER OF CYCLES FOR 60 DEGREE KEVLAR 49C/RIGIDITE 5216 EPOXY

NUMBER OF CYCLES	YOUNG'S MODULUS (MSI) FAST	SLOW
0	0.78	0.77
50	0.68	0.72
100	0.66	1.12
150	0.67	0.71

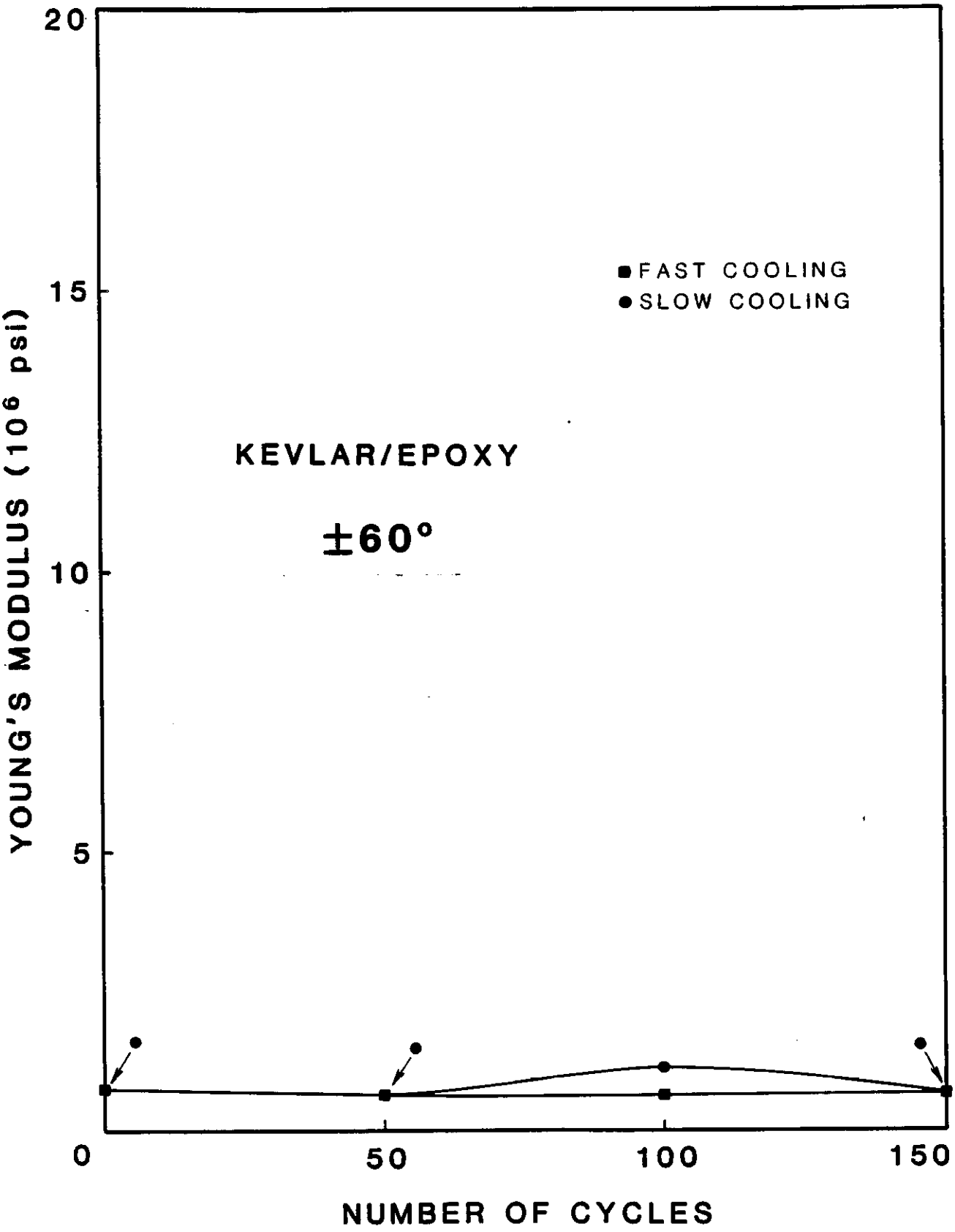

Figure 29. Young's Modulus vs. number of cycles for 60^{o} Kevlar 49C/Rigidite 5216 Epoxy.

TABLE 30. YOUNG'S MODULUS VS. NUMBER OF CYCLES FOR 60 DEGREE E-GLASS/RIGIDITE 5216 EPOXY

NUMBER OF CYCLES	YOUNG'S MODULUS (MSI) FAST	SLOW
0	3.20	2.73
50	2.24	2.43
100	2.30	2.19
150	2.35	2.15

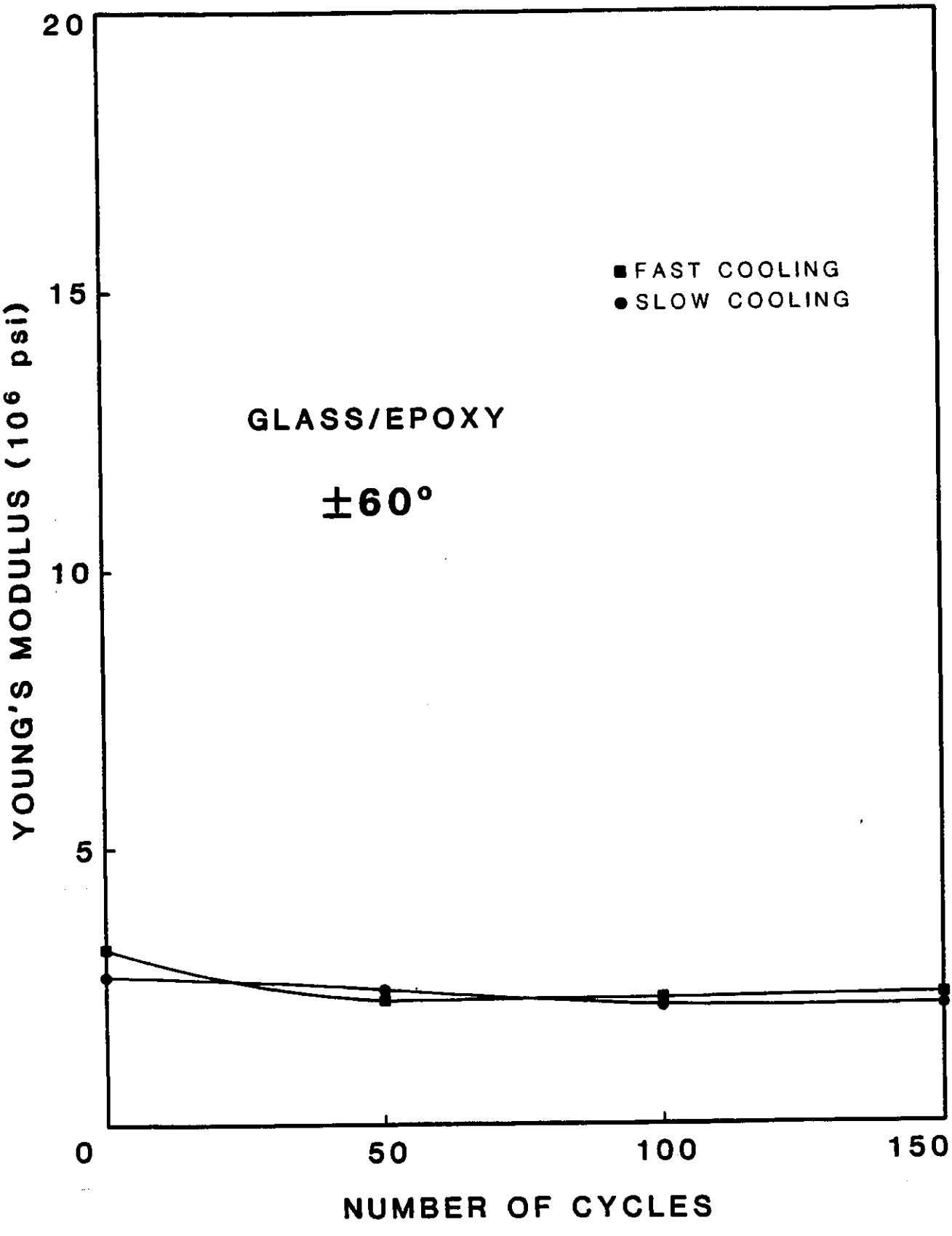

Figure 30. Young's Modulus vs. number of cycles for 60^{o} E-Glass/Rigidite 5216 Epoxy.

TABLE 31. YOUNG'S MODULUS VS. NUMBER OF CYCLES FOR 15 DEGREE T1 K-G-K HYBRID

NUMBER OF CYCLES	YOUNG'S MODULUS (MSI)	
	FAST	SLOW
0	7.73	7.38
50	7.02	7.10
100	7.02	6.77
150	6.97	7.33

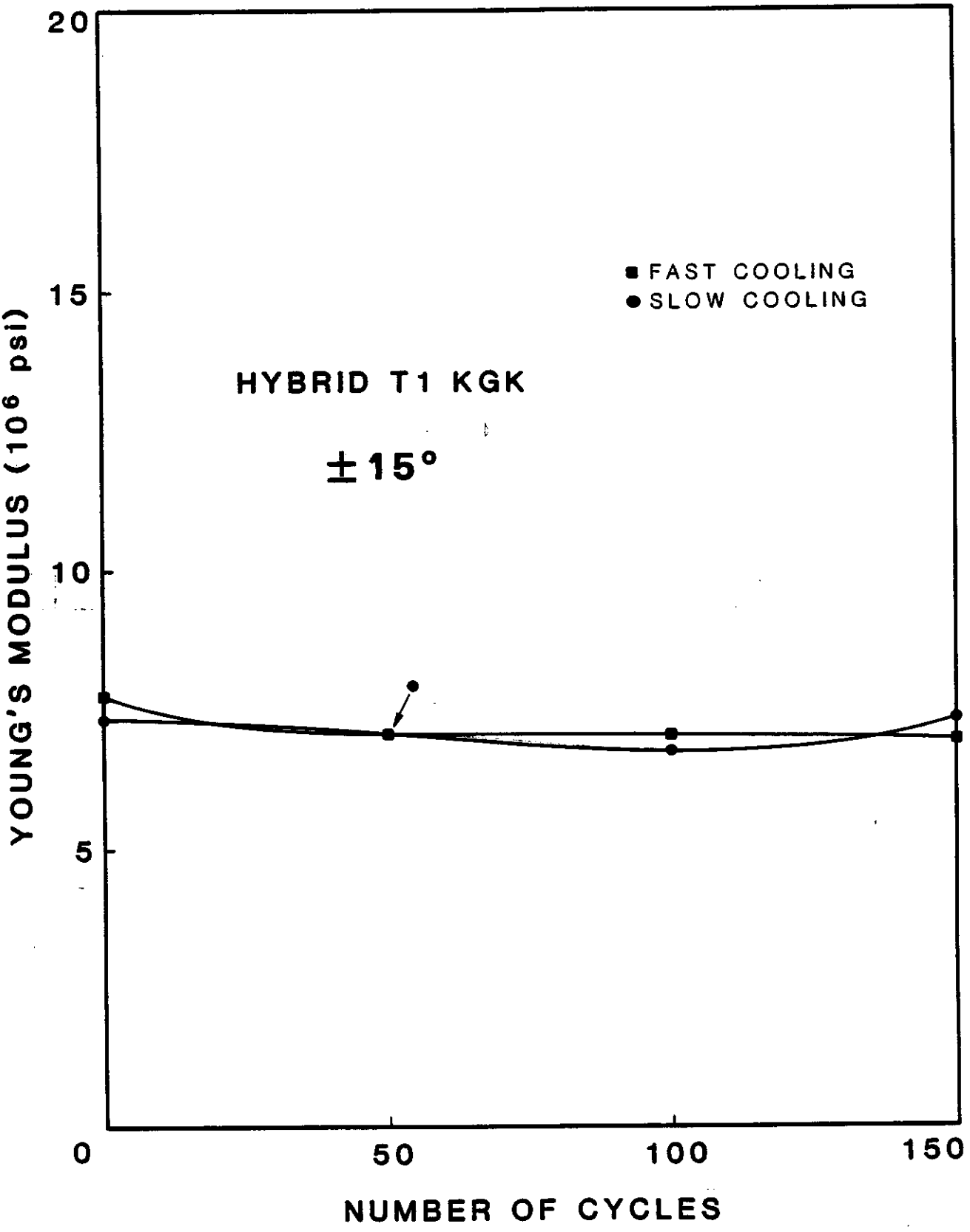

Figure 31. Young's Modulus vs. number of cycles for 15° T1 K-G-K Hybrid.

TABLE 32. YOUNG'S MODULUS VS. NUMBER OF CYCLES FOR 15 DEGREE T1 G-K-G HYBRID

NUMBER OF CYCLES	YOUNG'S MODULUS (MSI) FAST	SLOW
0	7.58	7.42
50	7.46	7.03
100	6.67	6.78
150	7.16	7.19

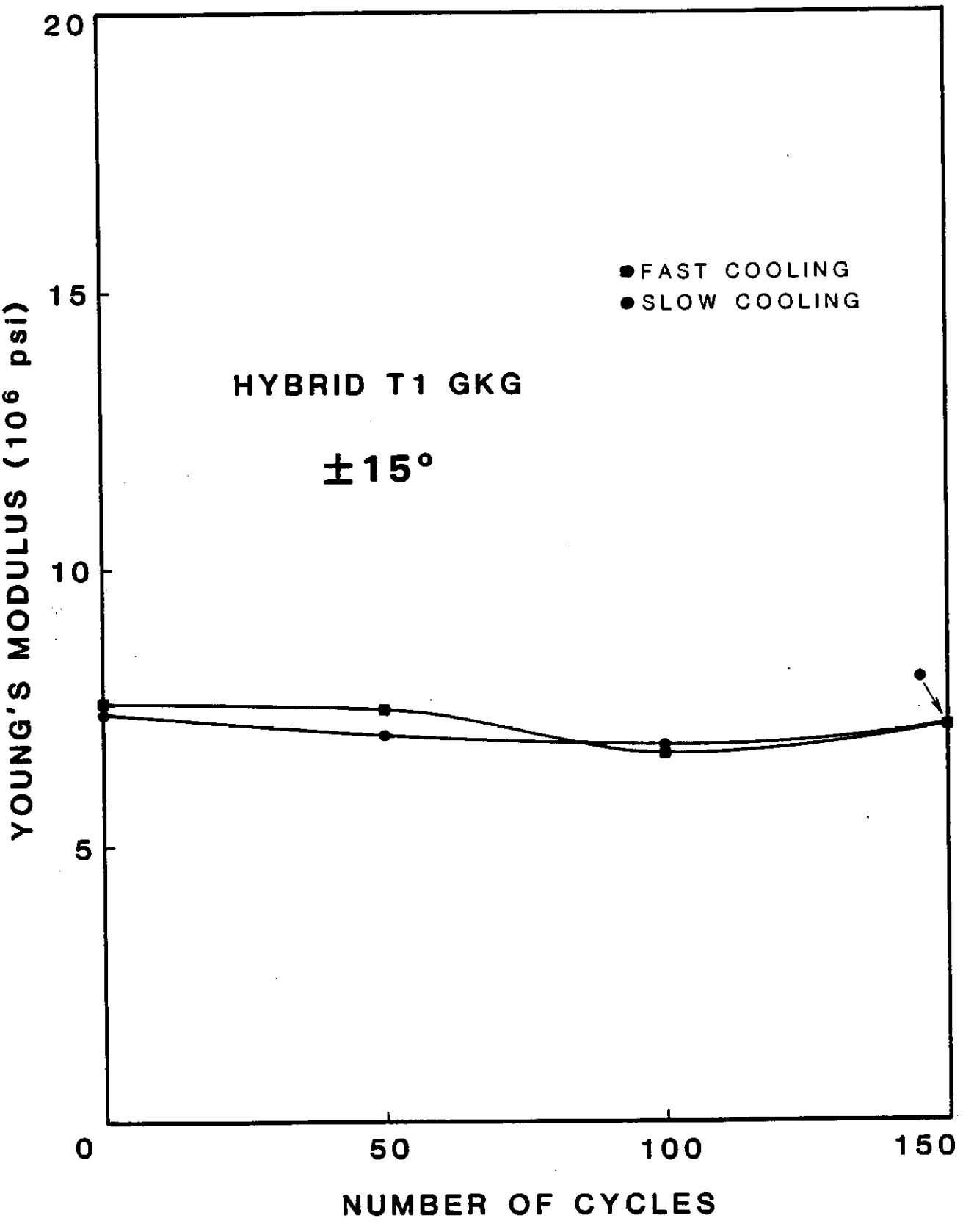

Figure 32. Young's Modulus vs. number of cycles for 15^{o} T1 G-K-G Hybrid.

TABLE 33. YOUNG'S MODULUS VS. NUMBER OF CYCLES FOR 15 DEGREE T2 HYBRID

NUMBER OF CYCLES	YOUNG'S MODULUS (MSI) FAST	SLOW
0	7.42	7.58
50	7.08	7.10
100	6.85	6.55
150	6.75	7.11

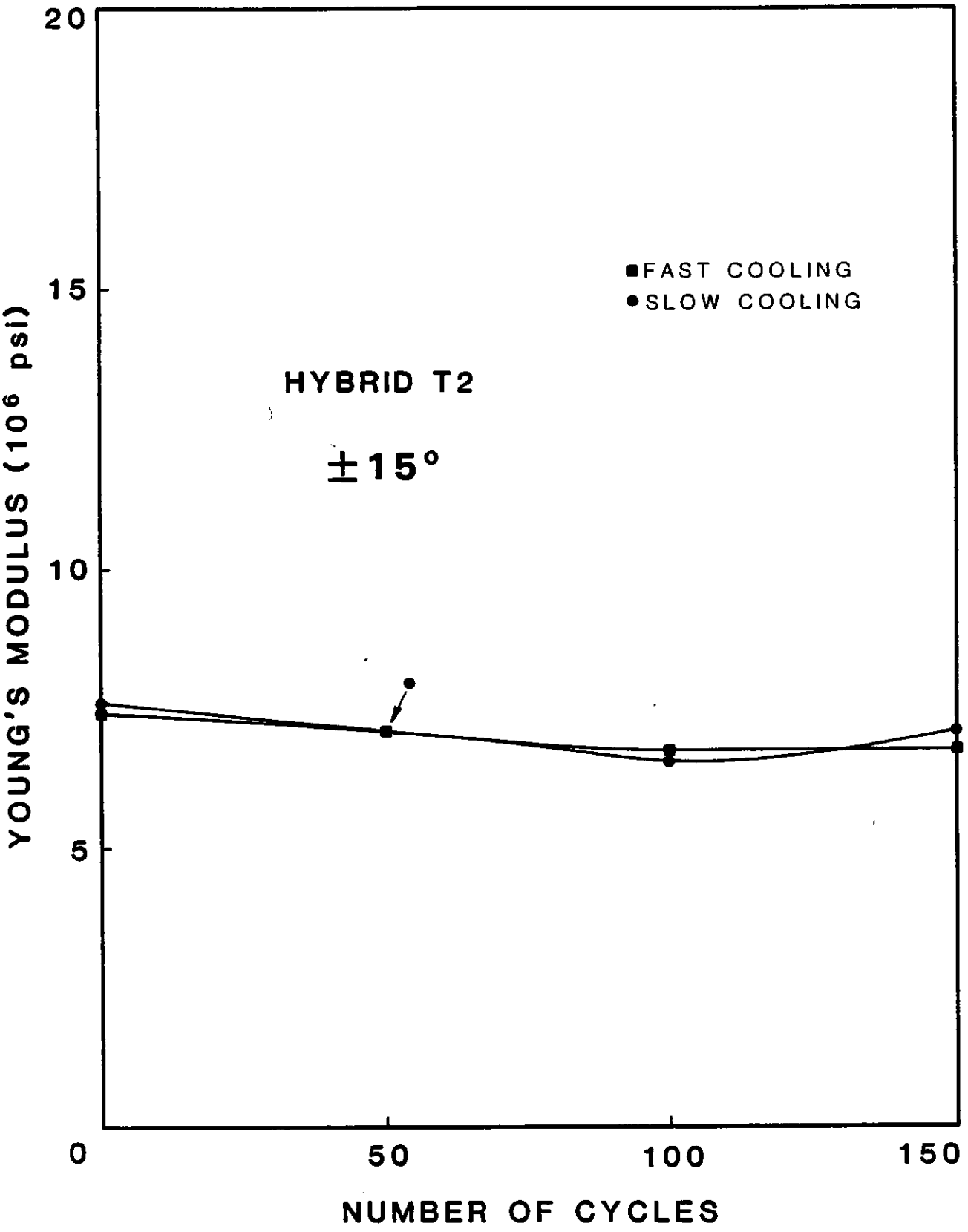

Figure 33. Young's Modulus vs. number of cycles for 15^{o} T2 Hybrid.

TABLE 34. YOUNG'S MODULUS VS. NUMBER OF CYCLES FOR 45 DEGREE T1 K-G-K HYBRID

NUMBER OF CYCLES	YOUNG'S MODULUS (MSI) FAST	SLOW
0	2.45	2.64
50	2.31	2.25
100	1.90	2.15
150	1.80	2.14

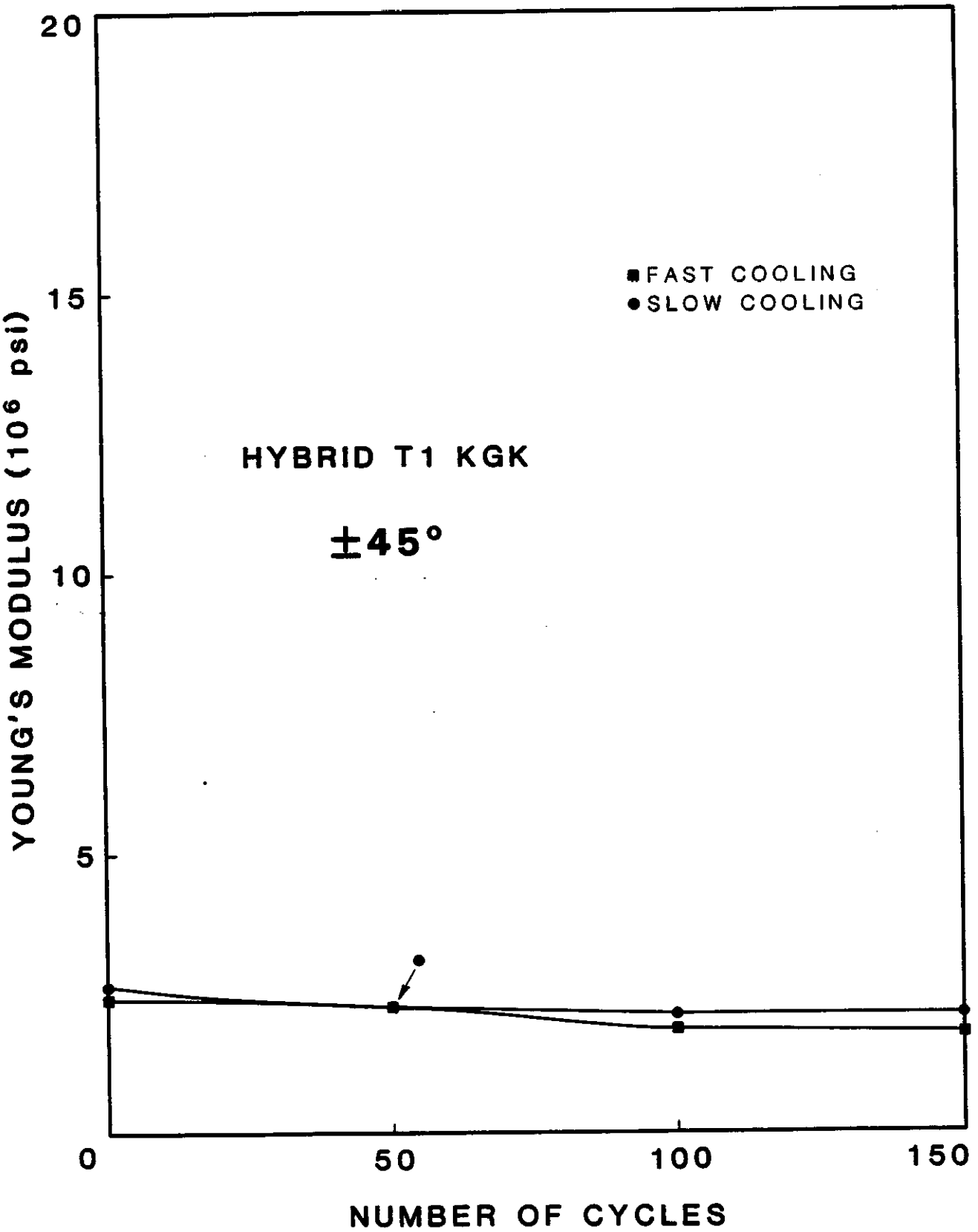

Figure 34. Young's Modulus vs. number of cycles for 45° T1 K-G-K Hybrid.

TABLE 35. YOUNG'S MODULUS VS. NUMBER OF CYCLES FOR 45 DEGREE T1 G-K-G HYBRID

NUMBER OF CYCLES	YOUNG'S MODULUS (MSI)	
	FAST	SLOW
0	2.43	2.31
50	2.39	2.03
100	1.83	1.98
150	2.08	1.98

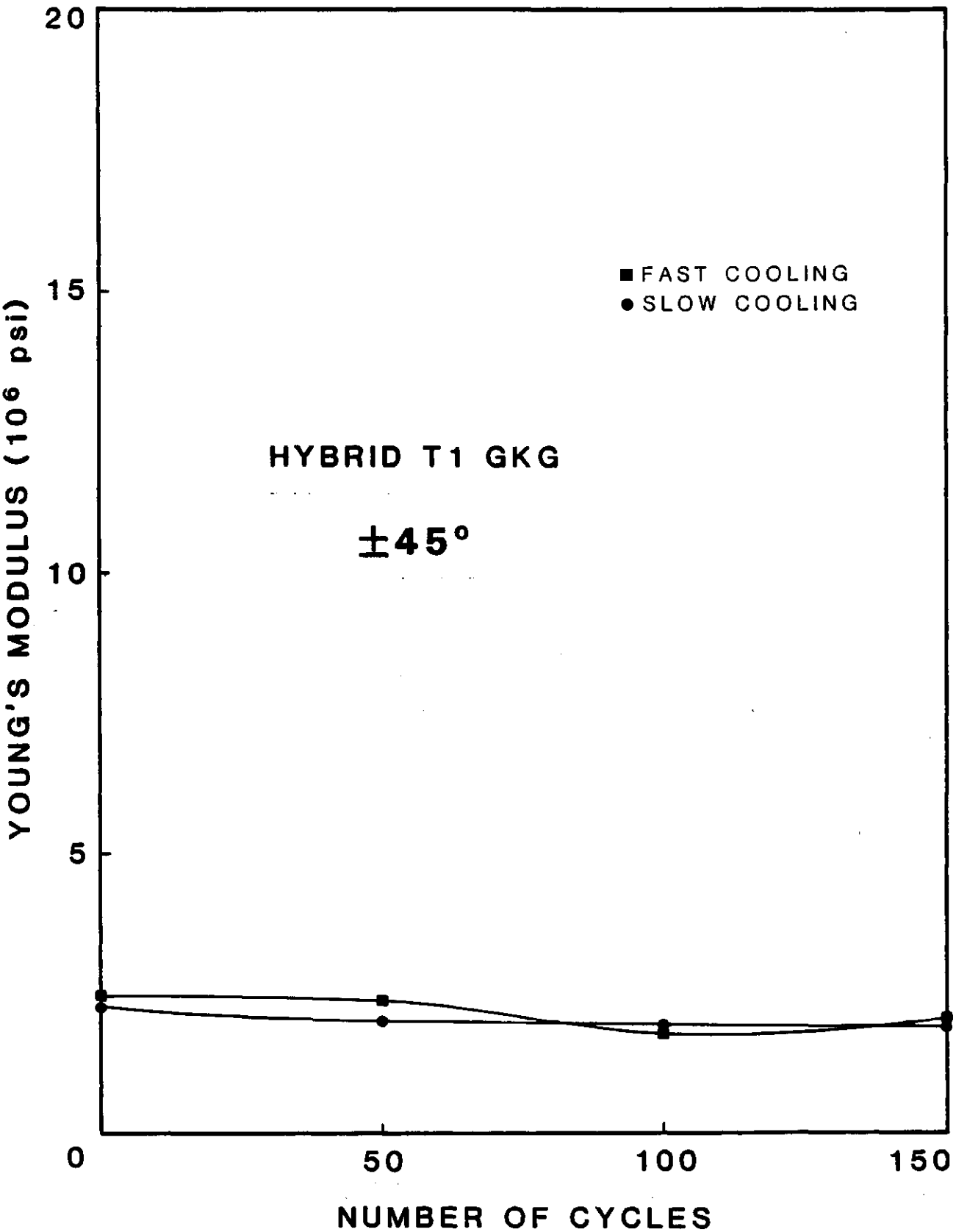

Figure 35. Young's Modulus vs. number of cycles for 45° T1 G-K-G Hybrid.

TABLE 36. YOUNG'S MODULUS VS. NUMBER OF CYCLES FOR 45 DEGREE T2 HYBRID

NUMBER OF CYCLES	YOUNG'S MODULUS (MSI) FAST	SLOW
0	2.46	2.39
50	2.15	2.08
100	1.87	2.01
150	2.05	1.89

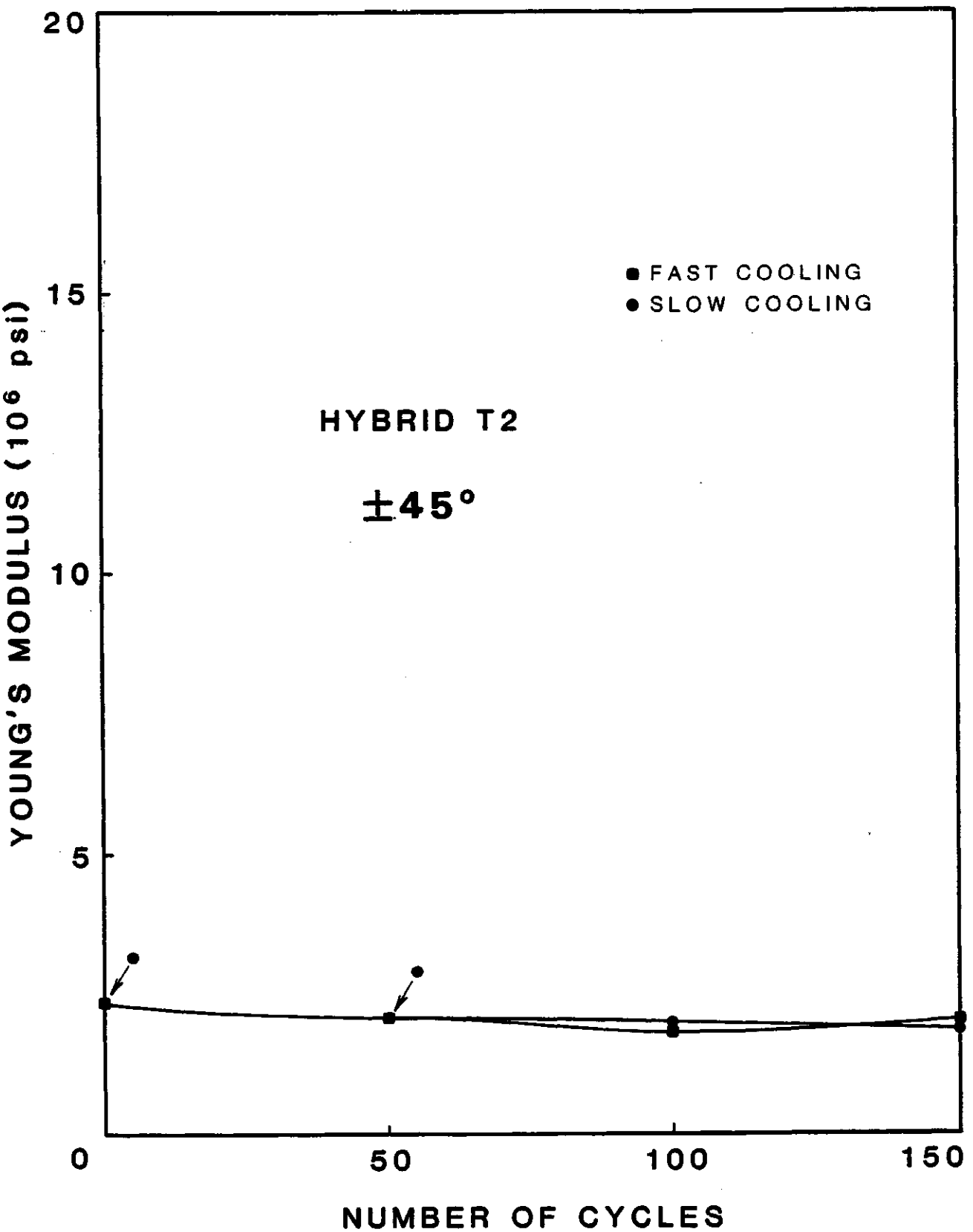

Figure 36. Young's Modulus vs. number of cycles for 45^{o} T2 Hybrid.

TABLE 37. POISSON'S RATIO VS. PLY ANGLE WITHOUT CYCLING FOR T300 GRAPHITE/RIGIDITE 5209 EPOXY

PLY ANGLE (DEGREES)	POISSON'S RATIO FAST	SLOW
0	0.37	0.35
15	1.09	0.98
30	1.44	1.53
45	0.98	0.79
60	0.40	0.19

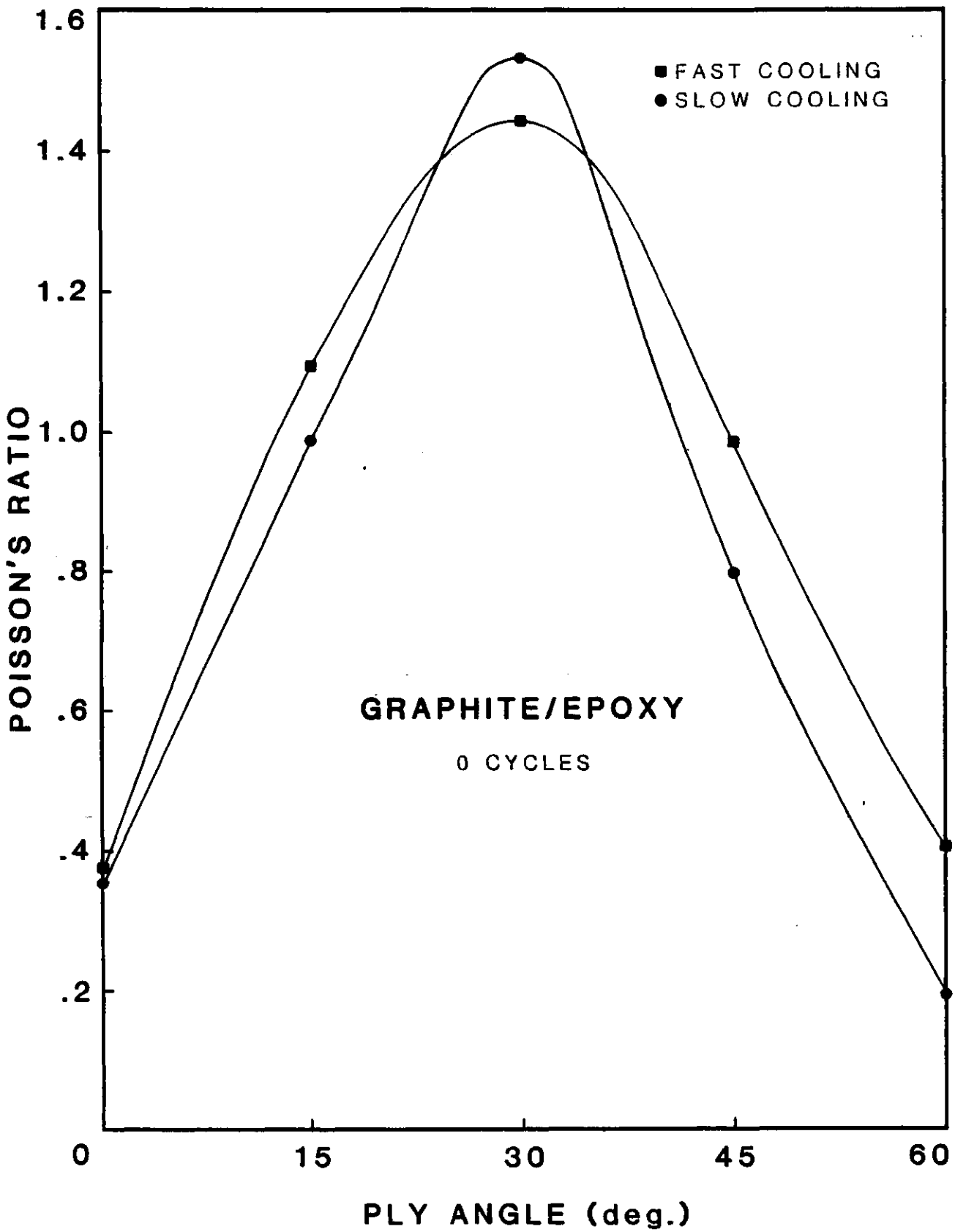

Figure 37. Poisson's Ratio vs. Ply Angle without cycling for T300 Graphite/Rigidite 5209 Epoxy.

TABLE 38. POISSON'S RATIO VS. PLY ANGLE WITHOUT CYCLING FOR KEVLAR 49C/RIGIDITE 5216 EPOXY

PLY ANGLE	POISSON'S RATIO	
(DEGREES)	FAST	SLOW
0	0.45	0.40
15	1.14	1.09
30	1.34	1.46
45	0.82	0.98
60	0.35	0.28

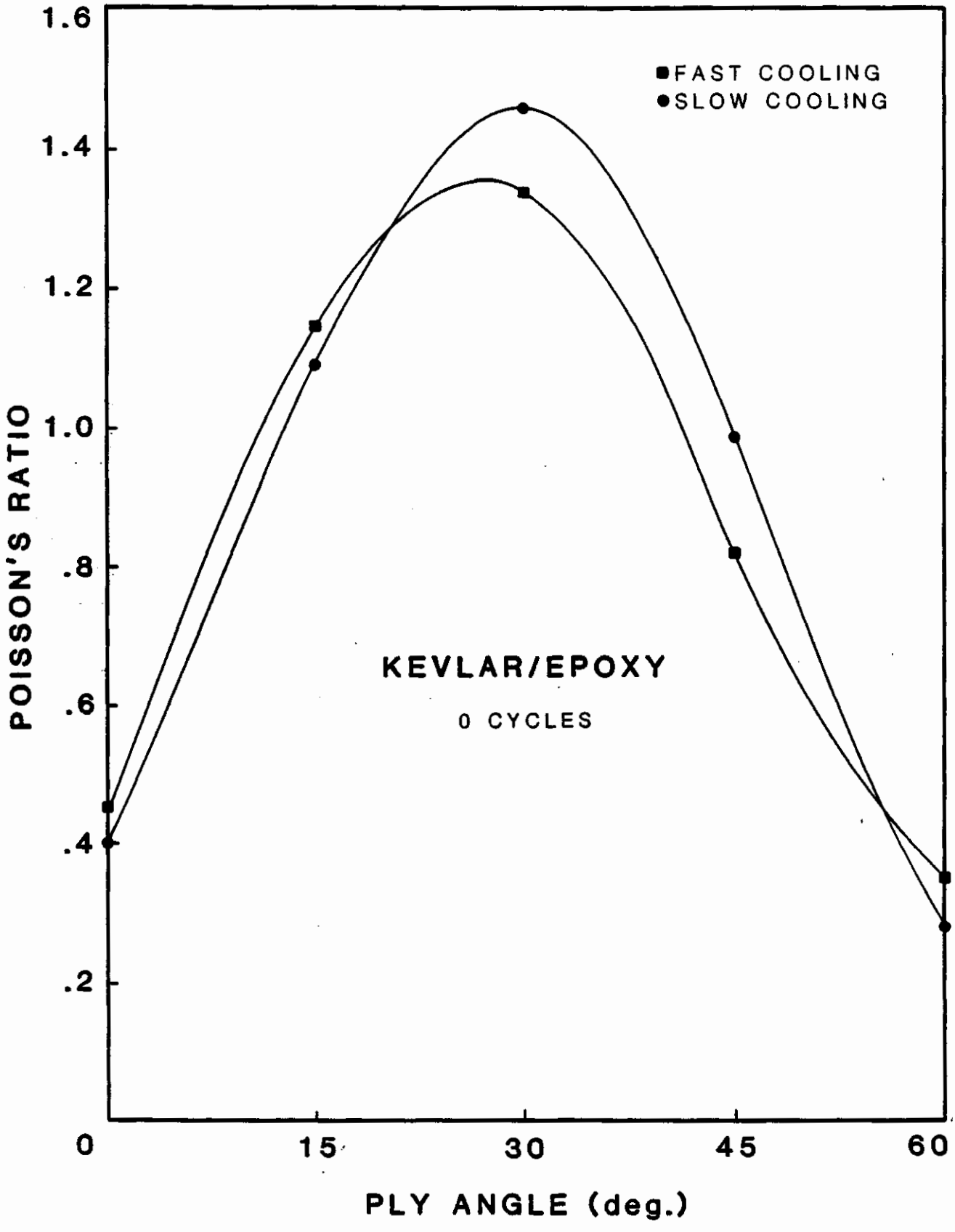

Figure 38. Poisson's Ratio vs. Ply Angle without cycling for Kevlar 49C/Rigidite 5216 Epoxy.

TABLE 39. POISSON'S RATIO VS. PLY ANGLE WITHOUT CYCLING FOR E-GLASS/RIGIDITE 5216 EPOXY

PLY ANGLE (DEGREES)	POISSON'S RATIO	
	FAST	SLOW
0	0.33	0.33
15	0.37	0.39
30	0.67	0.65
45	0.83	0.59
60	0.35	0.22

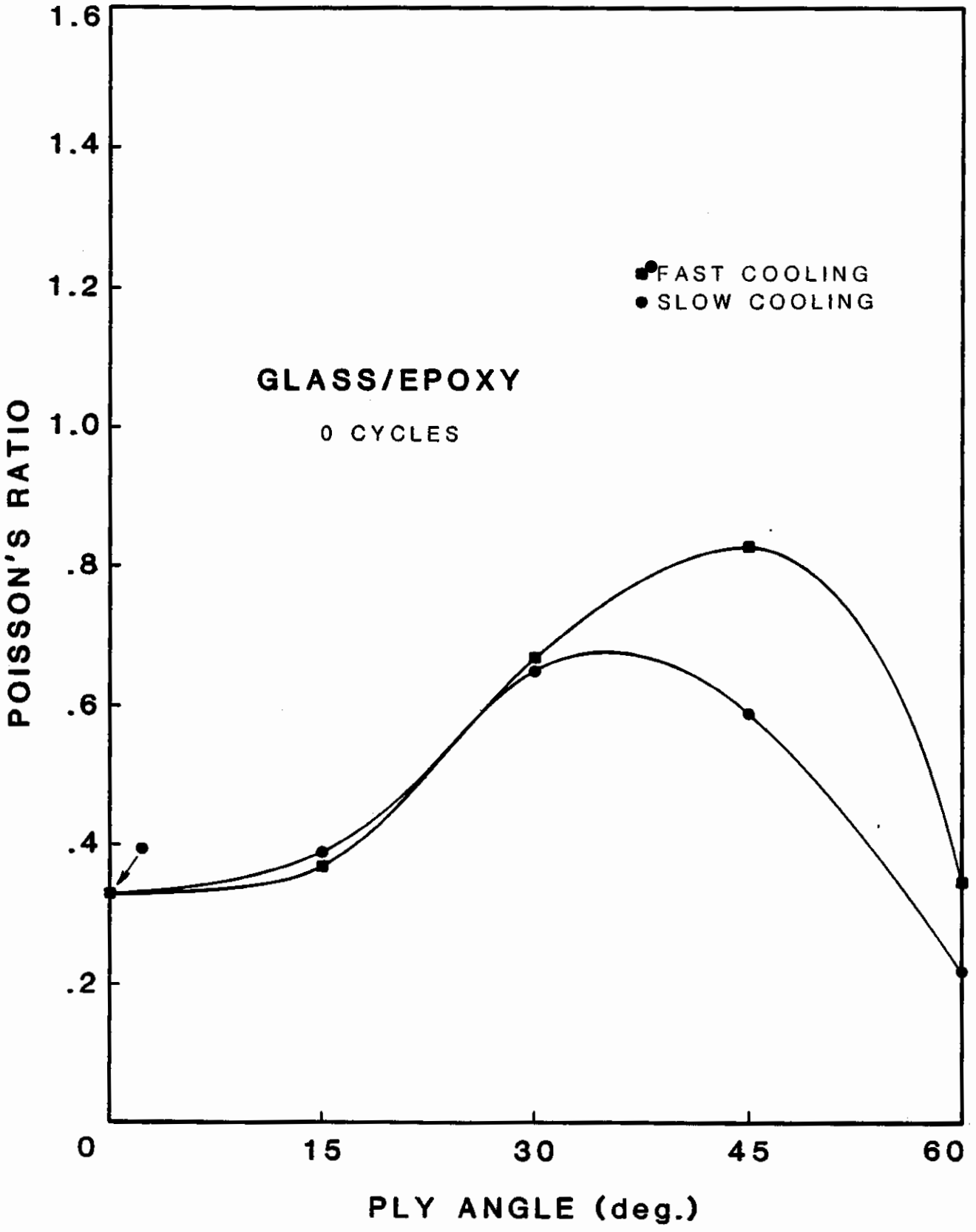

Figure 39. Poisson's Ratio vs. Ply Angle without cycling for E-Glass/Rigidite 5216 Epoxy.

TABLE 40. POISSON'S RATIO VS. PLY ANGLE AFTER 50 CYCLES FOR T300 GRAPHITE/RIGIDITE 5209 EPOXY

PLY ANGLE (DEGREES)	POISSON'S RATIO FAST	SLOW
0	0.32	0.32
15	1.08	0.72
30	1.05	1.38
45	0.92	0.82
60	0.36	0.27

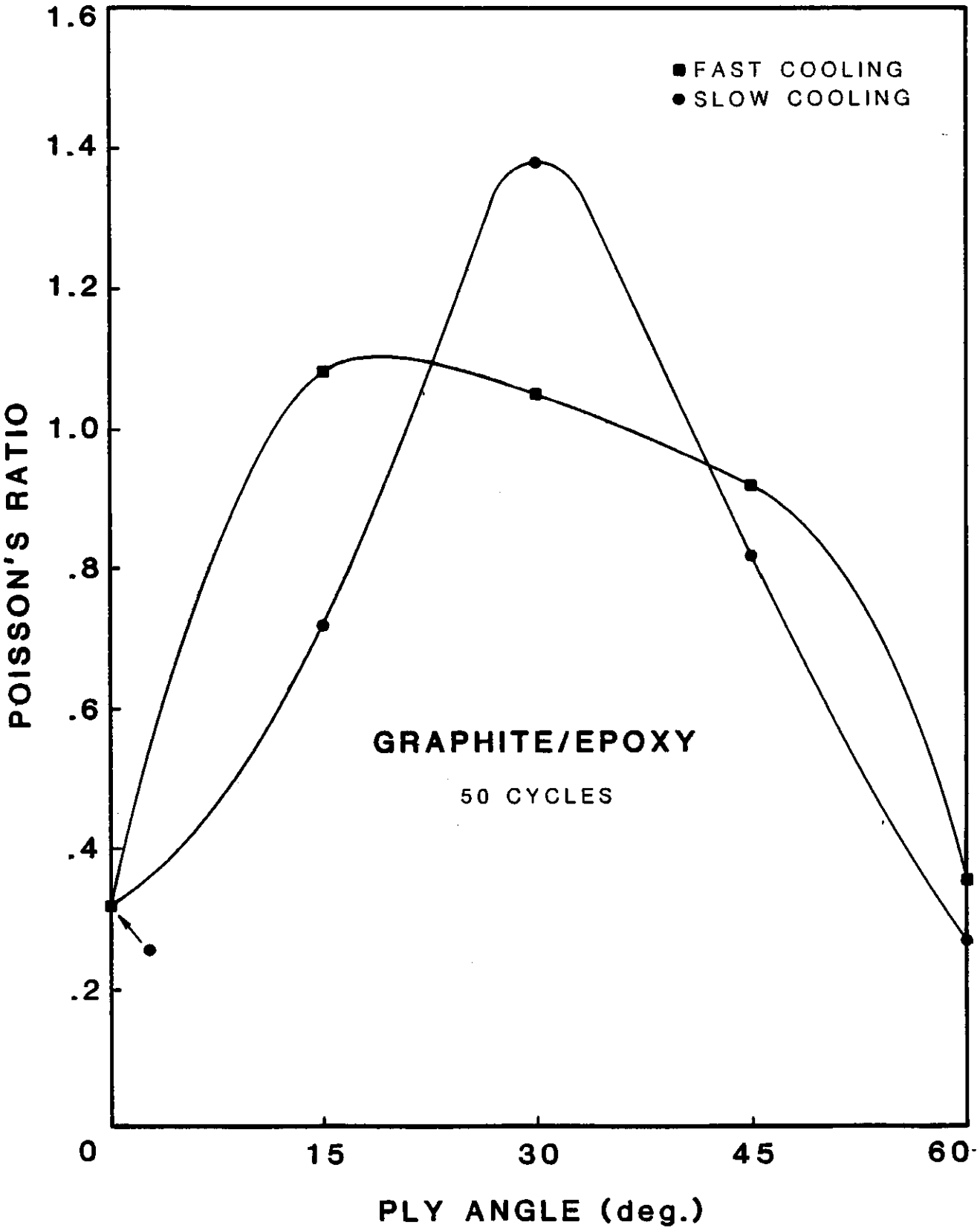

Figure 40. Poisson's Ratio vs. Ply Angle with 50 cycles for T300 Graphite/Rigidite 5209 Epoxy.

TABLE 41. POISSON'S RATIO VS. PLY ANGLE AFTER 50 CYCLES FOR KEVLAR 49C/RIGIDITE 5216 EPOXY

PLY ANGLE (DEGREES)	POISSON'S RATIO FAST	SLOW
0	0.40	0.39
15	1.12	1.17
30	1.44	1.41
45	0.83	0.93
60	0.33	0.33

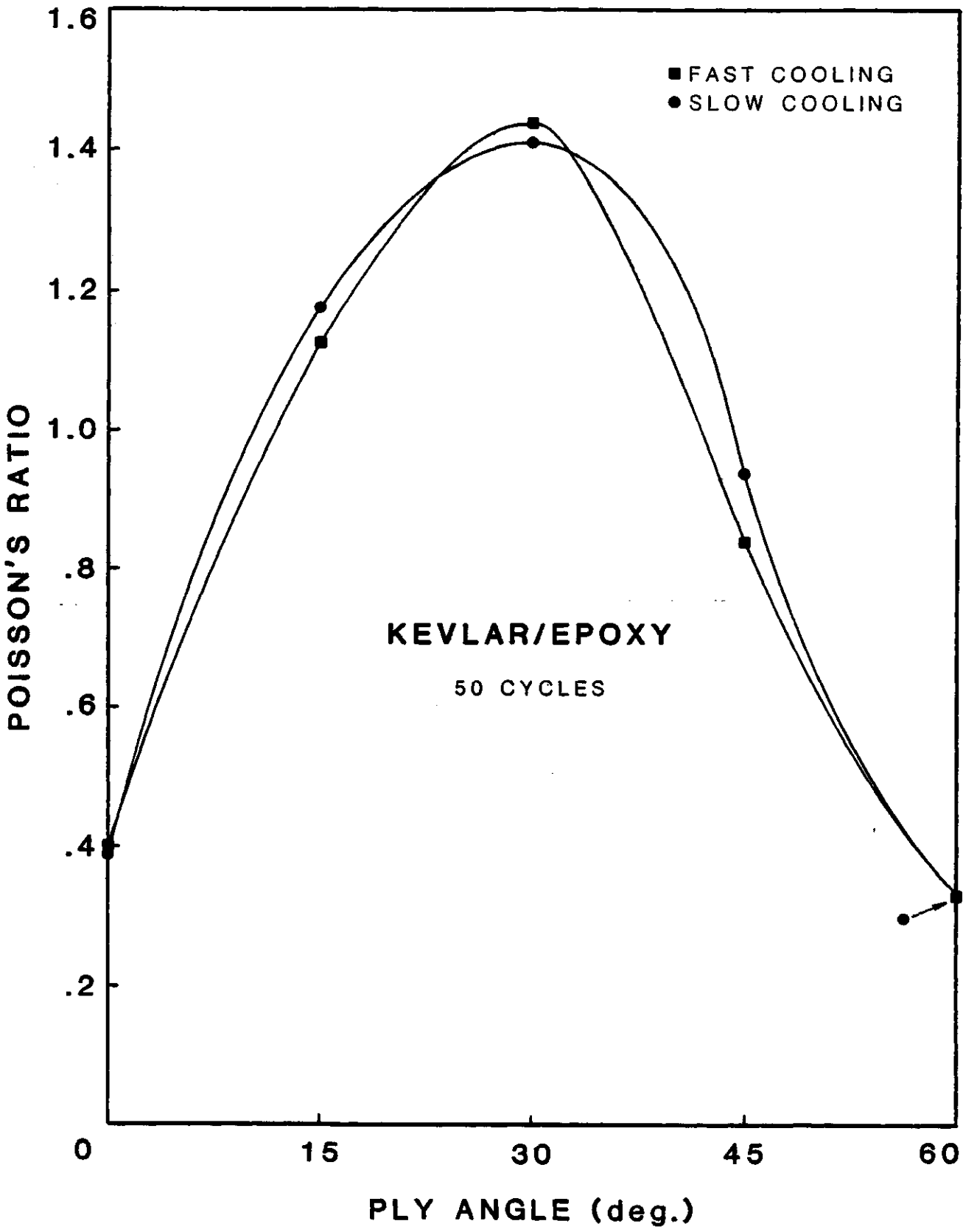

Figure 41. Poisson's Ratio vs. Ply Angle with 50 cycles for Kevlar 49C/Rigidite 5216 Epoxy.

TABLE 42. POISSON'S RATIO VS. PLY ANGLE AFTER 50 CYCLES FOR E-GLASS/RIGIDITE 5216 EPOXY

PLY ANGLE (DEGREES)	POISSON'S RATIO	
	FAST	SLOW
0	0.33	0.33
15	0.39	0.41
30	0.62	0.65
45	0.74	0.55
60	0.36	0.32

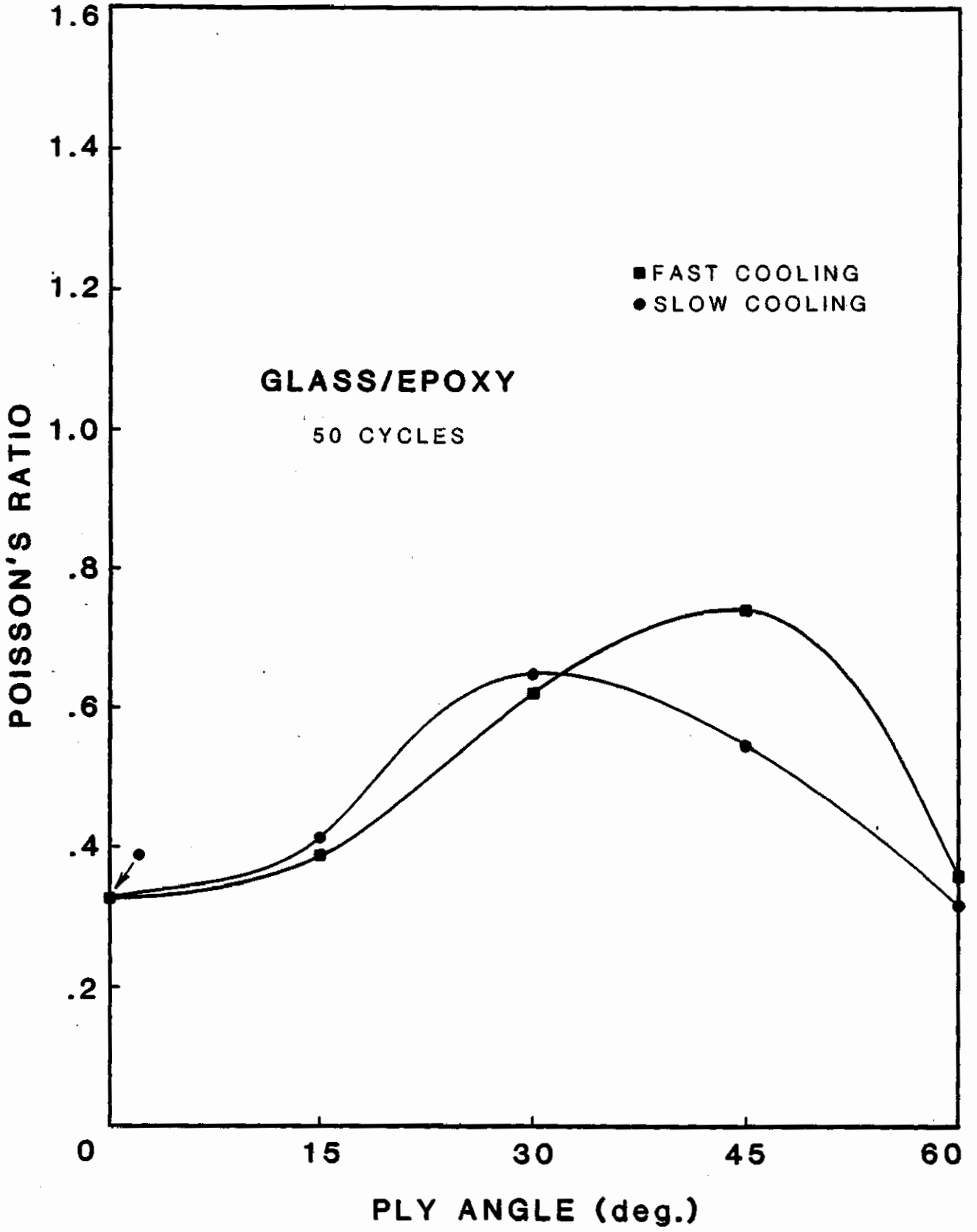

Figure 42. Poisson's Ratio vs. Ply Angle with 50 cycles for E-Glass/Rigidite 5216 Epoxy.

TABLE 43. POISSON'S RATIO VS. PLY ANGLE AFTER 100 CYCLES FOR T300 GRAPHITE/RIGIDITE 5209 EPOXY

PLY ANGLE (DEGREES)	POISSON'S RATIO FAST	SLOW
0	0.21	0.23
15	**.**	0.25
30	1.04	1.09
45	0.62	0.65
60	0.30	0.24

. Invalid data due to malfunctions of measurement devices.

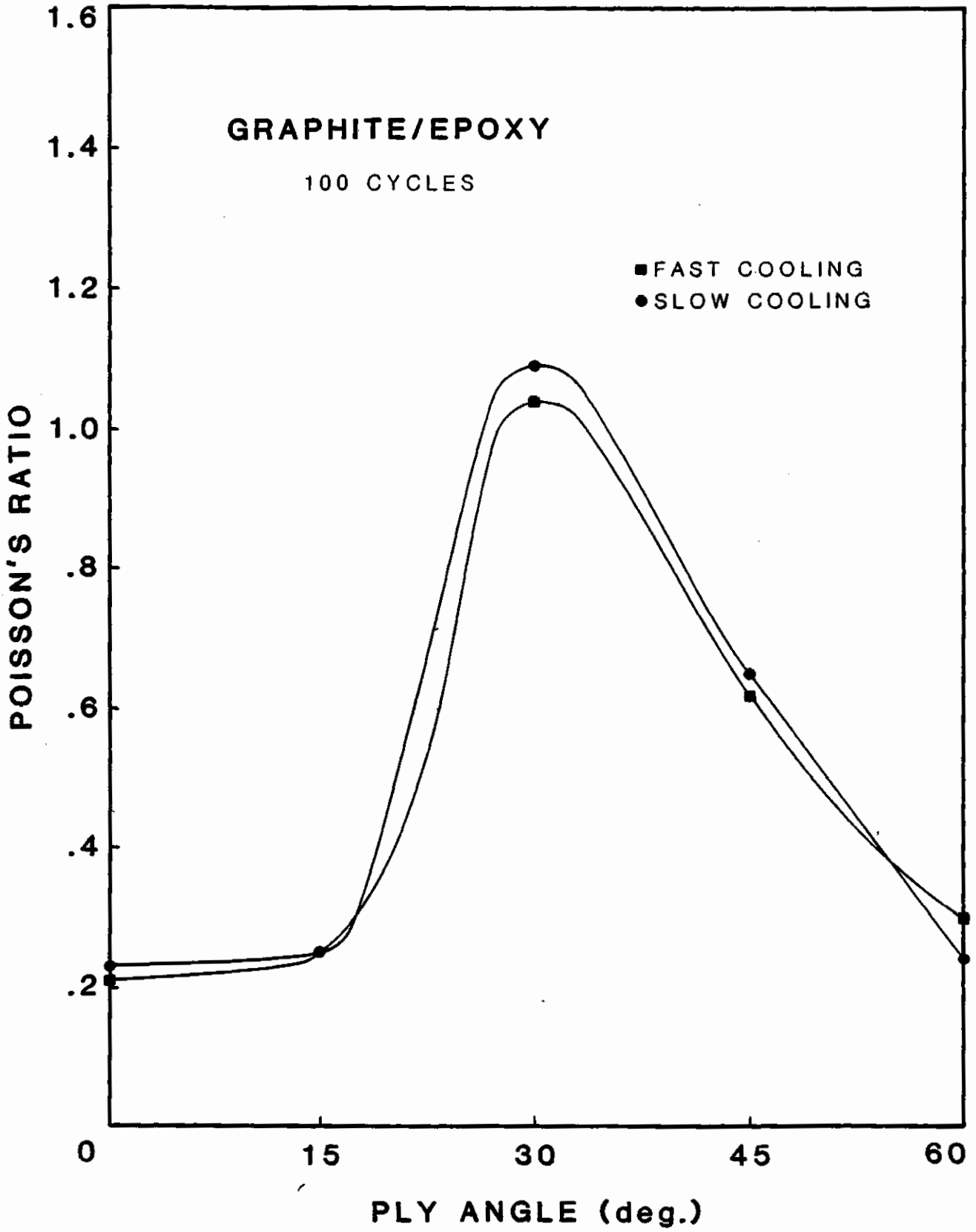

Figure 43. Poisson's Ratio vs. Ply Angle with 100 cycles for T300 Graphite/Rigidite 5209 Epoxy.

TABLE 44. POISSON'S RATIO VS. PLY ANGLE AFTER 100 CYCLES FOR KEVLAR 49C/RIGIDITE 5216 EPOXY

PLY ANGLE (DEGREES)	POISSON'S RATIO FAST	SLOW
0	0.29	0.28
15	0.78	0.79
30	1.09	0.95
45	0.61	0.69
60	0.27	0.25

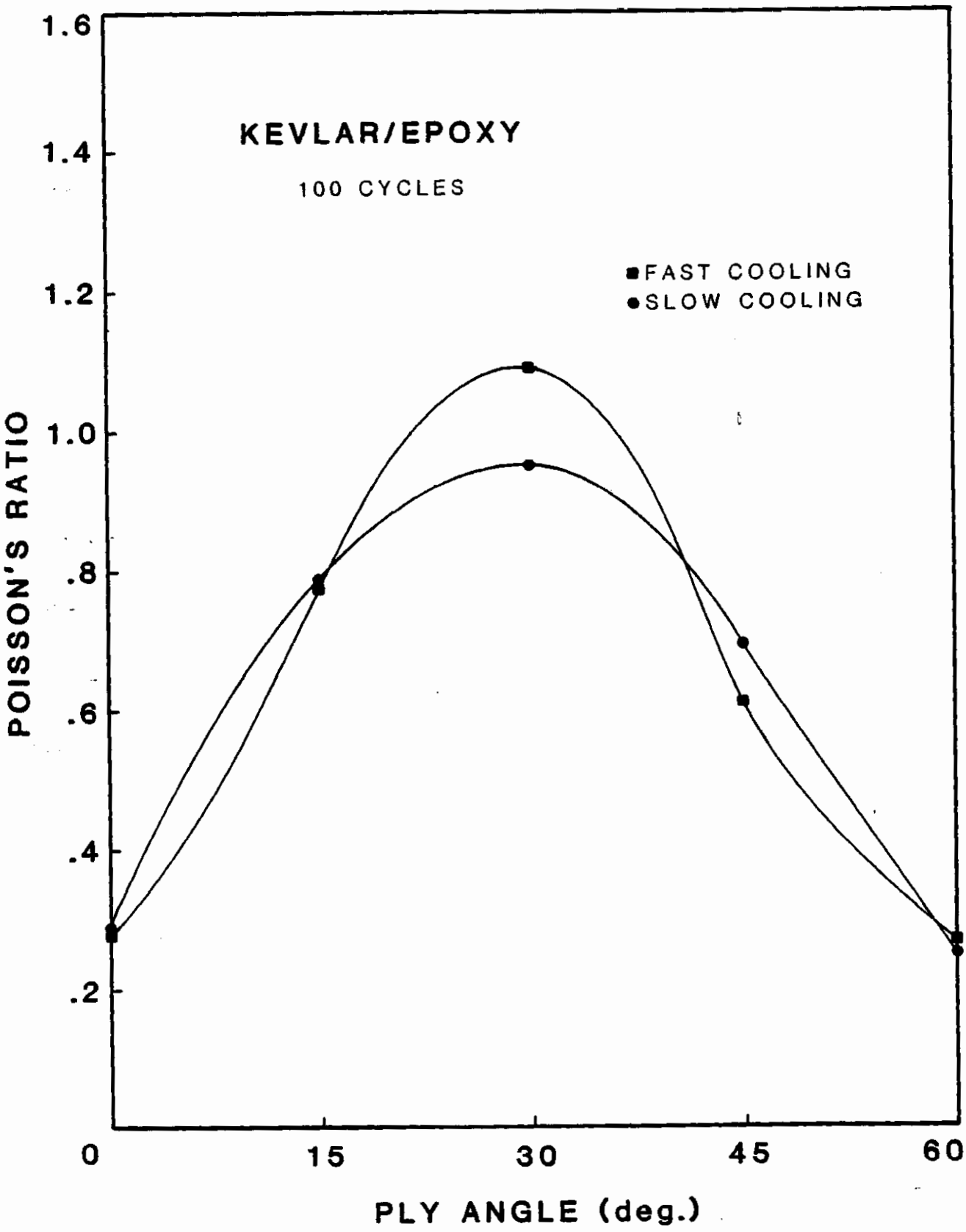

Figure 44. Poisson's Ratio vs. Ply Angle with 100 cycles for Kevlar 49C/Rigidite 5216 Epoxy.

TABLE 45. POISSON'S RATIO VS. PLY ANGLE AFTER 100 CYCLES FOR E-GLASS/RIGIDITE 5216 EPOXY

PLY ANGLE (DEGREES)	POISSON'S RATIO FAST	SLOW
0	0.21	0.23
15	0.25	0.28
30	0.36	0.47
45	0.59	0.40
60	0.27	0.29

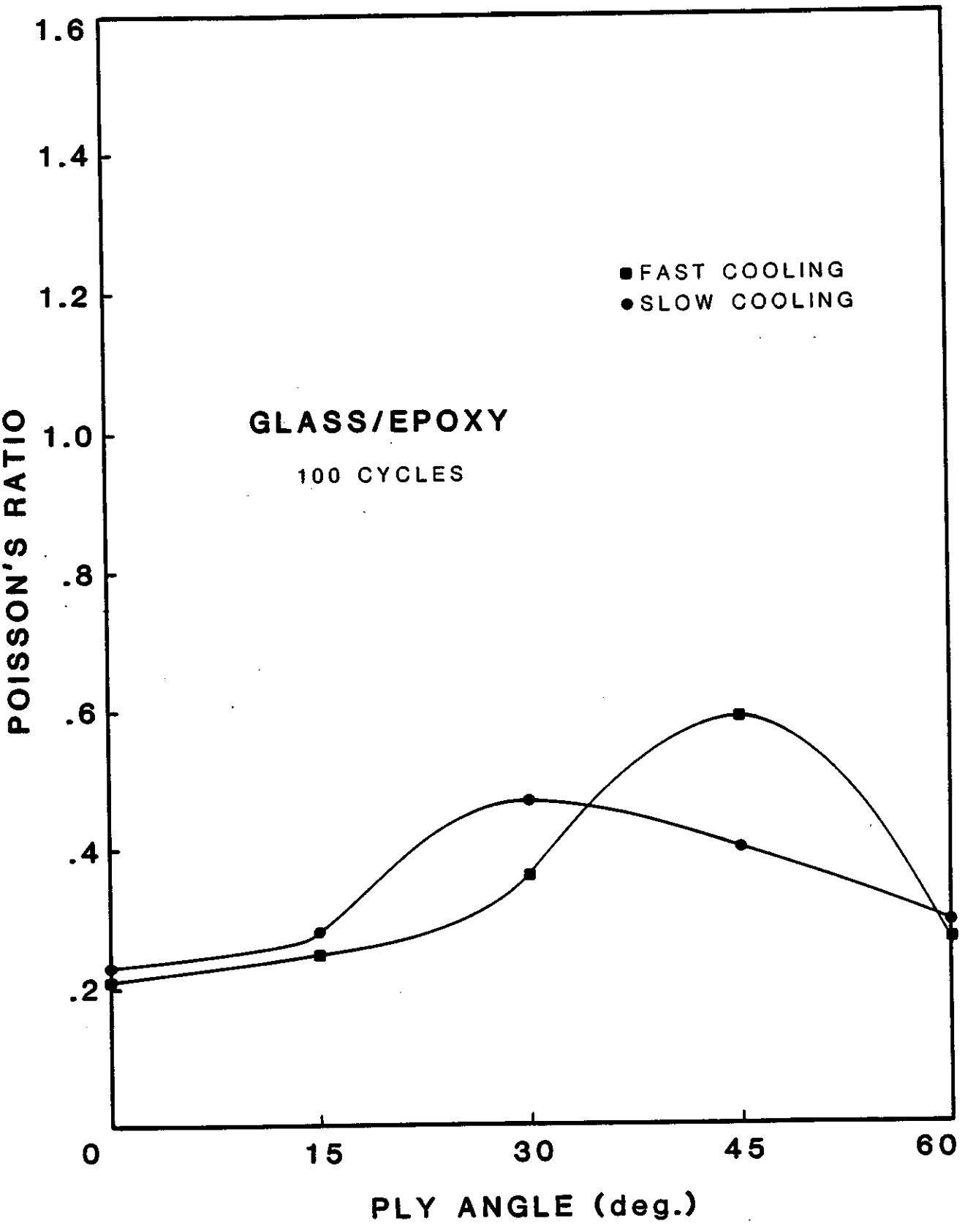
1.6
1.4
1.2
1.0
.8
.6
.4
.2
POISSON'S RATIO
FAST COOLING
SLOW COOLING
GLASS/EPOXY
100 CYCLES
0
15
30
45
60
PLY ANGLE (deg.)

TABLE 46. POISSON'S RATIO VS. PLY ANGLE AFTER 150 CYCLES FOR T300 GRAPHITE/RIGIDITE 5209 EPOXY

PLY ANGLE (DEGREES)	POISSON'S RATIO FAST	SLOW
0	0.28	0.27
15	**.**	0.21
30	1.22	1.22
45	0.75	0.59
60	0.28	0.23

. Invalid data due to malfunctions of measurement devices.

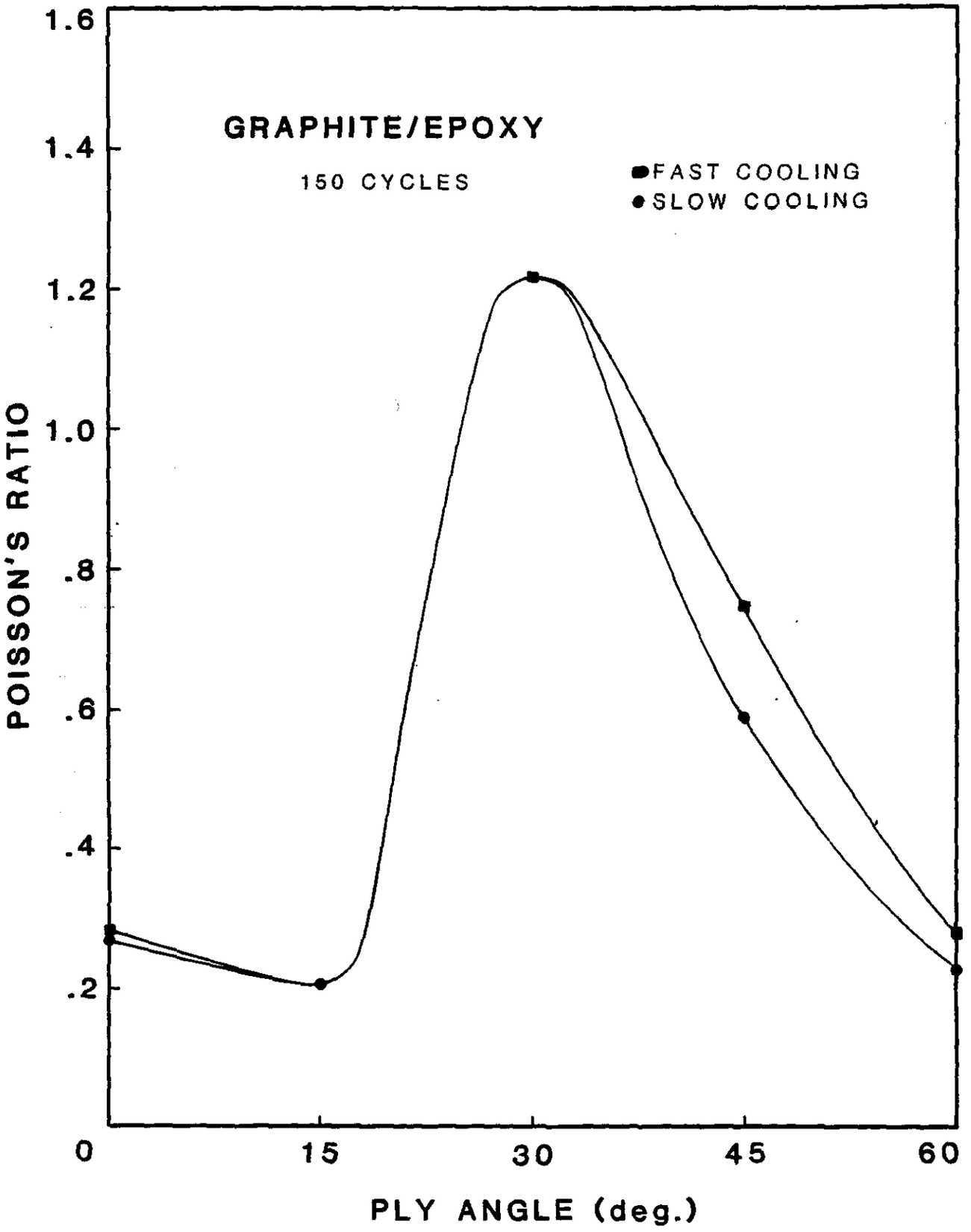

Figure 46. Poisson's Ratio vs. Ply Angle with 150 cycles for T300 Graphite/Rigidite 5209 Epoxy.

TABLE 47. POISSON'S RATIO VS. PLY ANGLE AFTER 150 CYCLES FOR KEVLAR 49C/RIGIDITE 5216 EPOXY

PLY ANGLE (DEGREES)	POISSON'S RATIO FAST	SLOW
0	0.35	0.33
15	0.82	0.83
30	0.99	1.01
45	0.64	0.66
60	0.25	0.35

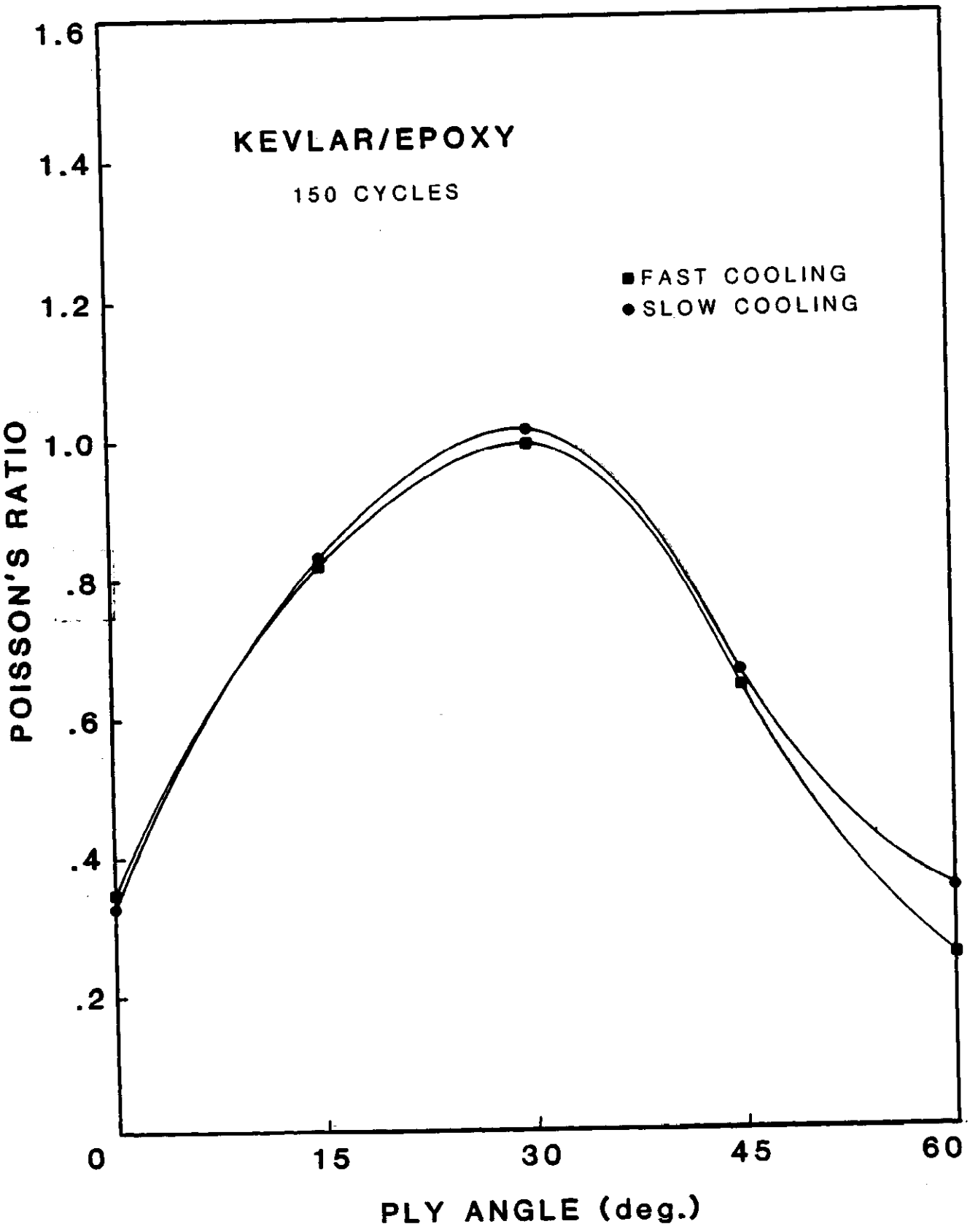

Figure 47. Poisson's Ratio vs. Ply Angle with 150 cycles for Kevlar 49C/Rigidite 5216 Epoxy.

TABLE 48. POISSON'S RATIO VS. PLY ANGLE AFTER 150 CYCLES FOR E-GLASS/RIGIDITE 5216 EPOXY

PLY ANGLE (DEGREES)	POISSON'S RATIO FAST	SLOW
0	0.27	0.29
15	0.32	0.35
30	0.54	**.**
45	0.60	0.57
60	0.33	0.35

. Invalid data due to malfunctions of measurement devices.

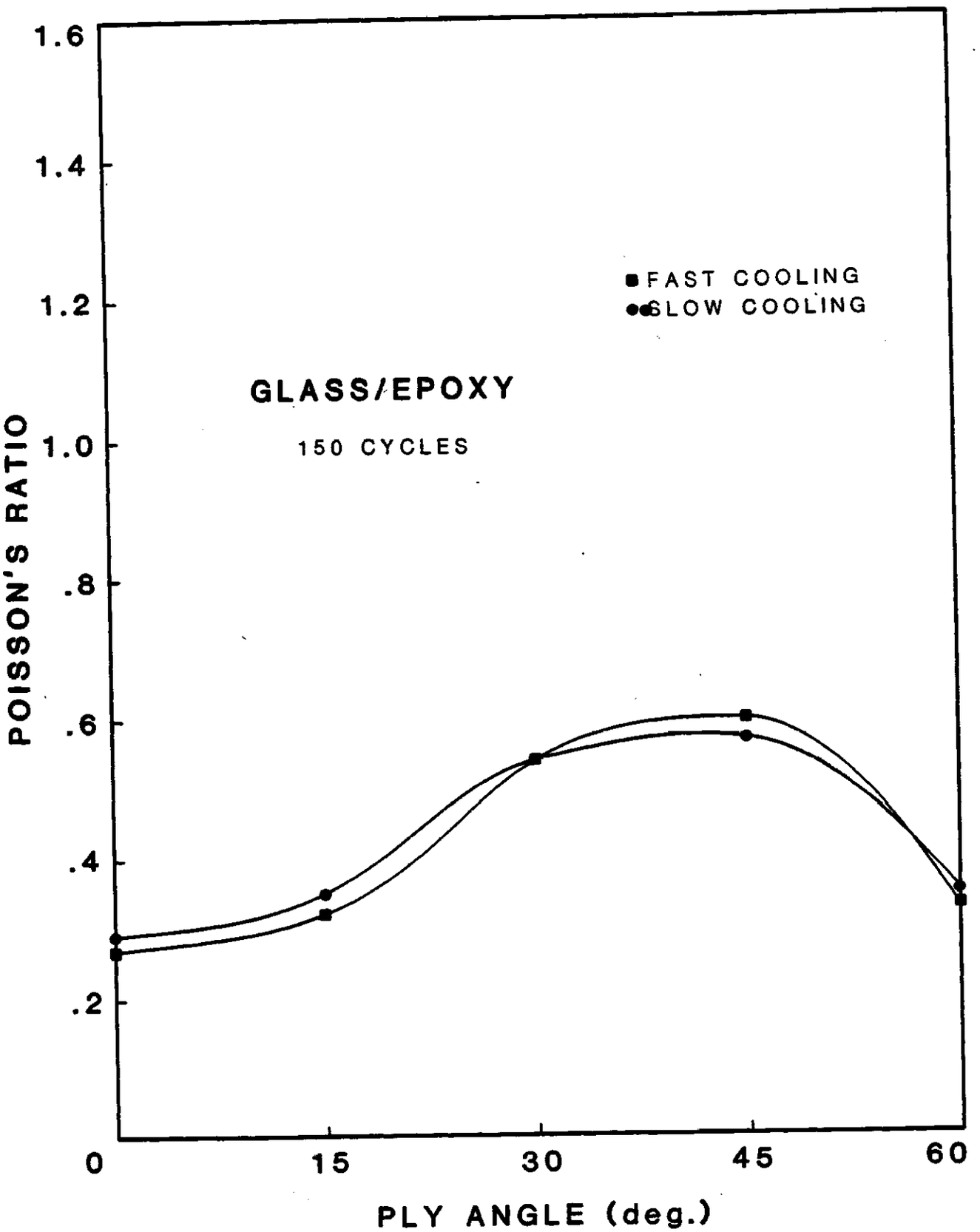

Figure 48. Poisson's Ratio vs. Ply Angle with 150 cycles for E-Glass/Rigidite 5216 Epoxy.

TABLE 49. POISSON'S RATIO VS. NUMBER OF CYCLES FOR UNIDIRECITONAL T300 GRAPHITE/RIGIDITE 5209 EPOXY

NUMBER OF CYCLES	POISSON'S RATIO	
	FAST	SLOW
0	0.37	0.35
50	0.32	0.32
100	0.21	0.23
150	0.28	0.27

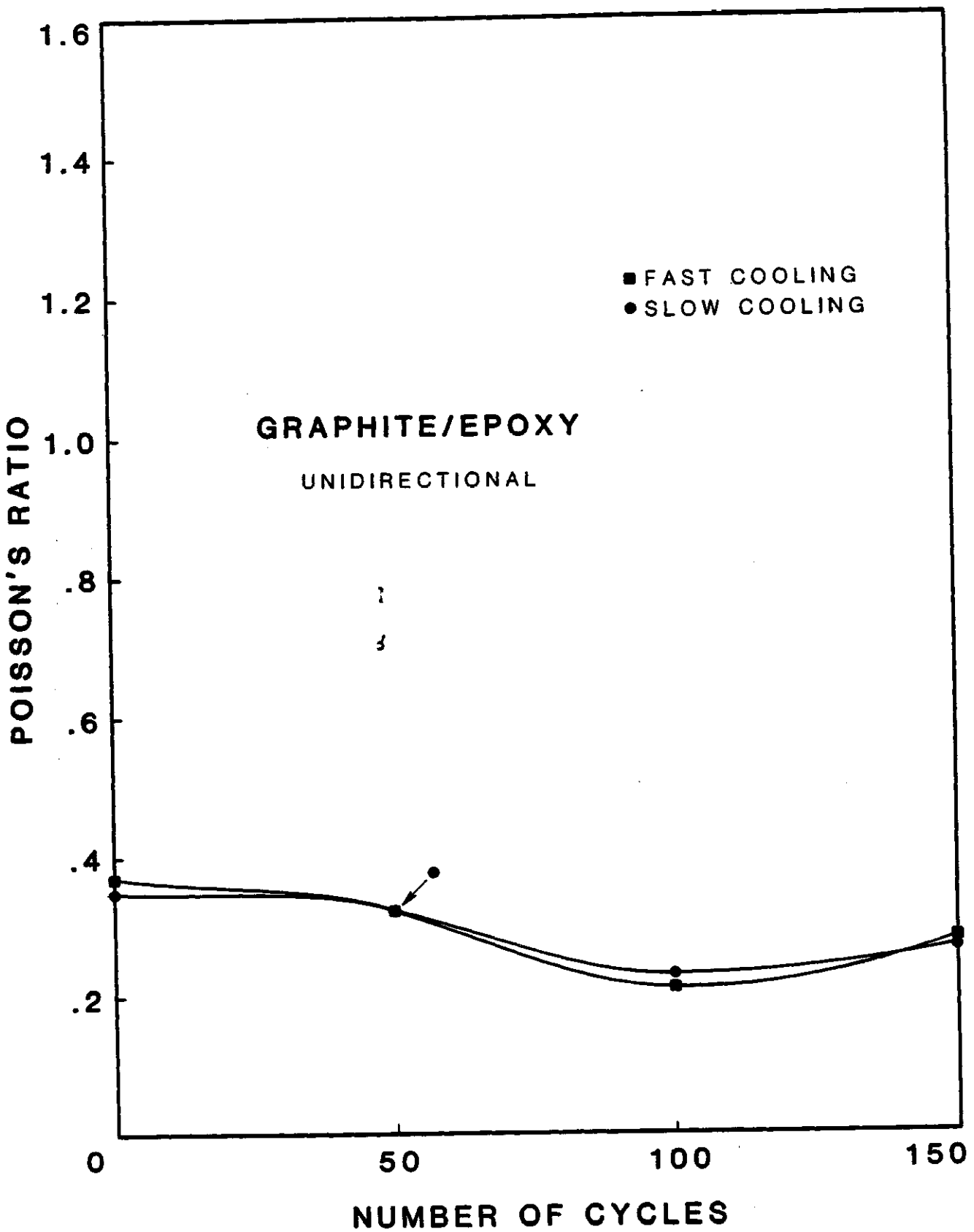

Figure 49. Poisson's Ratio vs. number of cycles for unidirectional T300 Graphite/Rigidite 5209 Epoxy.

TABLE 50. POISSON'S RATIO VS. NUMBER OF CYCLES FOR UNIDIRECTIONAL KEVLAR 49C/RIGIDITE 5216 EPOXY

NUMBER OF CYCLES	POISSON'S RATIO	
	FAST	SLOW
0	0.45	0.40
50	0.40	0.39
100	0.29	0.28
150	0.35	0.33

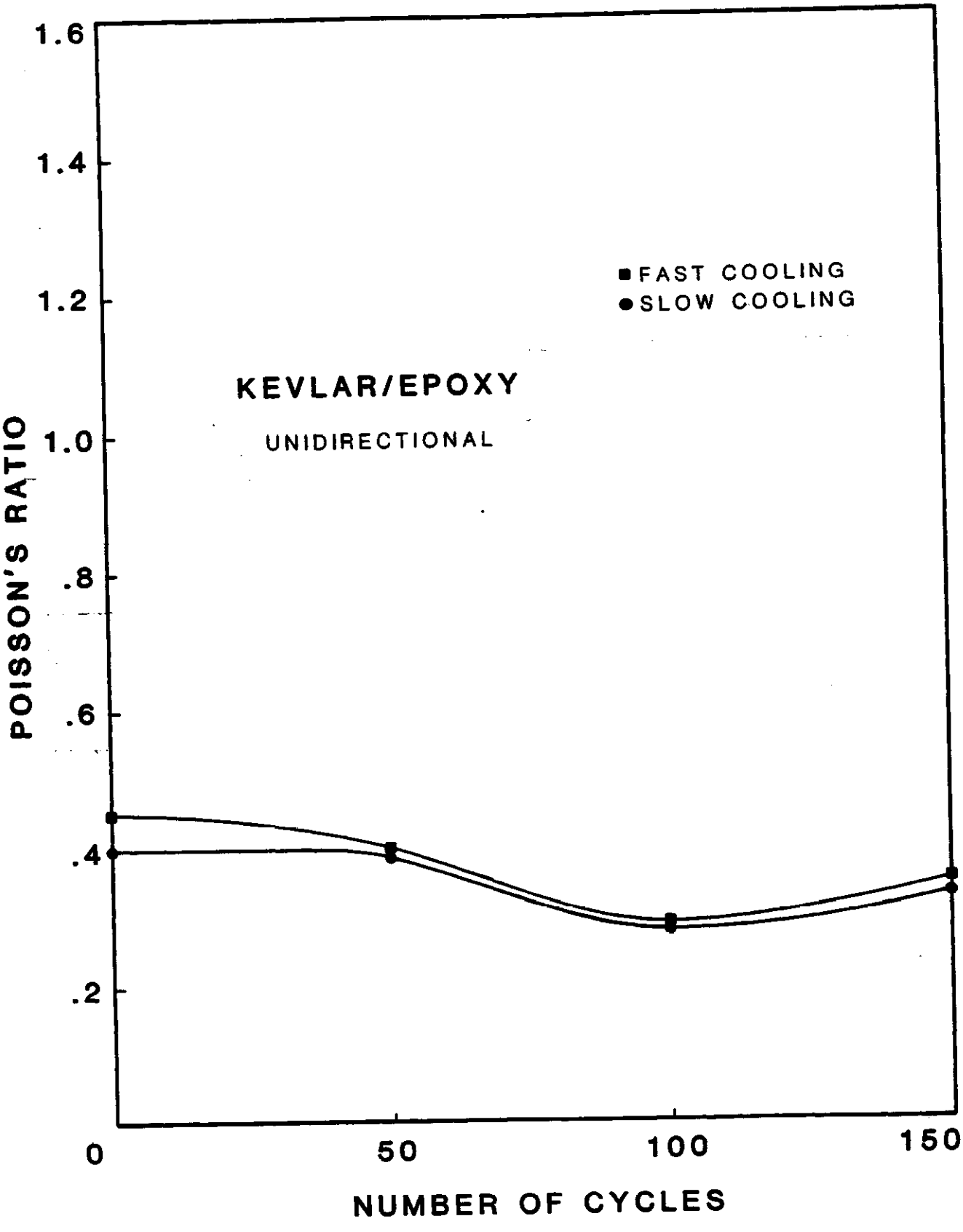

Figure 50. Poisson's Ratio vs. number of cycles for unidirectional Kevlar 49C/Rigidite 5216 Epoxy.

TABLE 51. POISSON'S RATIO VS. NUMBER OF CYCLES FOR UNIDIRECTIONAL E-GLASS/RIGIDITE 5216 EPOXY

NUMBER OF CYCLES	POISSON'S RATIO	
	FAST	SLOW
0	0.33	0.33
50	0.33	0.33
100	0.21	0.23
150	0.27	0.29

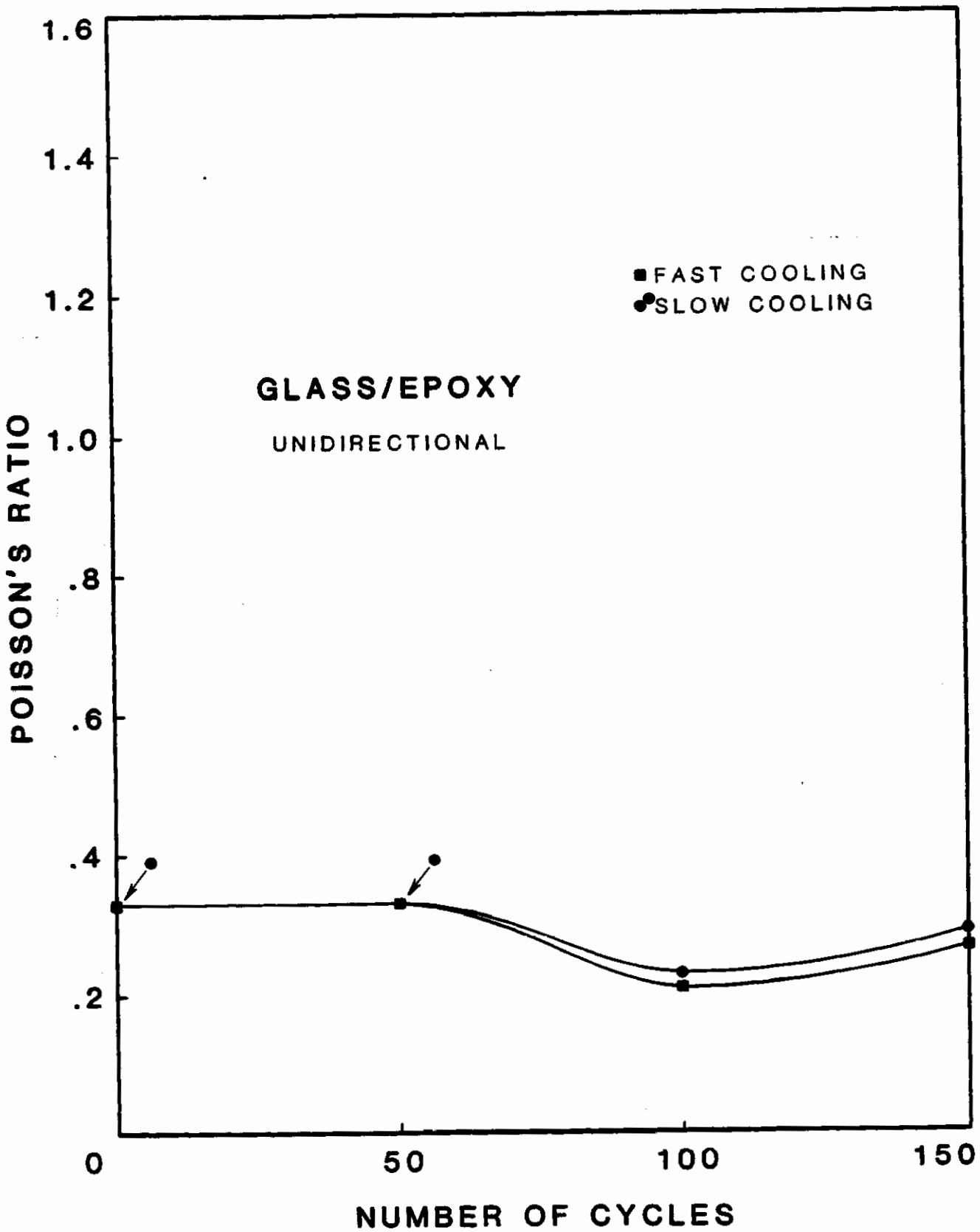

Figure 51. Poisson's Ratio vs. number of cycles for unidirectional E-Glass/Rigidite 5216 Epoxy.

TABLE 52. POISSON'S RATIO VS. NUMBER OF CYCLES FOR CROSS-PLY T300 GRAPHITE/RIGIDITE 5209 EPOXY

NUMBER OF CYCLES	POISSON'S RATIO	
	FAST	SLOW
0		
50		
100		
150		

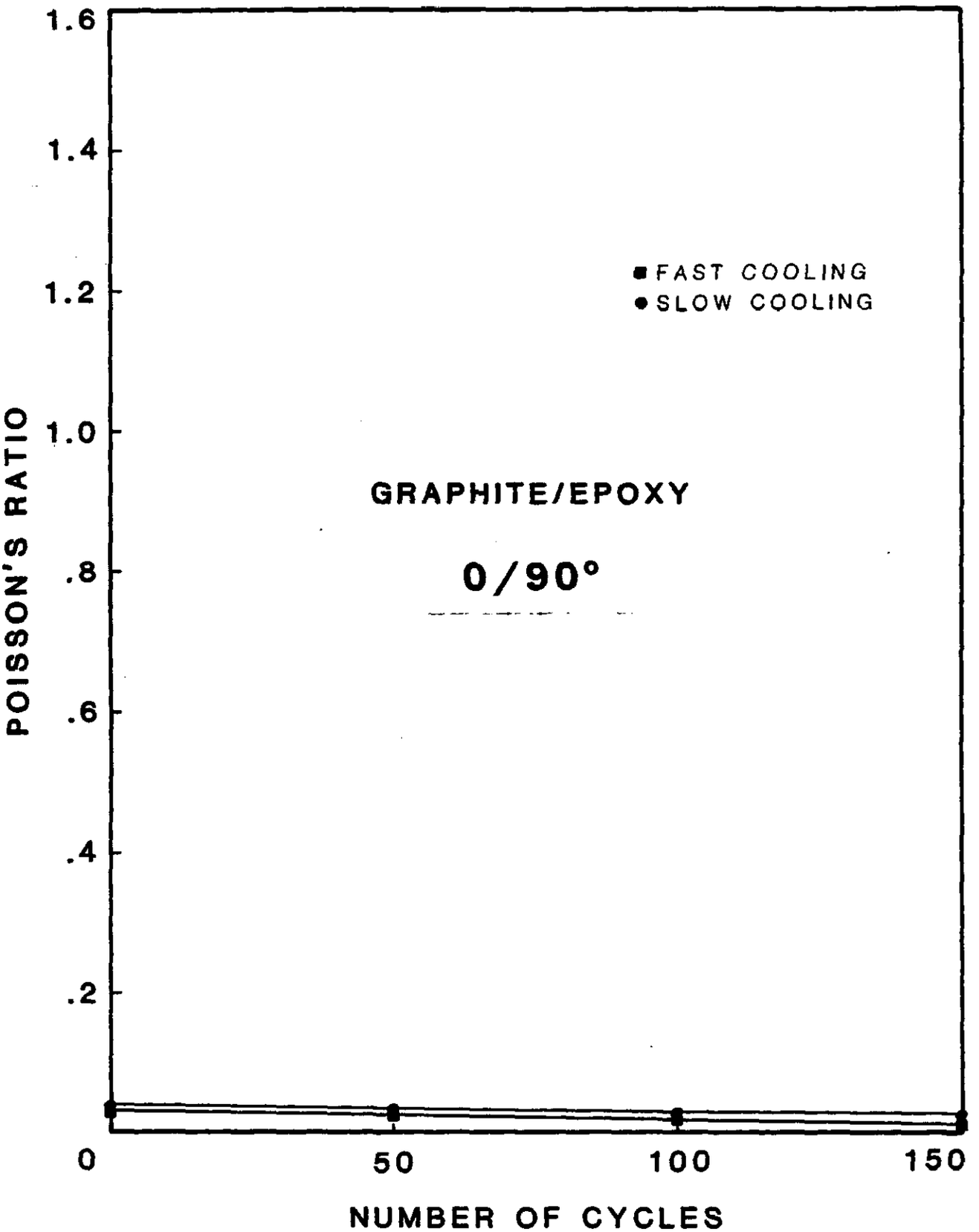

Figure 52. Poisson's Ratio vs. number of cycles for cross-ply T300 Graphite/Rigidite 5209 Epoxy.

TABLE 53. POISSON'S RATIO VS. NUMBER OF CYCLES FOR CROSS-PLY KEVLAR 49C/RIGIDITE 5216 EPOXY

NUMBER OF CYCLES	POISSON'S RATIO	
	FAST	SLOW
0		
50		
100		
150		

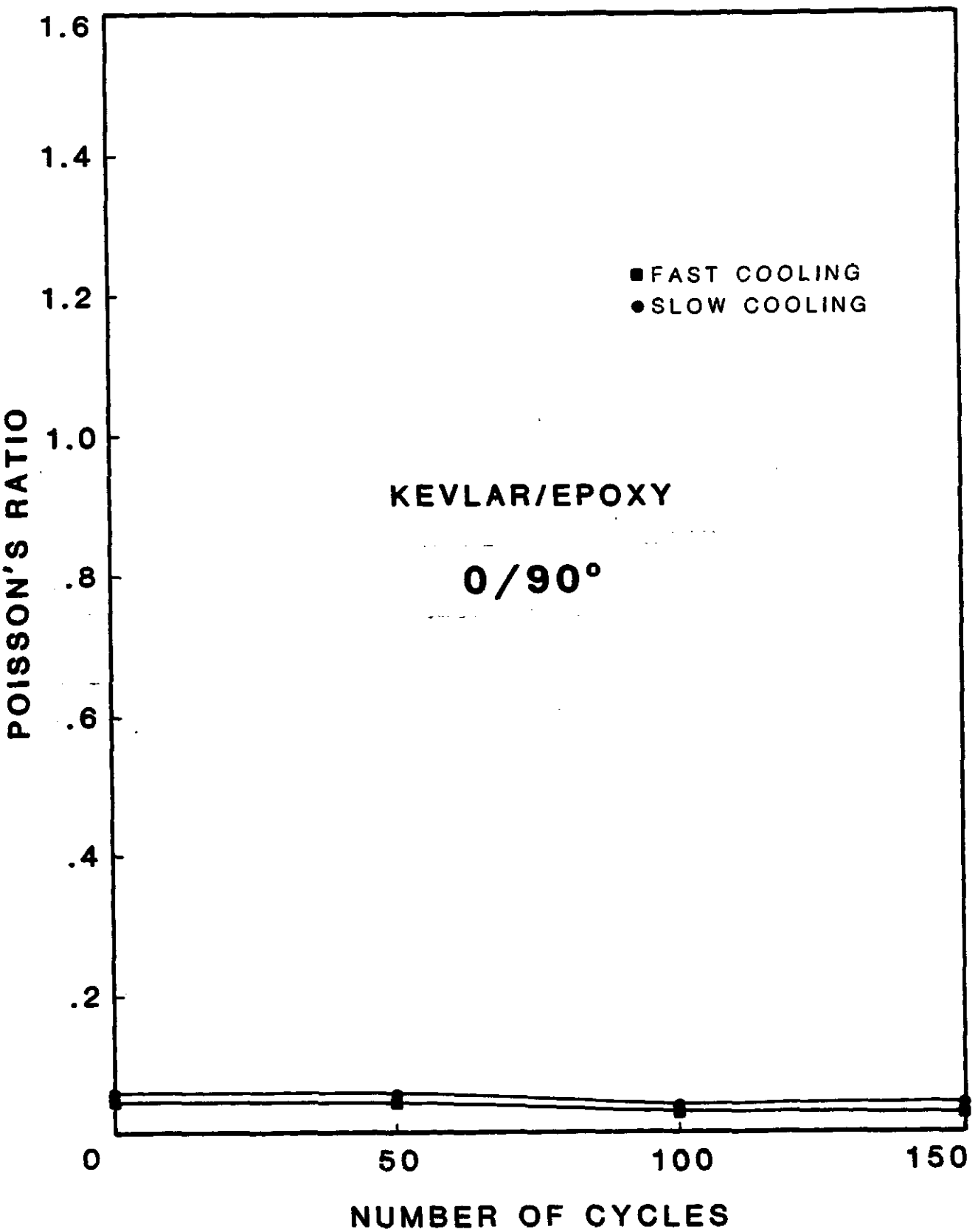

Figure 53. Poisson's Ratio vs. number of cycles for cross-ply Kevlar 49C/Rigidite 5216 Epoxy.

TABLE 54. POISSON'S RATIO VS. NUMBER OF CYCLES FOR CROSS-PLY E-GLASS/RIGIDITE 5216 EPOXY

NUMBER OF CYCLES	POISSON'S RATIO	
	FAST	SLOW
0	0.17	0.17
50	0.15	0.16
100	0.11	0.097
150	0.13	0.11

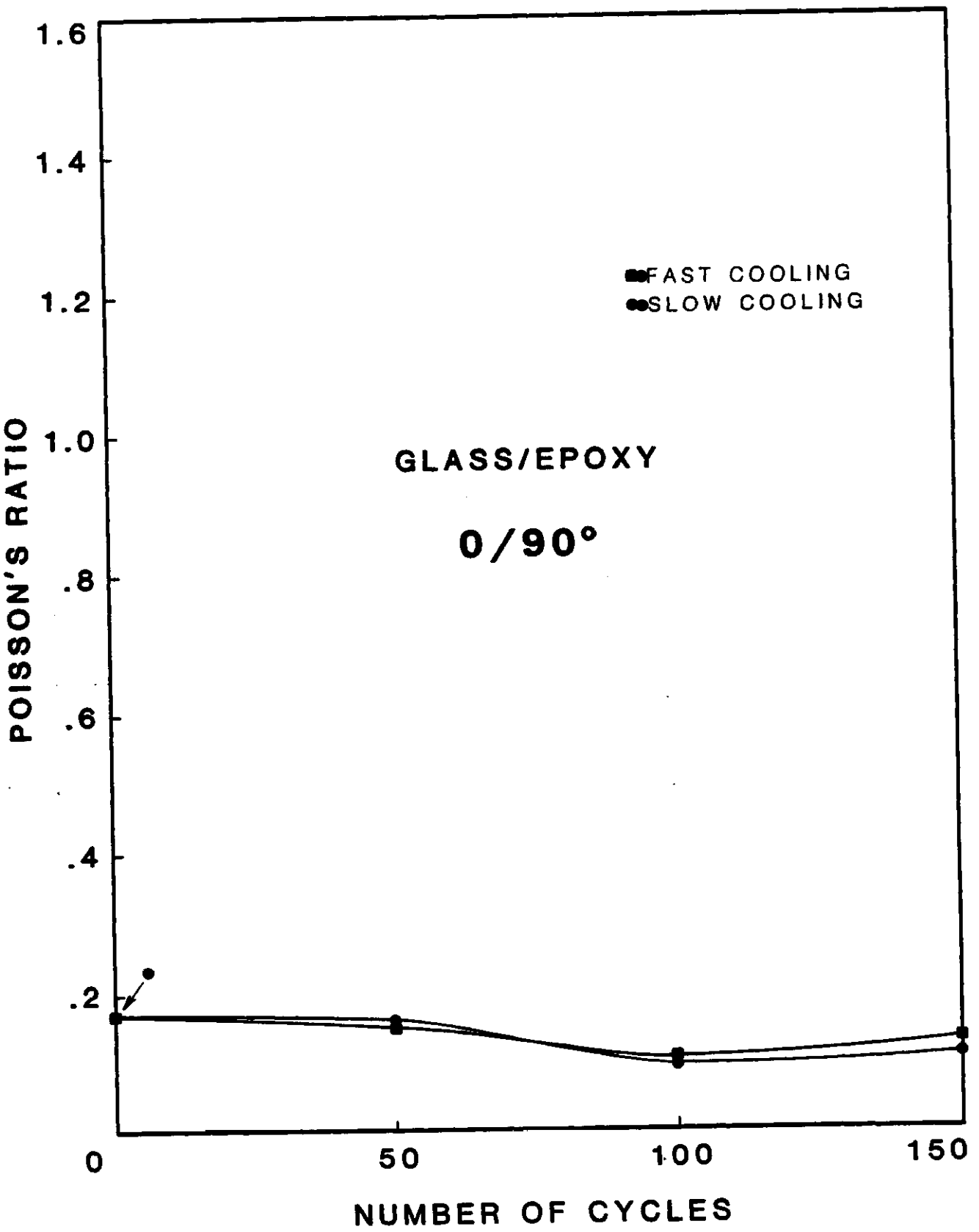

Figure 54. Poisson's Ratio vs. number of cycles for cross-ply E-Glass/Rigidite 5216 Epoxy.

TABLE 55. POISSON'S RATIO VS. NUMBER OF CYCLES FOR 15 DEGREES T300 GRAPHITE 5209 EPOXY

NUMBER OF CYCLES	POISSON'S RATIO	
	FAST	SLOW
0	1.09	0.98
50	1.08	0.72
100	**.**	0.25
150	**.**	0.21

. Invalid data due to malfunctions of measurement devices.

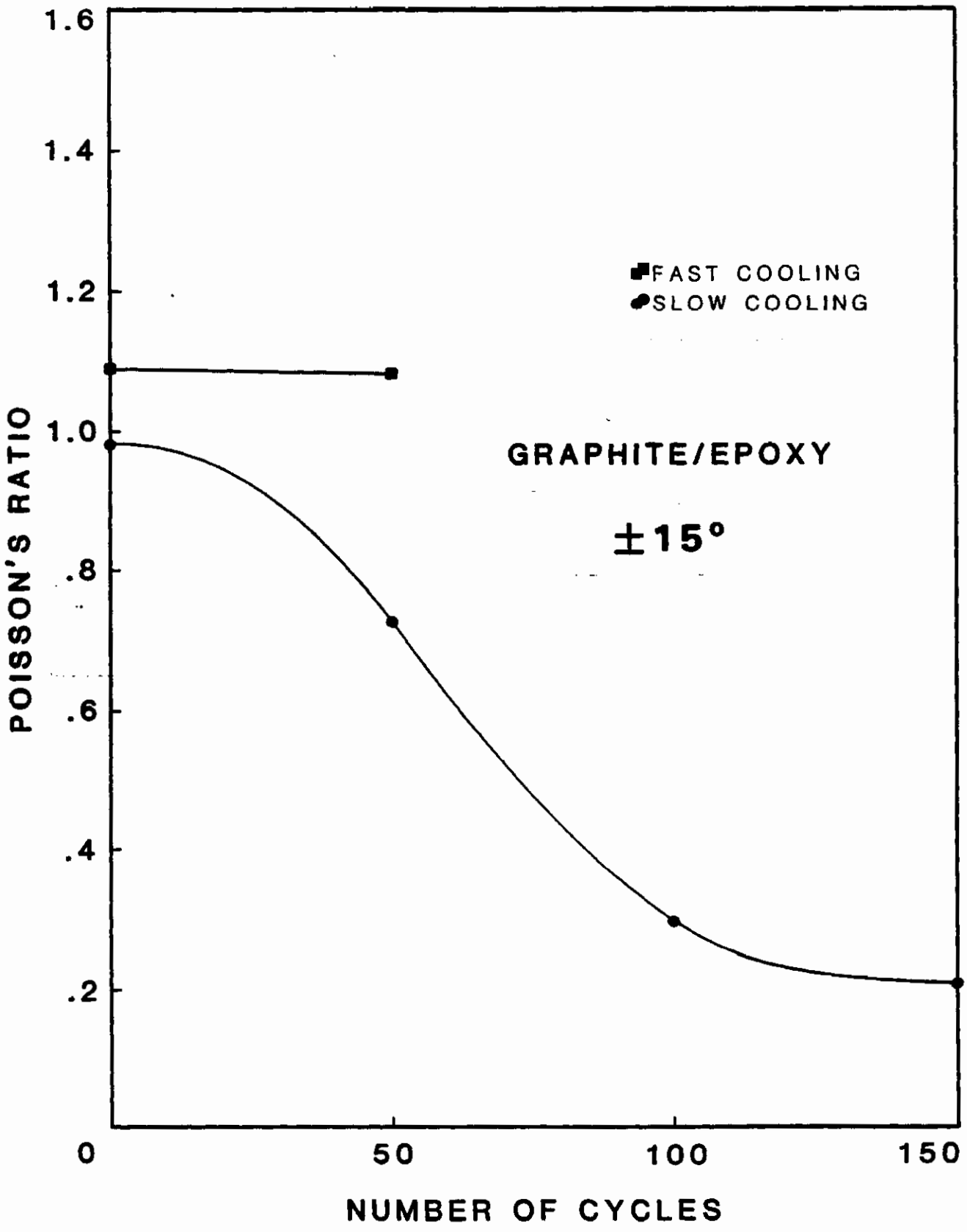

Figure 55. Poisson's Ratio vs. number of cycles for 15° T300 Graphite/Rigidite 5209 Epoxy.

TABLE 56. POISSON'S RATIO VS. NUMBER OF CYCLES FOR 15 DEGREE KEVLAR 49C/RIGIDITE 5216 EPOXY

NUMBER OF CYCLES	POISSON'S RATIO	
	FAST	SLOW
0	1.14	1.09
50	1.12	1.17
100	0.78	0.79
150	0.82	0.83

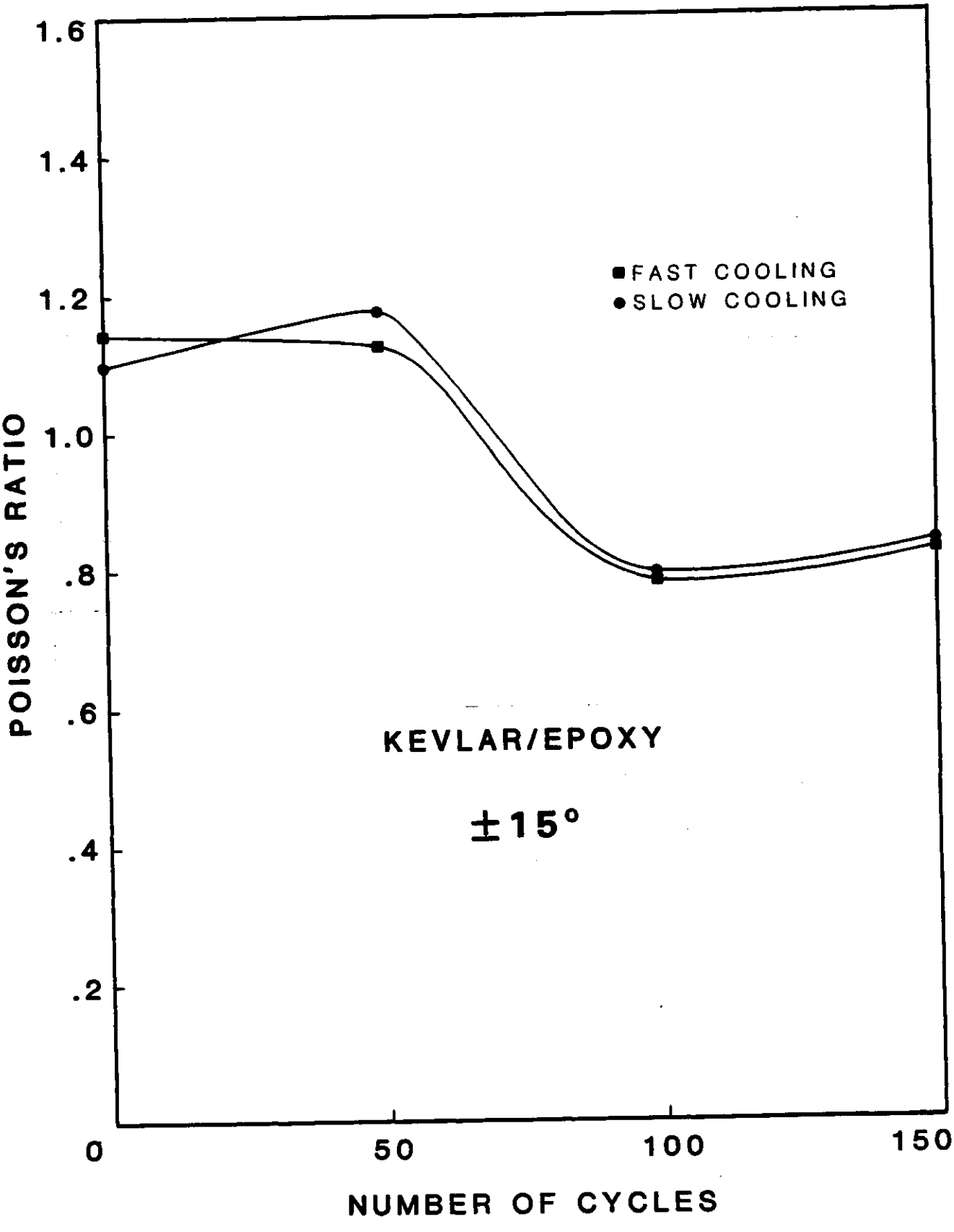

Figure 56. Poisson's Ratio vs. number of cycles for 15^{o} Kevlar 49C/Rigidite 5216 Epoxy.

TABLE 57. POISSON'S RATIO VS. NUMBER OF CYCLES FOR 15 DEGREE E-GLASS/RIGIDITE 5216 EPOXY

NUMBER OF CYCLES	POISSON'S RATIO	
	FAST	SLOW
0	0.37	0.39
50	0.39	0.41
100	0.25	0.28
150	0.32	0.35

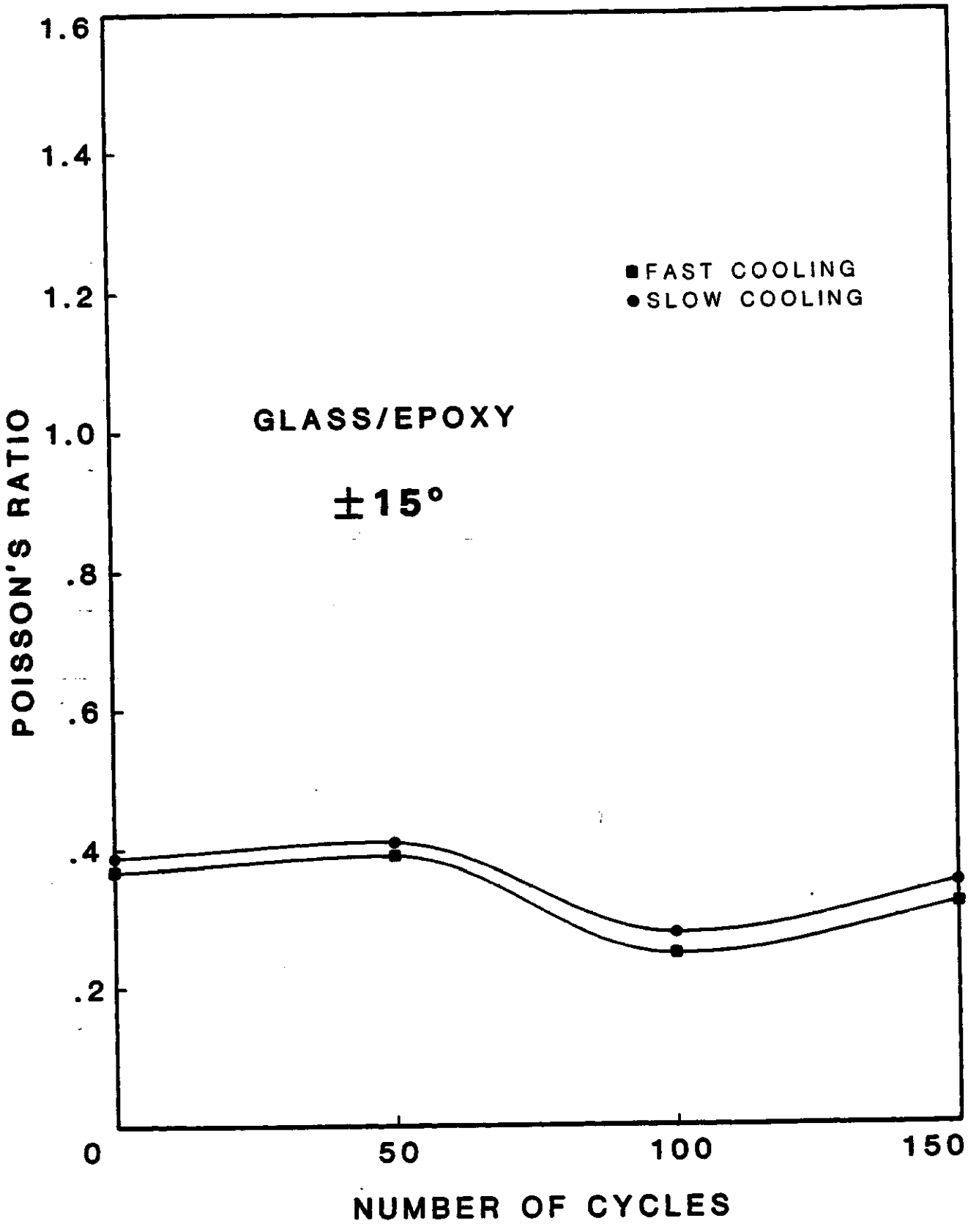

Figure 57. Poisson's Ratio vs. number of cycles for 15^{o} E-Glass/Rigidite 5216 Epoxy.

TABLE 58. POISSON'S RATIO VS. NUMBER OF CYCLES FOR 30 DEGREE T300 GRAPHITE/RIGIDITE 5209 EPOXY

NUMBER OF CYCLES	POISSON'S RATIO	
	FAST	SLOW
0	1.44	1.53
50	1.05	1.38
100	1.04	1.09
150	1.22	1.21

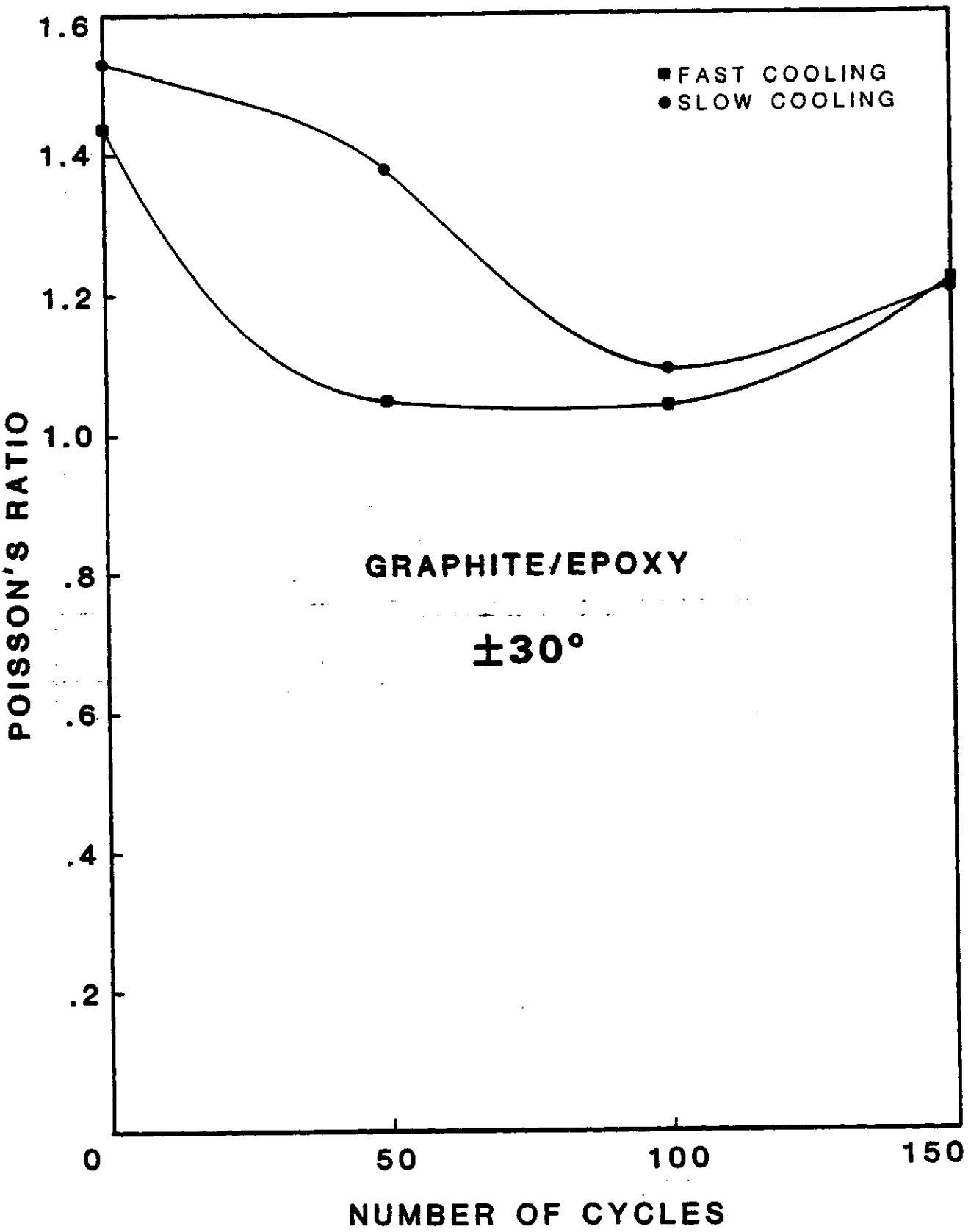

Figure 58. Poisson's Ratio vs. number of cycles for 30^{o} T300 Graphite/Rigidite 5209 Epoxy.

TABLE 59. POISSON'S RATIO VS. NUMBER OF CYCLES FOR 30 DEGREE KEVLAR 49C/RIGIDITE 5216 EPOXY

NUMBER OF CYCLES	POISSON'S RATIO	
	FAST	SLOW
0	1.34	1.46
50	1.44	1.41
100	1.09	0.95
150	0.99	1.01

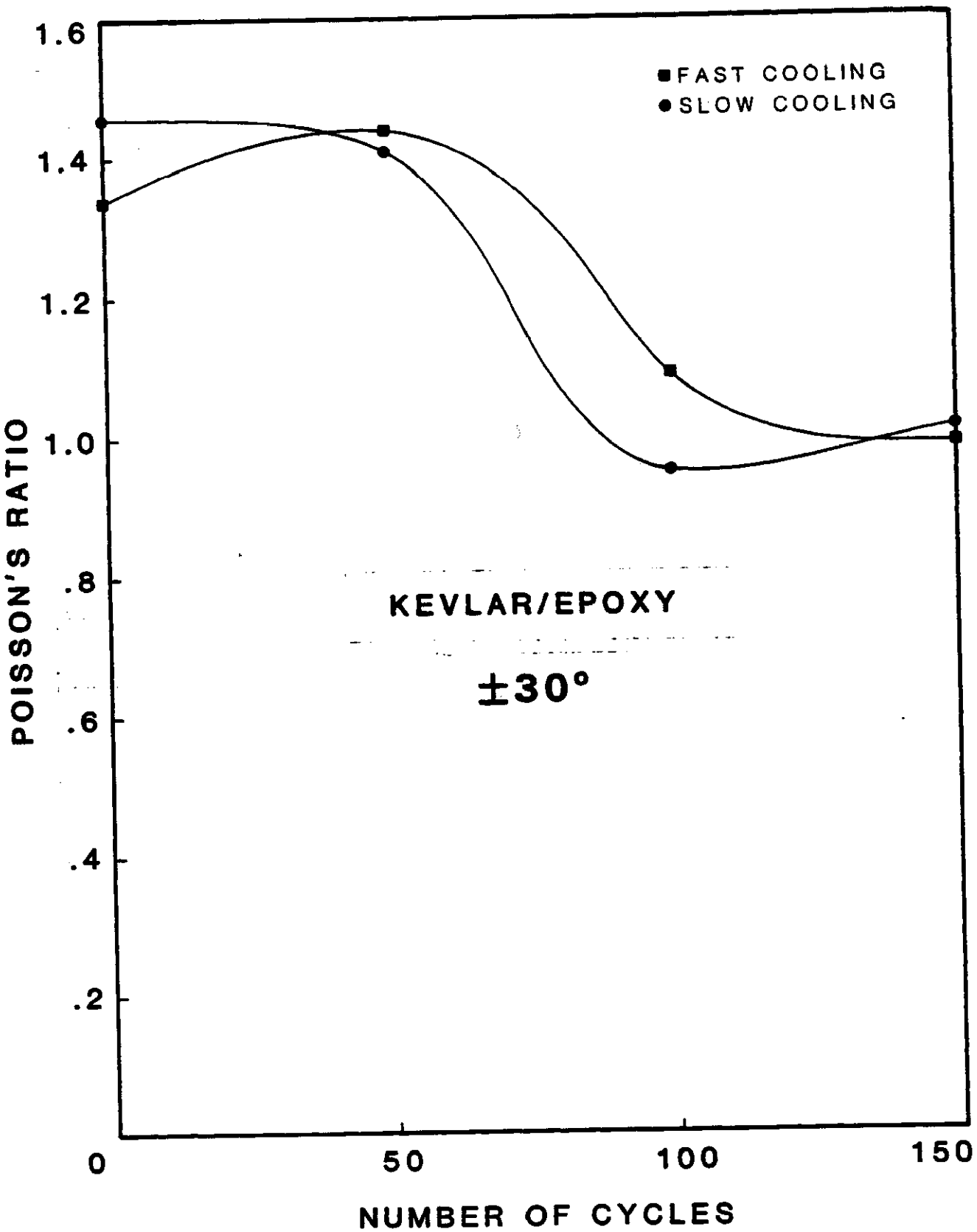

Figure 59. Poisson's Ratio vs. number of cycles for 30^{o} Kevlar 49C/Rigidite 5216 Epoxy.

TABLE 60. POISSON'S RATIO VS. NUMBER OF CYCLES FOR 30 DEGREE E-GLASS/RIGIDITE 5216 EPOXY

NUMBER OF CYCLES	POISSON'S RATIO	
	FAST	SLOW
0	0.67	0.65
50	0.62	0.65
100	0.36	0.47
150	0.54	**.**

. Invalid data due to malfunctions of measurement devices.

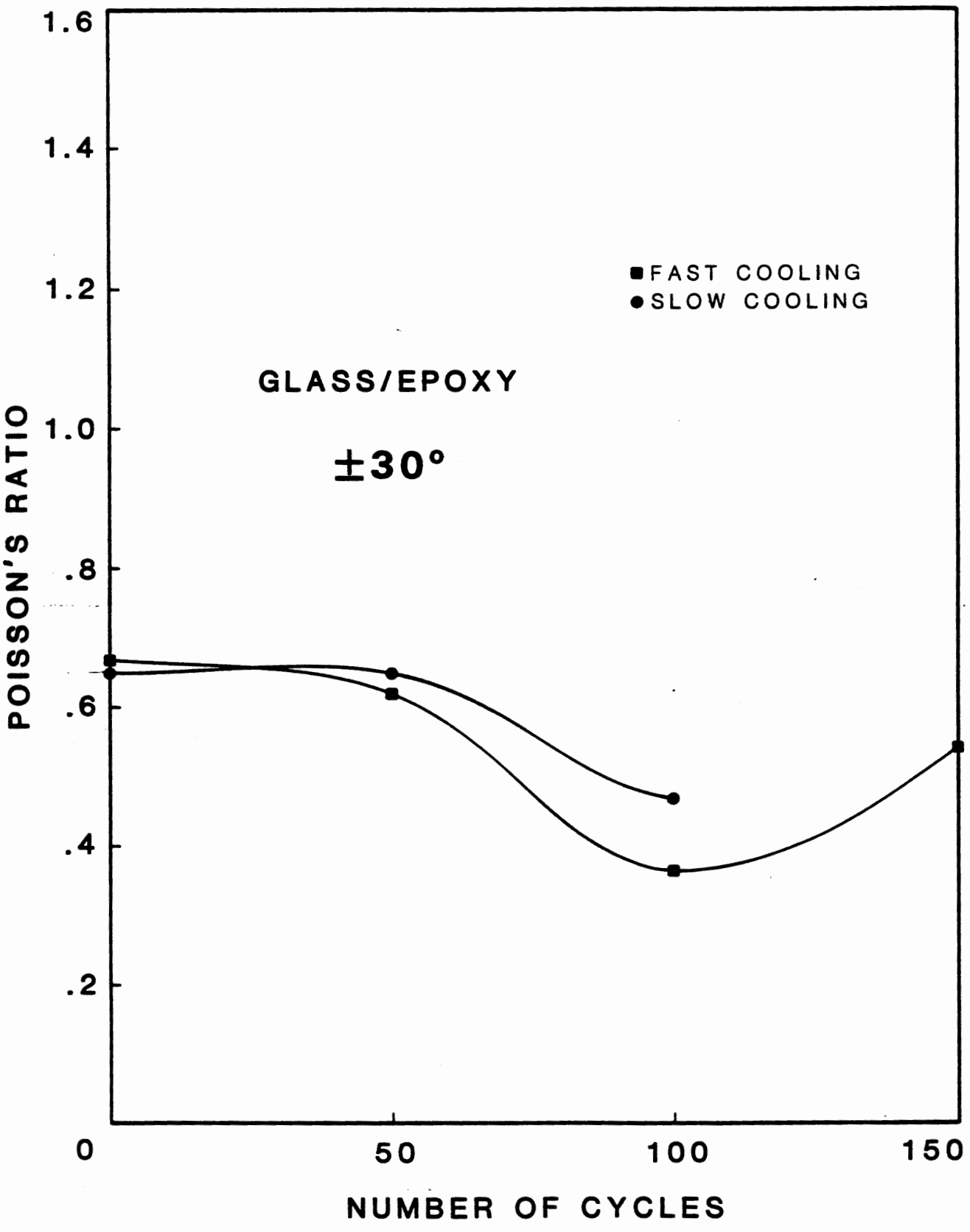

Figure 60. Poisson's Ratio vs. number of cycles for 30^{o} E-Glass/Rigidite 5216 Epoxy.

TABLE 61. POISSON'S RATIO VS. NUMBER OF CYCLES FOR 45 DEGREE T300 GRAPHITE/RIGIDITE 5209 EPOXY

NUMBER OF CYCLES	POISSON'S RATIO	
	FAST	SLOW
0	0.98	0.79
50	0.92	0.82
100	0.62	0.65
150	0.75	0.59

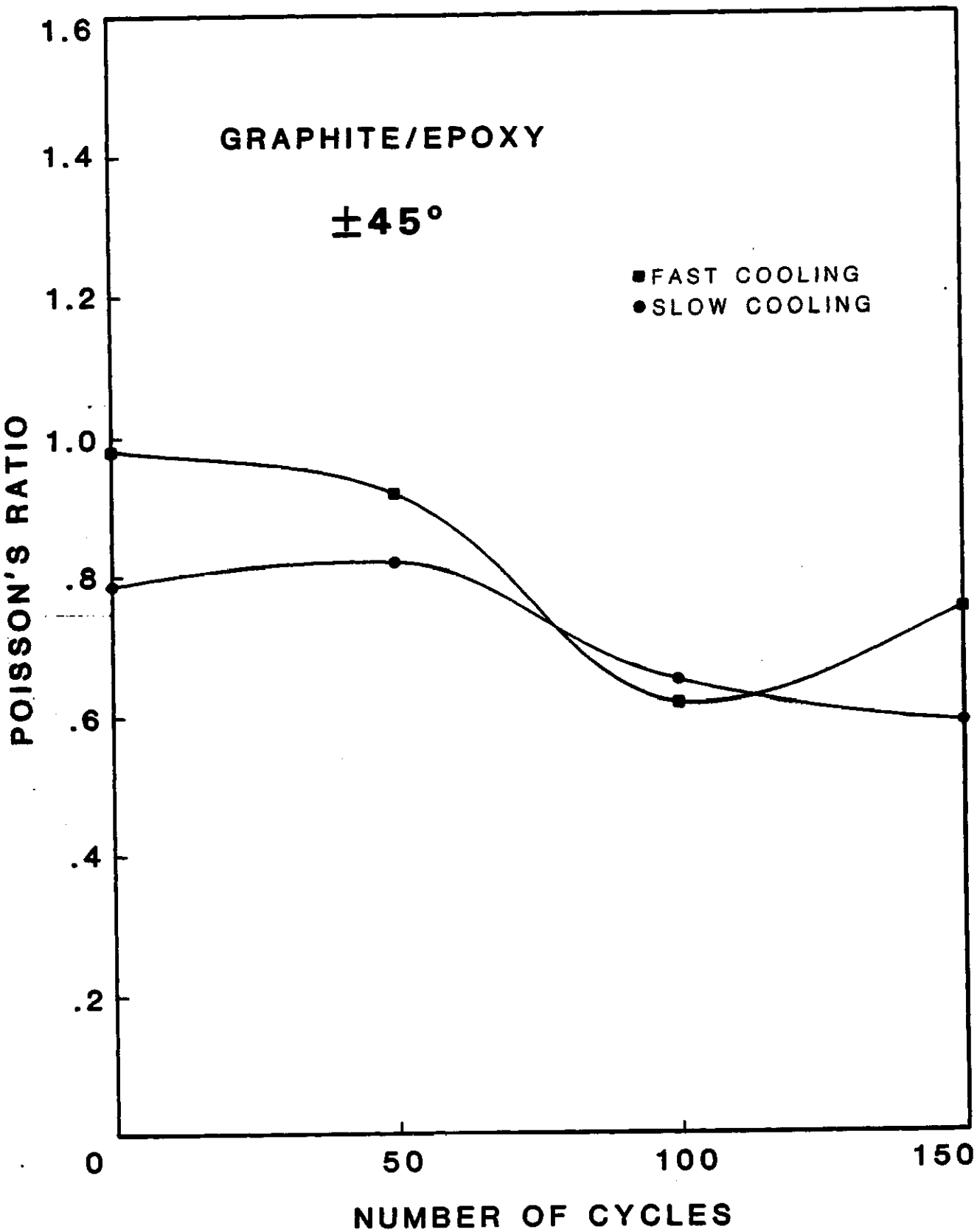

Figure 61. Poisson's Ratio vs. number of cycles for 45° T300 Graphite/Rigidite 5209 Epoxy.

TABLE 62. POISSON'S RATIO VS. NUMBER OF CYCLES FOR 45 DEGREE KEVLAR 49C/RIGIDITE 5216 EPOXY

NUMBER OF CYCLES	POISSON'S RATIO FAST	SLOW
0	0.82	0.98
50	0.83	0.93
100	0.61	0.69
150	0.64	0.66

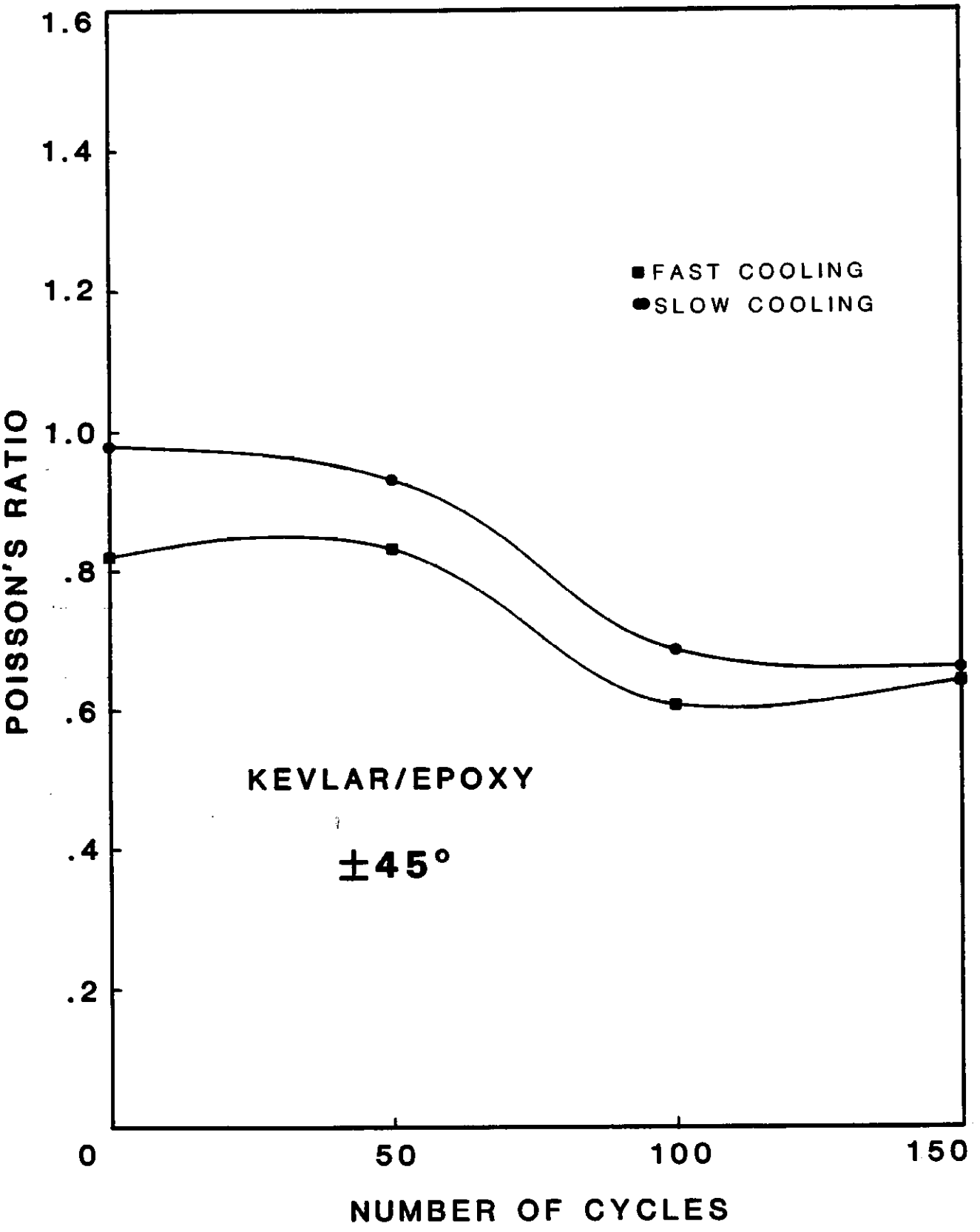

Figure 62. Poisson's Ratio vs. number of cycles for 45° Kevlar 49C/Rigidite 5216 Epoxy.

TABLE 63. POISSON'S RATIO VS. NUMBER OF CYCLES FOR 45 DEGREE E-GLASS/RIGIDITE 5216 EPOXY

NUMBER OF CYCLES	POISSON'S RATIO	
	FAST	SLOW
0	0.83	0.59
50	0.74	0.55
100	0.59	0.40
150	0.60	0.57

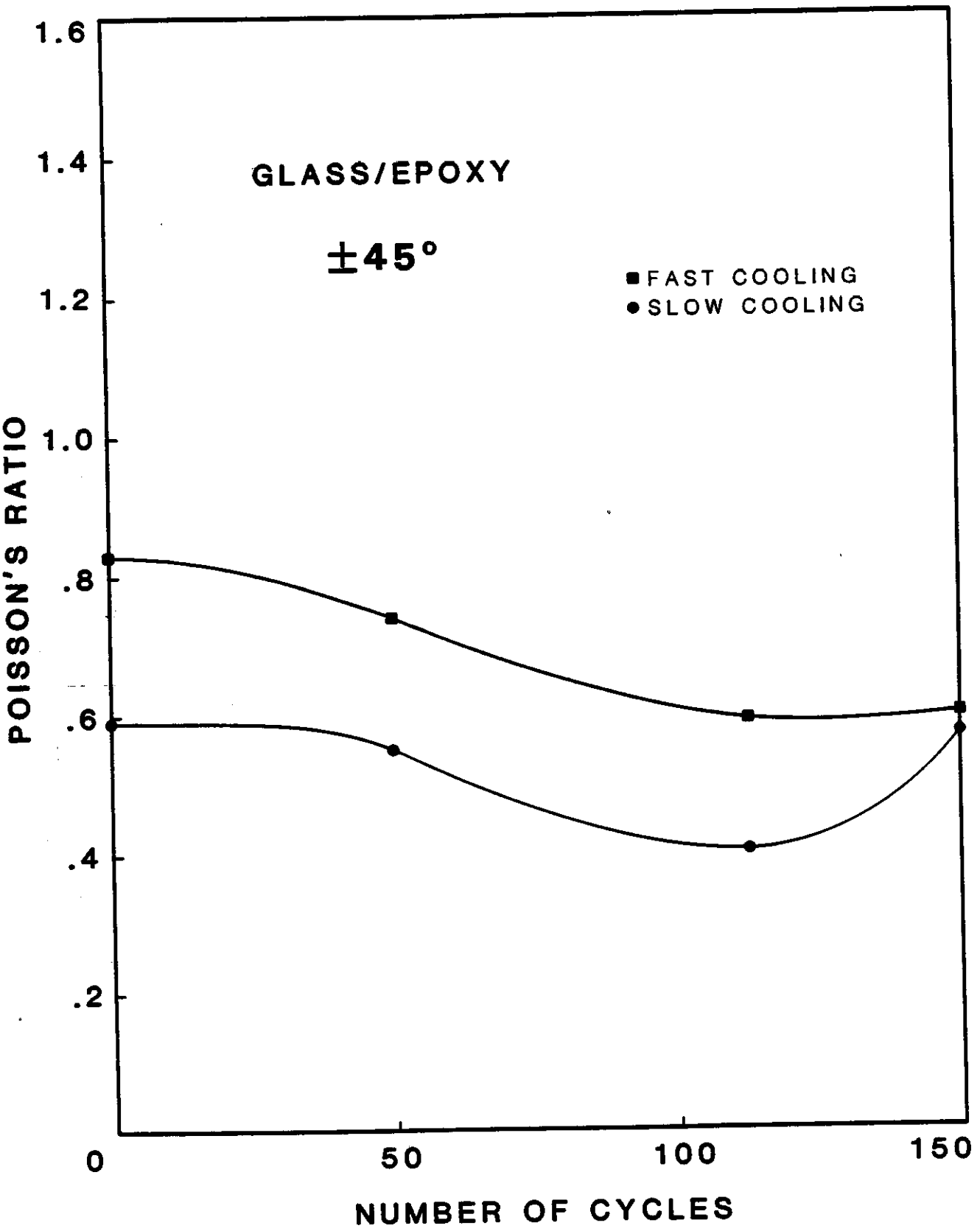

Figure 63. Poisson's Ratio vs. number of cycles for 45° E-Glass/Rigidite 5216 Epoxy.

TABLE 64. POISSON'S RATIO VS. NUMBER OF CYCLES FOR 60 DEGREE T300 GRAPHITE/RIGIDITE 5209 EPOXY

NUMBER OF CYCLES	POISSON'S RATIO	
	FAST	SLOW
0	0.40	0.19
50	0.36	0.27
100	0.30	0.24
150	0.28	0.23

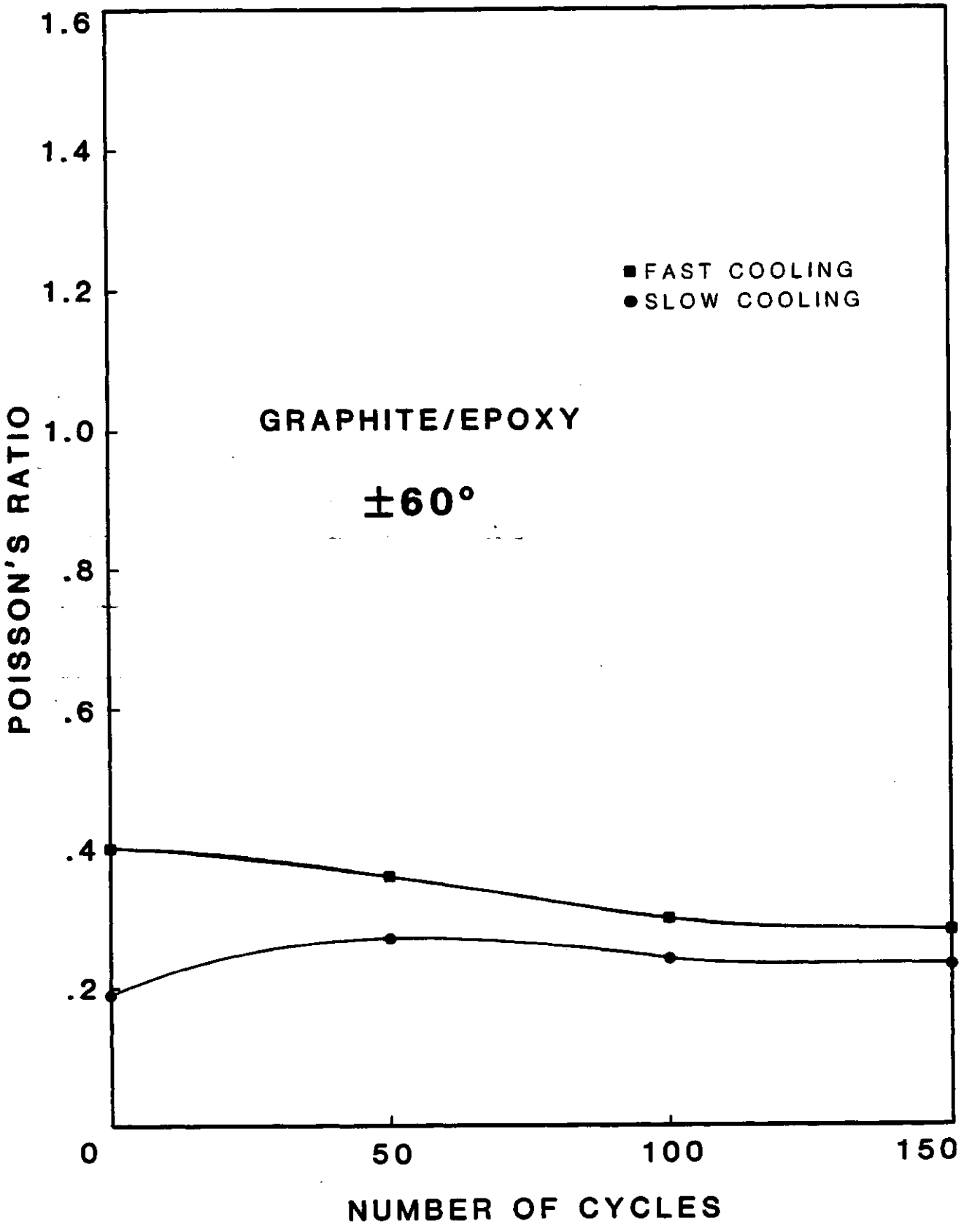

Figure 64. Poisson's Ratio vs. number of cycles for 60^{o} T300 Graphite/Rigidite 5209 Epoxy.

TABLE 65. POISSON'S RATIO VS. NUMBER OF CYCLES FOR 60 DEGREE KEVLAR 49C/RIGIDITE 5216 EPOXY

NUMBER OF CYCLES	POISSON'S RATIO	
	FAST	SLOW
0	0.35	0.28
50	0.33	0.33
100	0.27	0.25
150	0.25	0.35

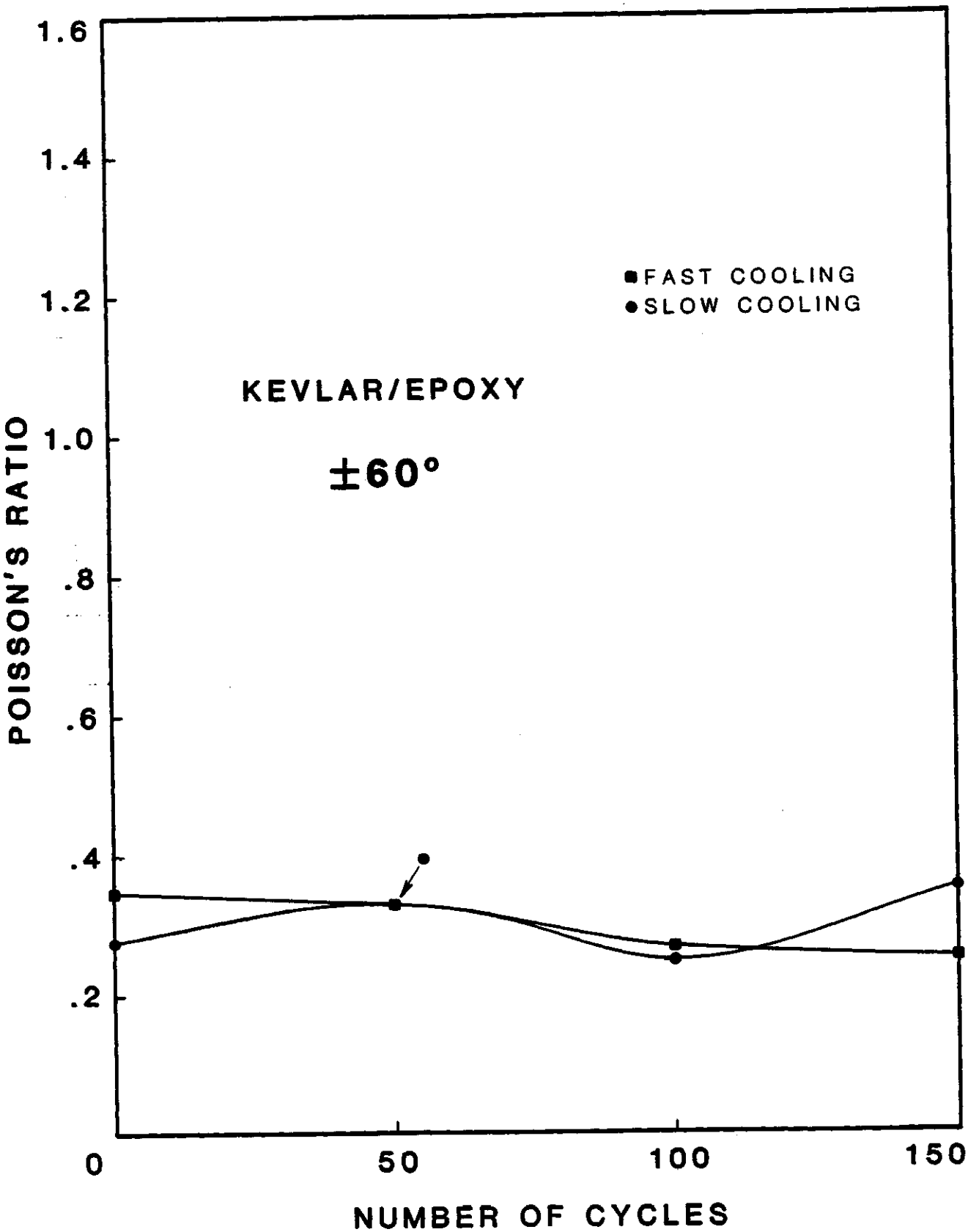

Figure 65. Poisson's Ratio vs. number of cycles for 60^{o} Kevlar 49C/Rigidite 5216 Epoxy.

TABLE 66. POISSON'S RATIO VS. NUMBER OF CYCLES FOR 60 DEGREE E-GLASS/RIGIDITE 5216 EPOXY

NUMBER OF CYCLES	POISSON'S RATIO	
	FAST	SLOW
0	0.35	0.22
50	0.36	0.32
100	0.27	0.29
150	0.33	0.35

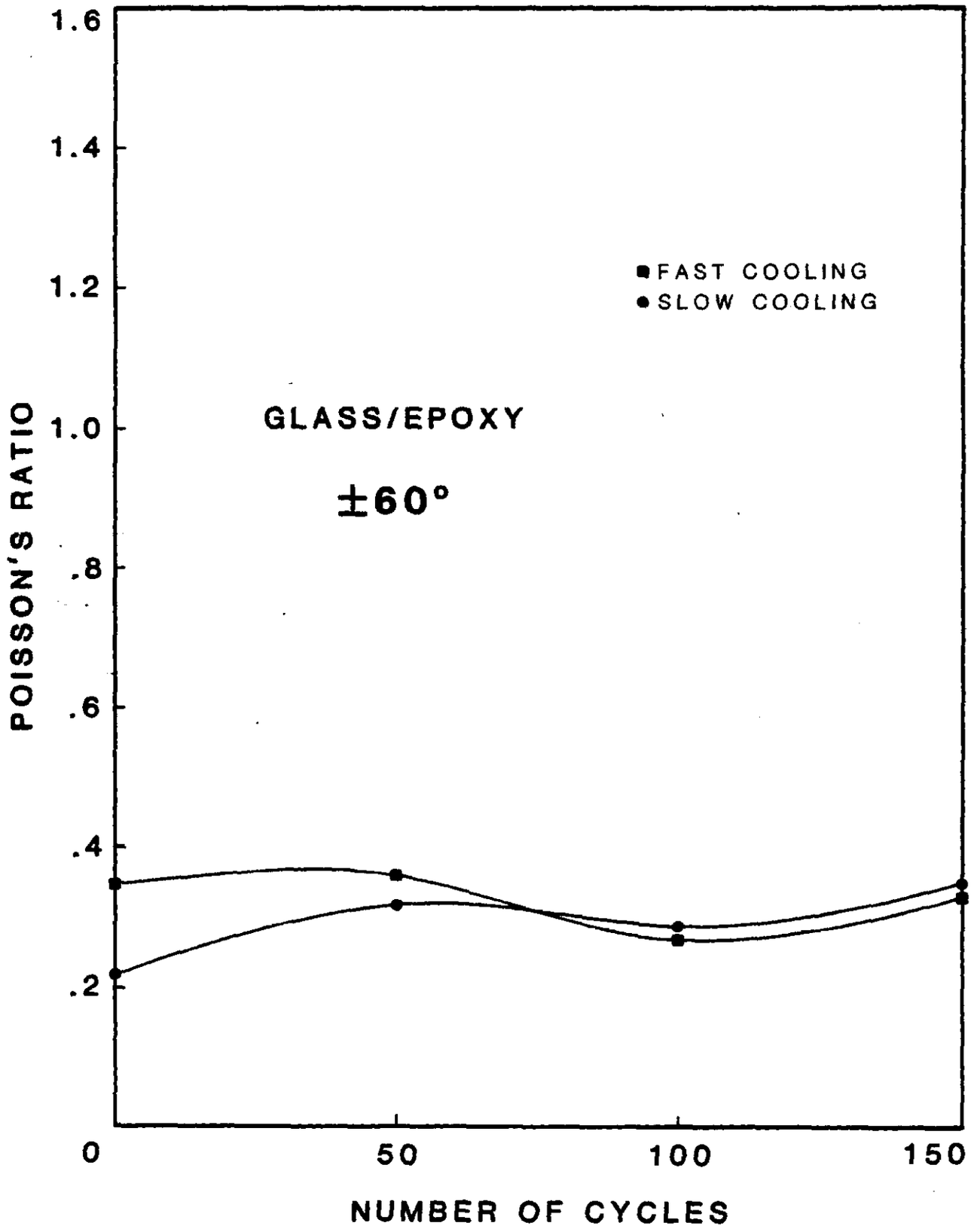

Figure 66. Poisson's Ratio vs. number of cycles for 60° E-Glass/Rigidite 5216 Epoxy.

TABLE 67. POISSON'S RATIO VS. NUMBER OF CYCLES FOR 15 DEGREE T1 K-G-K HYBRID

NUMBER OF CYCLES	POISSON'S RATIO	
	FAST	SLOW
0	0.49	0.56
50	0.53	0.36
100	0.34	0.36
150	0.38	0.38

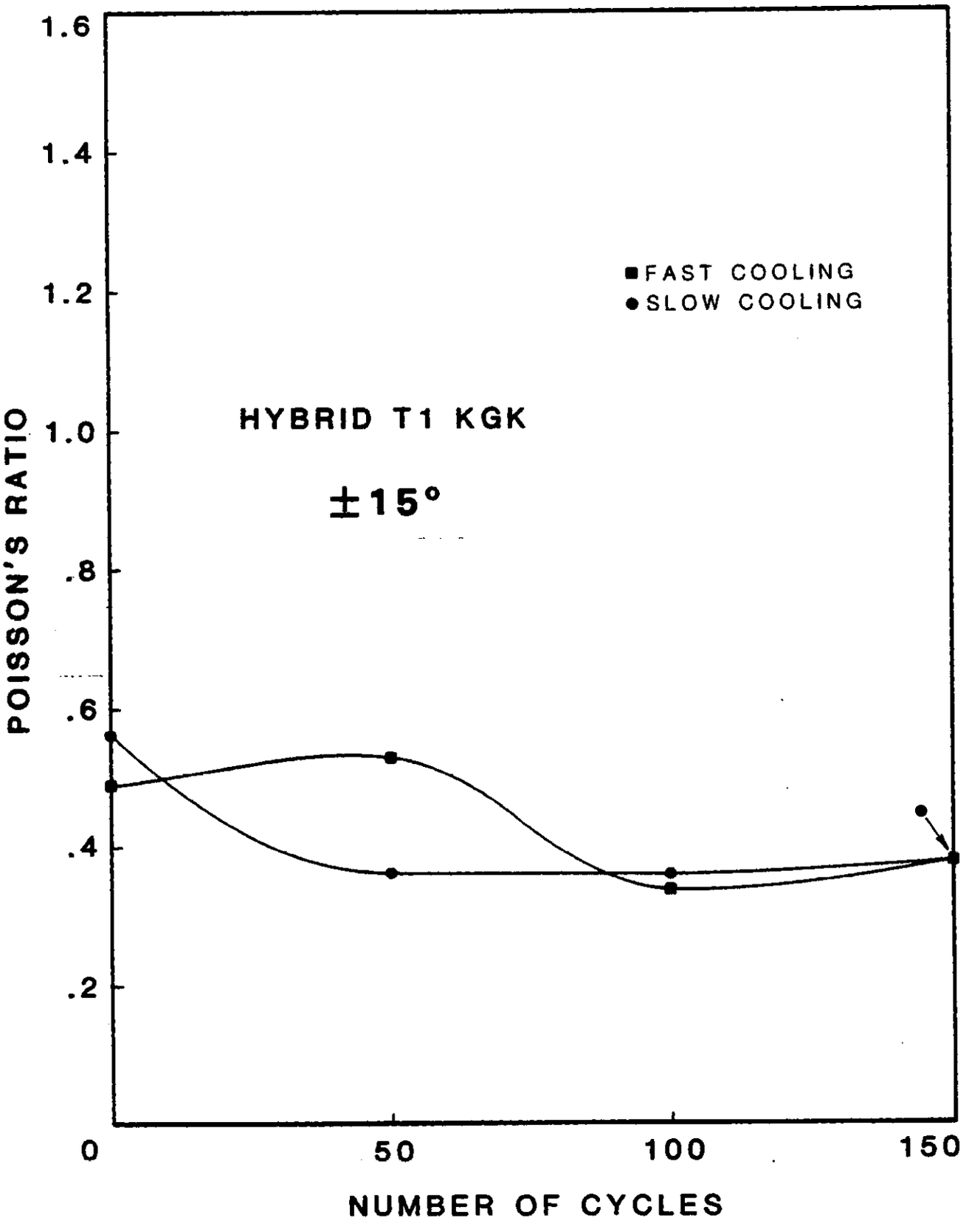

Figure 67. Poisson's Ratio vs. number of cycles for 15° T1 K-G-K Hybrid.

TABLE 68. POISSON'S RATIO VS. NUMBER OF CYCLES FOR 15 DEGREE T1 G-K-G HYBRID

NUMBER OF CYCLES	POISSON'S RATIO	
	FAST	SLOW
0	0.60	0.51
50	0.61	0.52
100	0.44	0.38
150	0.47	0.41

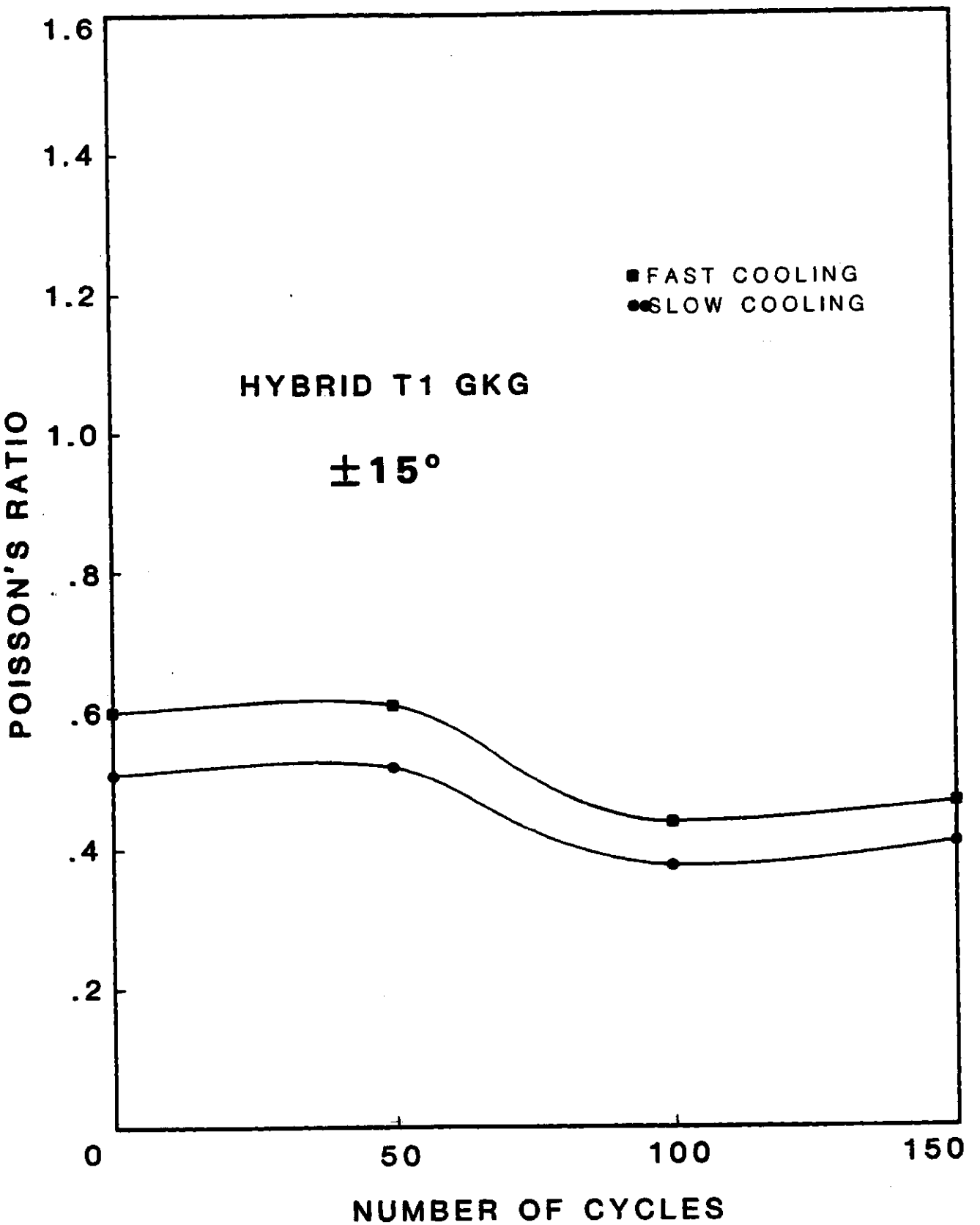

Figure 68. Poisson's Ratio vs. number of cycles for 15° T1 G-K-G Hybrid.

TABLE 69. POISSON'S RATIO VS. NUMBER OF CYCLES FOR 15 DEGREE T2 HYBRID

NUMBER OF CYCLES	POISSON'S RATIO	
	FAST	SLOW
0	0.66	0.52
50	0.53	0.55
100	0.38	0.45
150	0.40	0.38

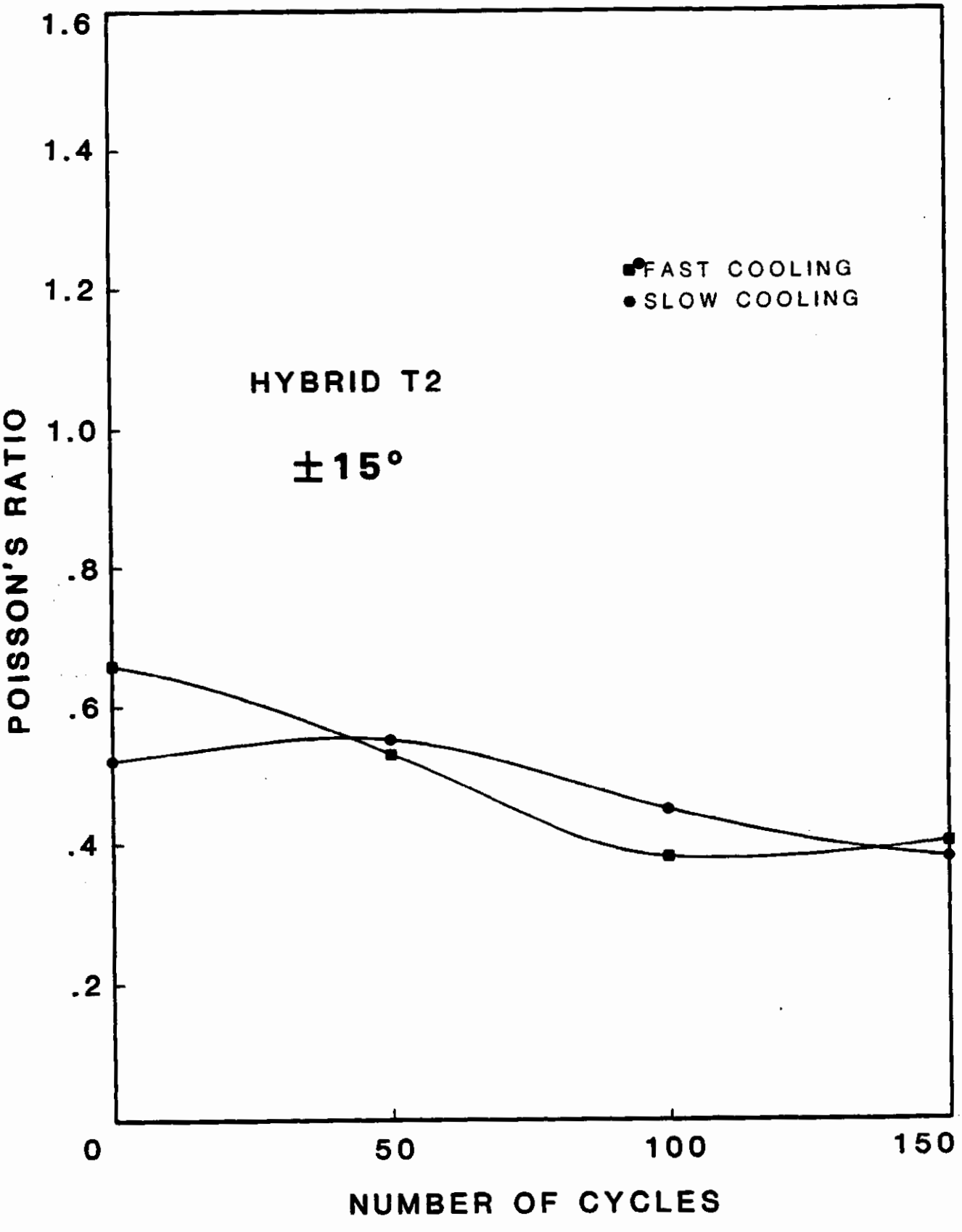

Figure 69. Poisson's Ratio vs. number of cycles for 15° T2 Hybrid.

TABLE 70. POISSON'S RATIO VS. NUMBER OF CYCLES FOR 45 DEGREE TI K-G-K HYBRID

NUMBER OF CYCLES	POISSON'S RATIO	
	FAST	SLOW
0	0.73	0.59
50	0.67	0.56
100	0.71	0.64
150	0.49	0.51

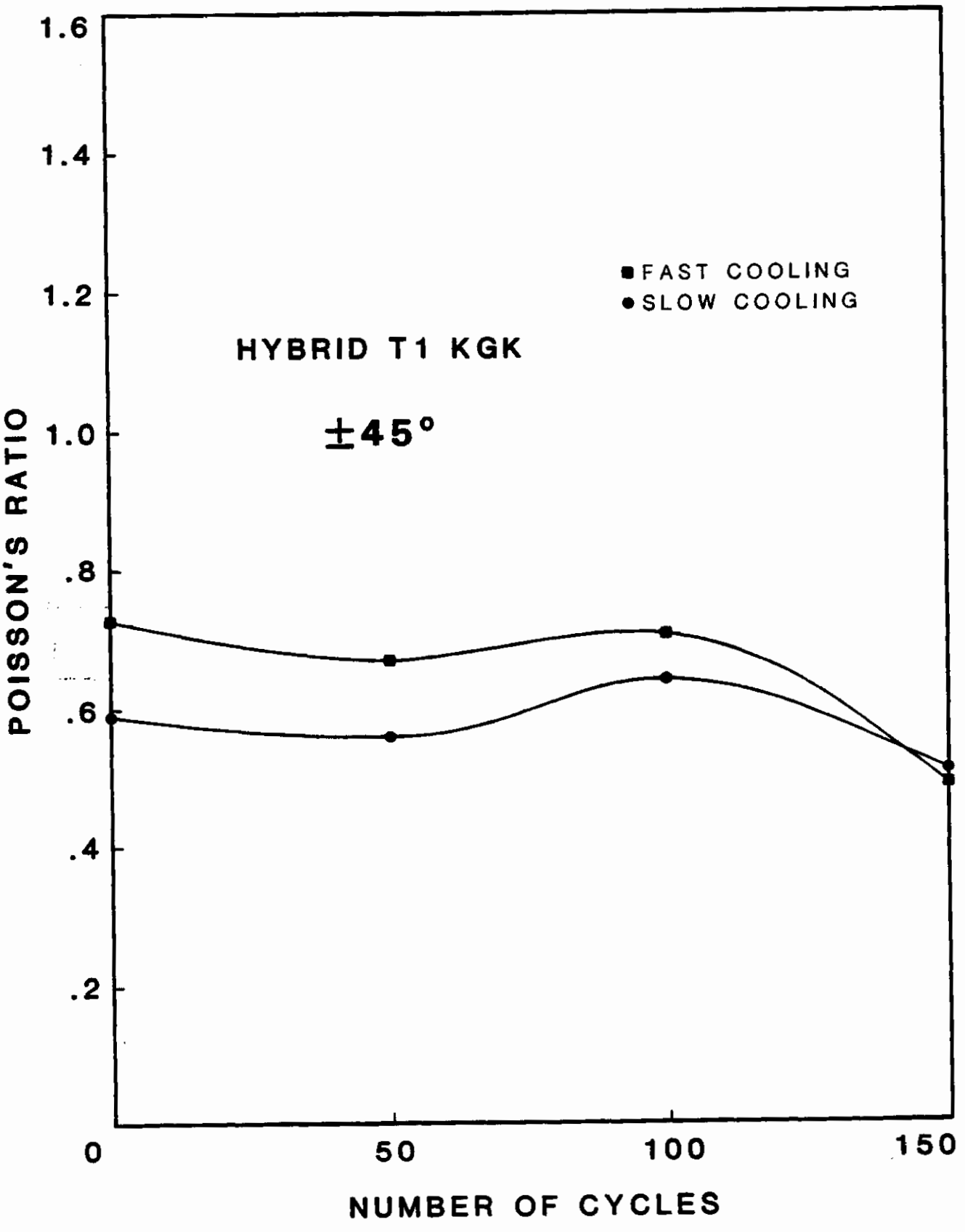

Figure 70. Poisson's Ratio vs. number of cycles for 45° T1 K-G-K Hybrid.

TABLE 71. POISSON'S RATIO VS. NUMBER OF CYCLES FOR 45 DEGREE T1 G-K-G HYBRID

NUMBER OF CYCLES	POISSON'S RATIO	
	FAST	SLOW
0	0.73	0.60
50	0.68	0.61
100	0.61	0.60
150	0.51	0.45

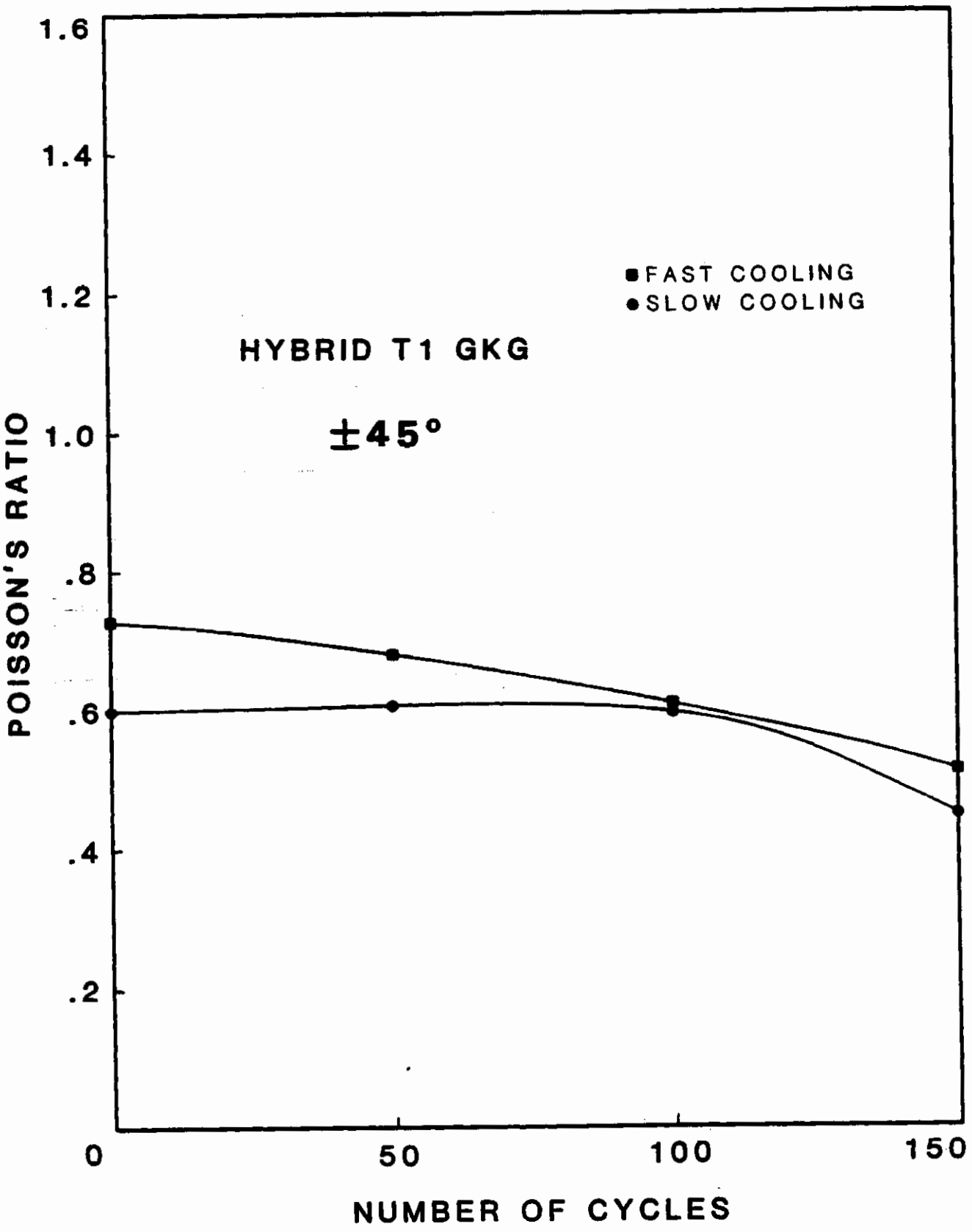

Figure 71. Poisson's Ratio vs. number of cycles for 45° T1 G-K-G Hybrid.

TABLE 72. POISSON'S RATIO VS. NUMBER OF CYCLES FOR 45 DEGREE T2 HYBRID

NUMBER OF CYCLES	POISSON'S RATIO	
	FAST	SLOW
0	0.73	0.75
50	0.73	0.72
100	0.70	0.67
150	0.49	0.55

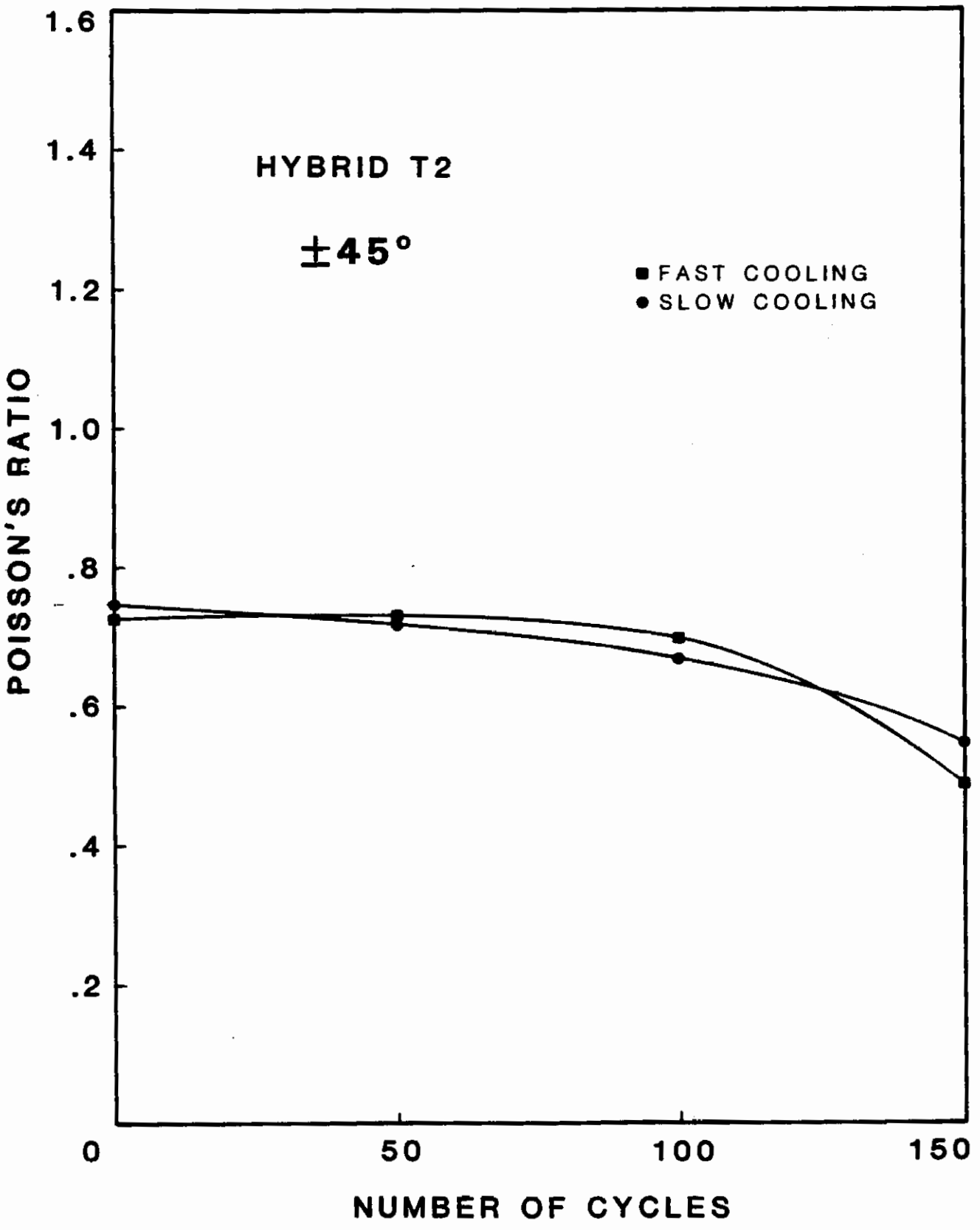

Figure 72. Poisson's Ratio vs. number of cycles for 45° T2 Hybrid.

TABLE 73. FRACTURE STRESS VS. PLY ANGLE: EXPERIMENTAL AND TSAI-HILL CRITERION FOR T300 GRAPHITE/RIGIDITE 5209 EPOXY

ANGLE	EXPERIMENTAL(PSI)	TSAI-HILL(PSI)
0	206300	206300
15	129040	33393
30	74056	16216
45	34743	10539
60	16256	8000
75	11380	6840
90	6500	6500

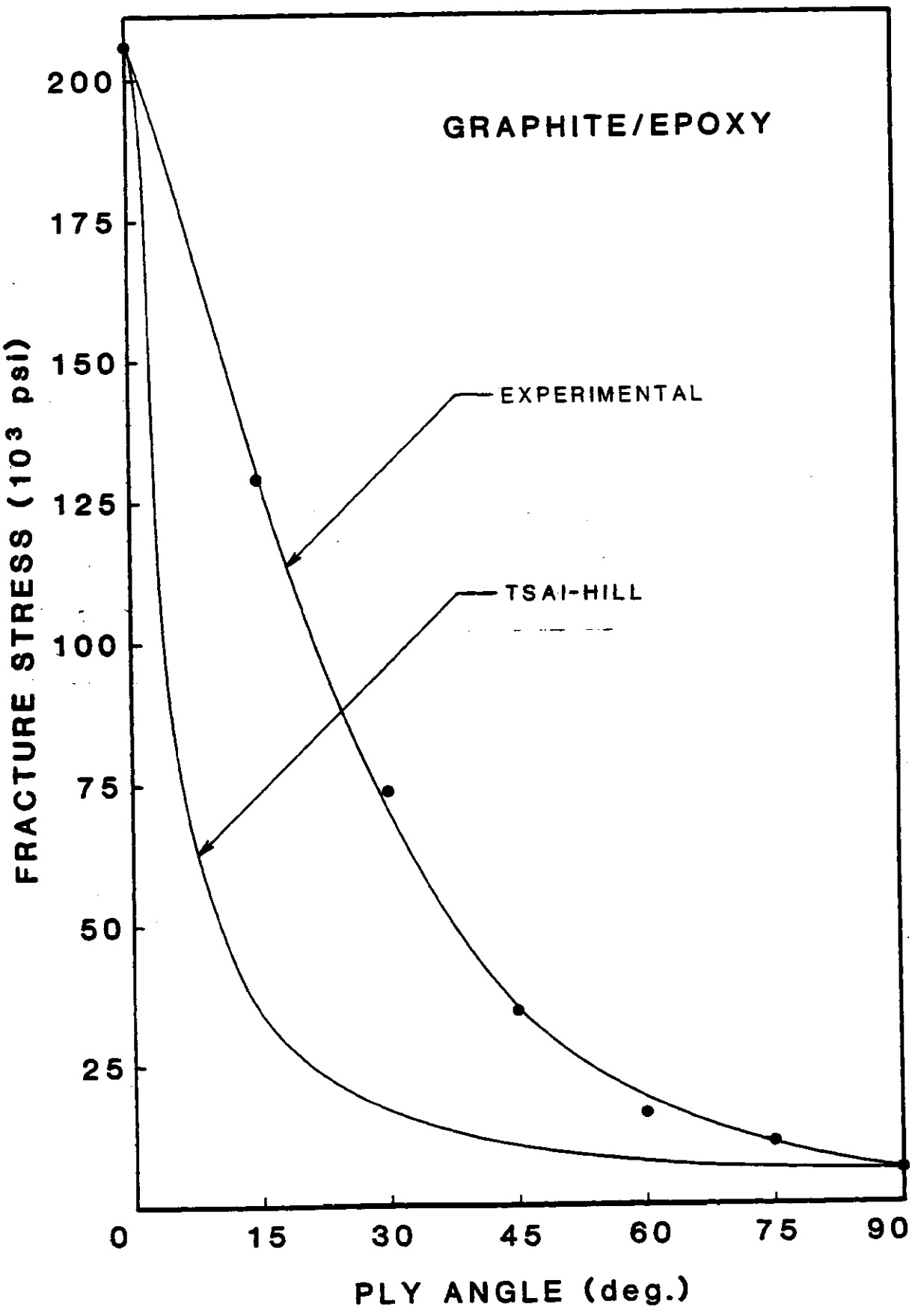

Figure 73. Fracture Strength vs. Ply Angle for T300 Graphite/Rigidite 5209 Epoxy.

TABLE 74. FRACTURE STRESS VS. PLY ANGLE: EXPERIMENTAL AND TSAI-HILL CRITERION FOR KEVLAR 49C/RIGIDITE 5216 EPOXY

ANGLE	EXPERIMENTAL(PSI)	TSAI-HILL(PSI)
0	189186	189186
15	101080	29944
30	66378	12694
45	25444	7418
60	7039	5275
75	4565	4360
90	4100	4100

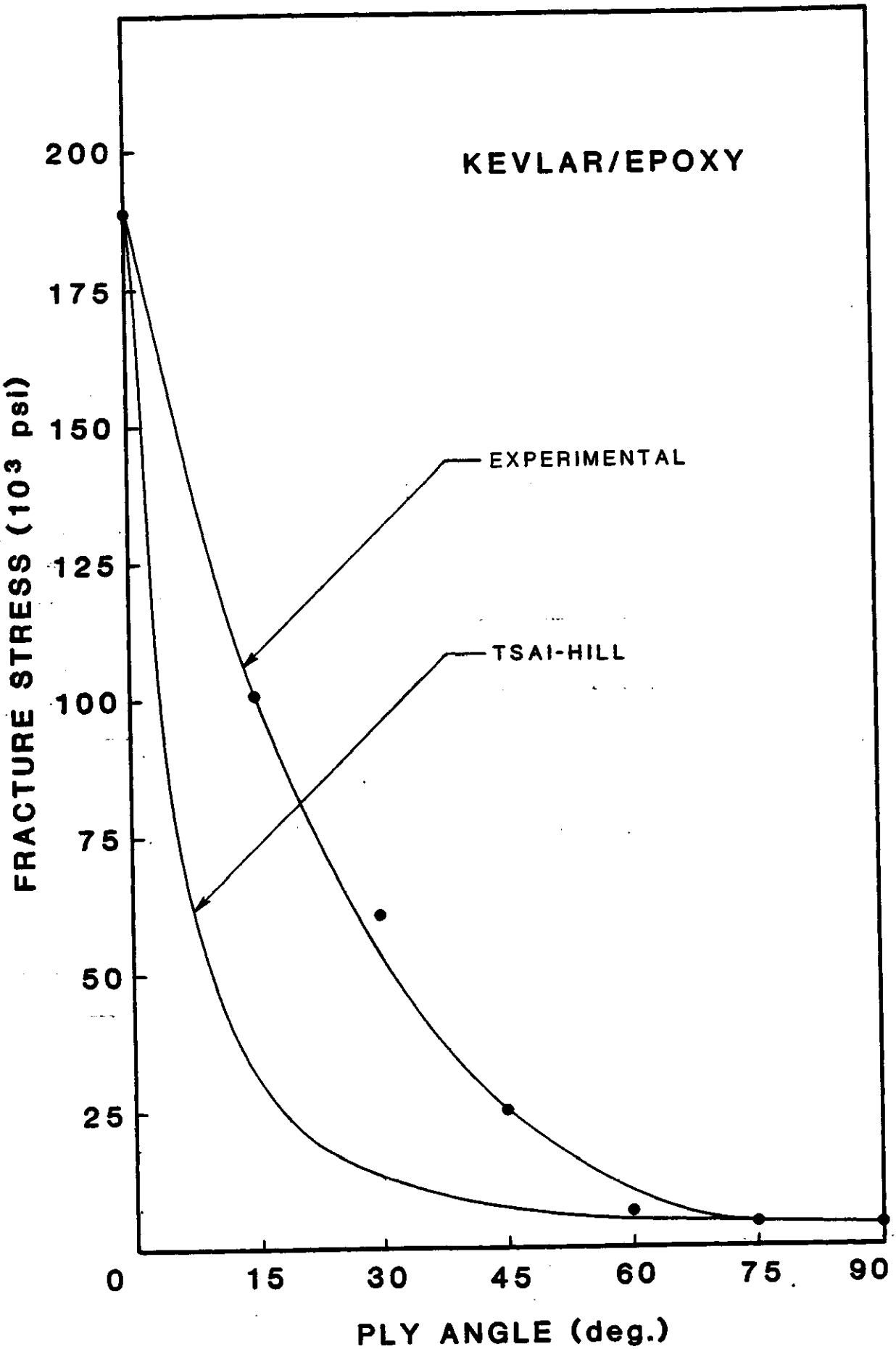

Figure 74. Fracture Strength vs. Ply Angle for Kevlar 49C/Rigidite 5216 Epoxy.

TABLE 75. FRACTURE STRESS VS. PLY ANGLE: EXPERIMENTAL AND TSAI-HILL CRITERION FOR E-GLASS/RIGIDITE 5216 EPOXY

ANGLE	EXPERIMENTAL(PSI)	TSAI-HILL (PSI)
0	212237	212237
15	99148	44863
30	71703	22731
45	31366	15364
60	13397	12017
75	11039	10461
90	10000	10000

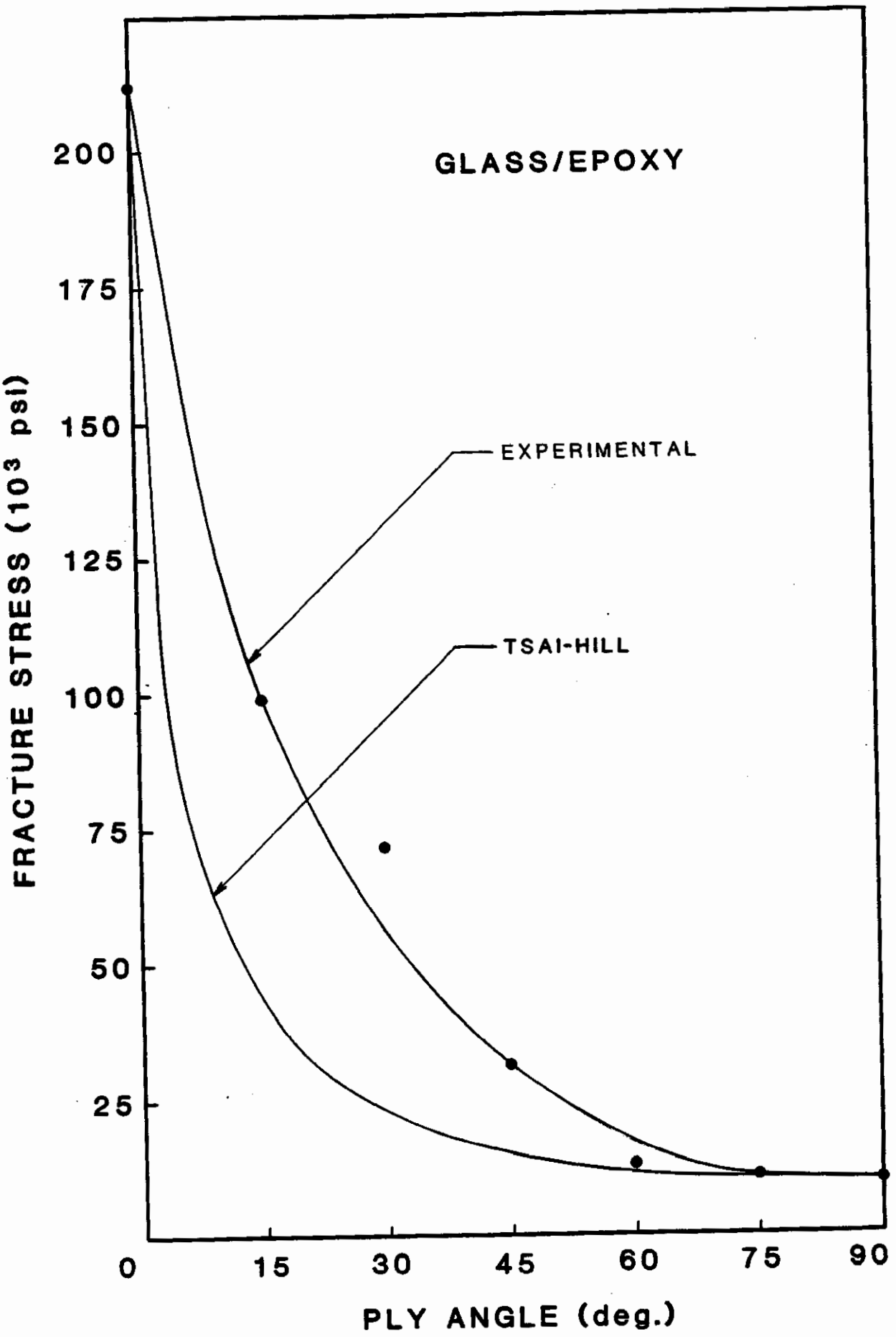

Figure 75. Fracture Strength vs. Ply Angle for E-Glass/ Rigidite 5216 Epoxy.

TABLE 76. SHEAR DISTORTION COEFFICIENT (M_1) VS. PLY ANGLE

ANGLE	GRAPHITE	KEVLAR	GLASS
	M_1	M_1	M_1
0	0	0	0
15	7.874	8.514	2.376
30	10.890	11.632	2.838
45	8.240	8.517	1.263
60	3.383	3.121	-0.651
75	0.367	0.003	-1.113
90	0	0	0

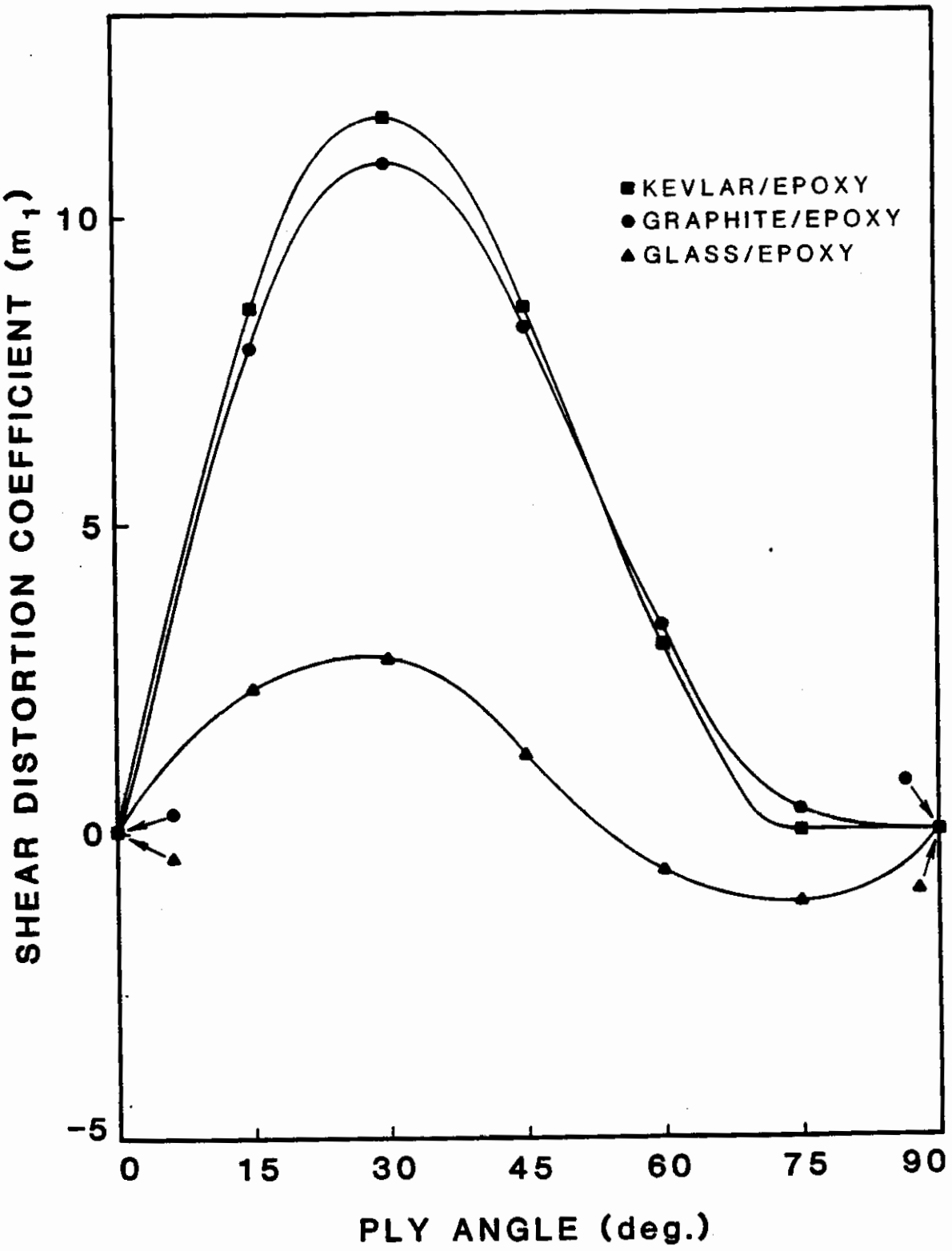

Figure 76. Shear Distortion Coefficient vs. Ply Angle for T300 Graphite/Rigidite 5209 Epoxy, Kevlar 49C/ Rigidite 5216 Epoxy, and E-Glass/Rigidite 5216 Epoxy.

TABLE 77. FRACTURE IN-PLANE SHEAR STRESS VS. PLY ANGLE

ANGLE	GRAPHITE(PSI	KEVLAR(PSI	GLASS(PSI)
0	0	0	0
15	31550	24850	20967
30	34266	31127	28240
45	14911	10895	7629
60	2337	866	-1210
75	130	0.4	-1094
90	0	0	0

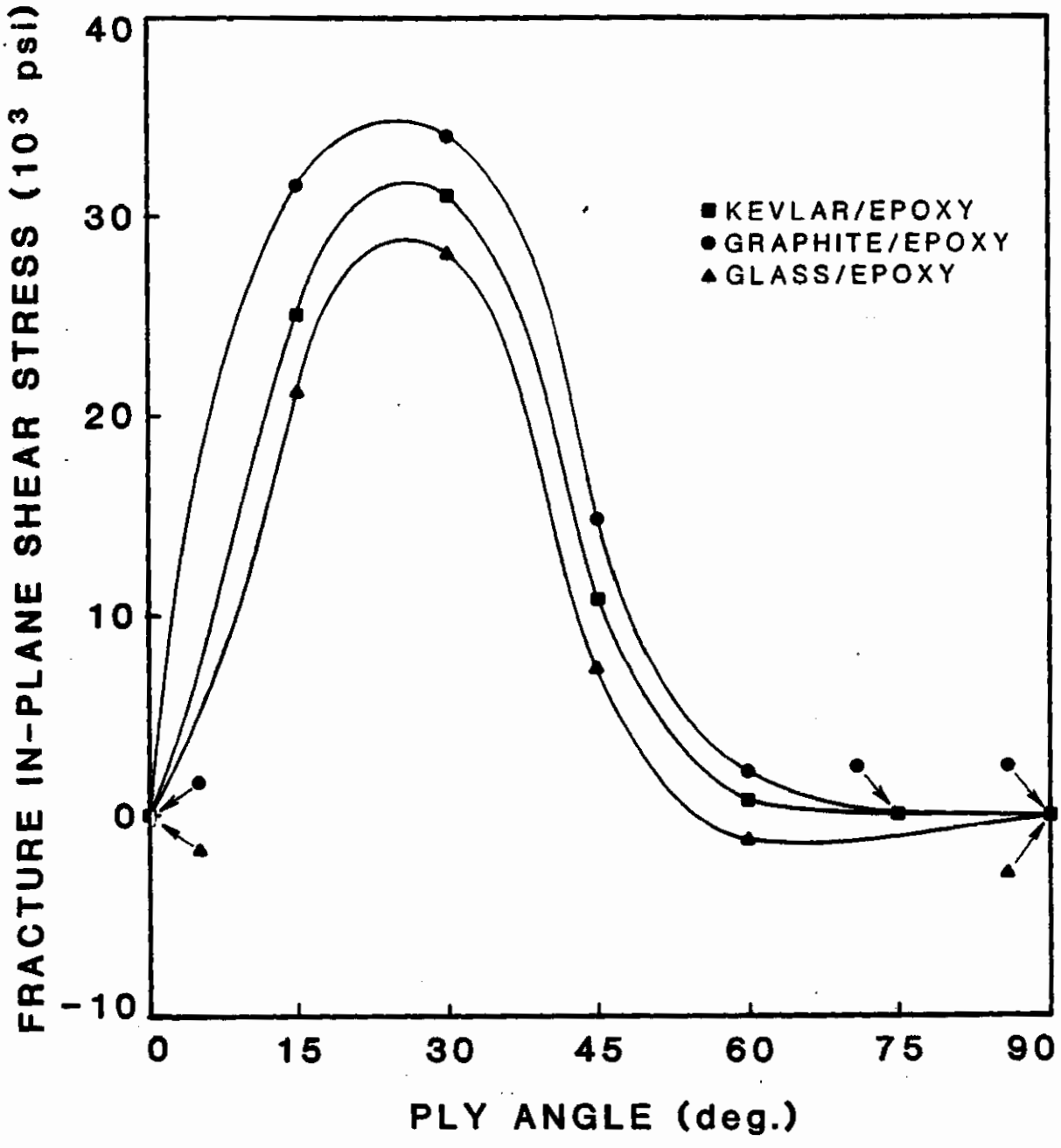

Figure 77. In-Plane Shear Stress vs. Ply Angle for T300 Graphite/Rigidite 5209 Epoxy, Kevlar 49C/ Rigidite 5216 Epoxy and E-Glass/Rigidite 5216 Epoxy.

TABLE 78. STRAIN VS. PLY ANGLE

ANGLE	GRAPHITE(%)	KEVLAR(%)	GLASS(%)
0	4.5	5.1	10.0
15	4.3	4.55	6.50
30	6.8	9.2	10.95
45	21.7	22.5	27.22
60	3.9	2.82	2.11
75	1.90	1.17	1.44

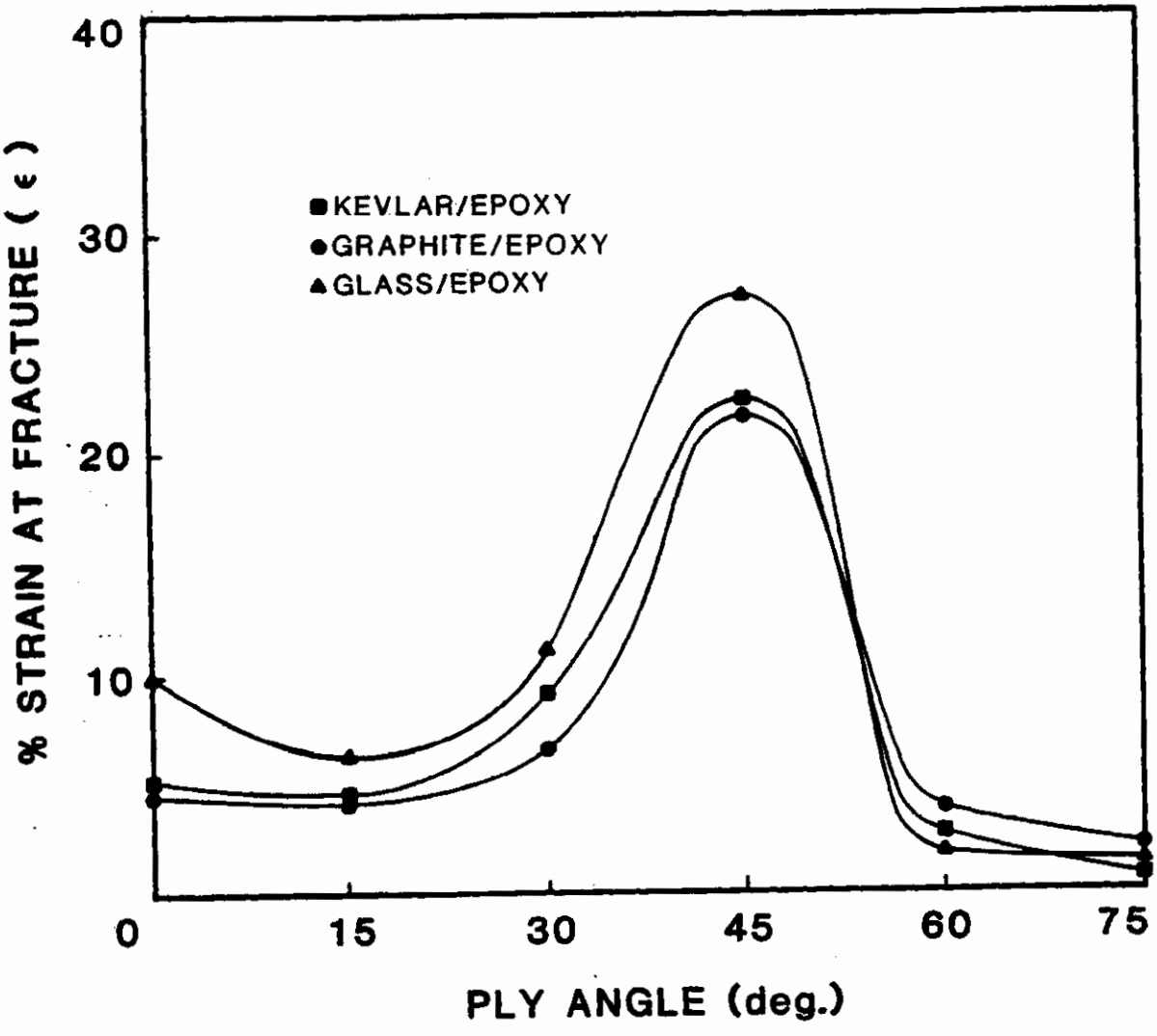

Figure 78. Percent Strain at Fracture vs. Ply Angle for T300 Graphite/Rigidite 5209 Epoxy, Kevlar 49C/ Rigidite 5216 Epoxy, E-Glass/Rigidite 5216 Epoxy.

TABLE 79. RESOLVED STRESSES AND FAILURE MODES

GRAPHITE

ANGLE	σ_1	σ_L	σ_T	τ_{LT}	MODE
0	206300	206300	0	0	FB
15	129040	136171	-7131	-4937	FS-PD-FB
30	74056	85217	-11161	-14934	FS-PD-FB
45	34743	32283	2461	-17372	FS-PD
60	16256	6088	10168	-8208	FS-PD
75	11380	827	10553	-2957	FS
90	6500	0	6500	0	FS

KEVLAR

0	189186	189186	0	0	FB
15	101080	106734	-5654	-3749	FS-PD-FB
30	66378	76740	-10362	-13179	FS-PD-FB
45	25444	23617	1827	-12722	FS-PD
60	7039	2527	4512	-3491	FS-PD
75	4565	306	4259	1142	FS
90	4100	0	4100	0	FS

GLASS

0	212237	212237	0	0	FB
15	99148	102990	-3842	-6629	FS-PD-FB
30	71703	78234	-6531	-16928	FS-PD-FB
45	31366	23312	8054	-15683	FS-PD
60	13397	2301	11096	-5196	FS-PD
75	11039	192	1084	-1812	FS
90	10000	0	10000	0	FS

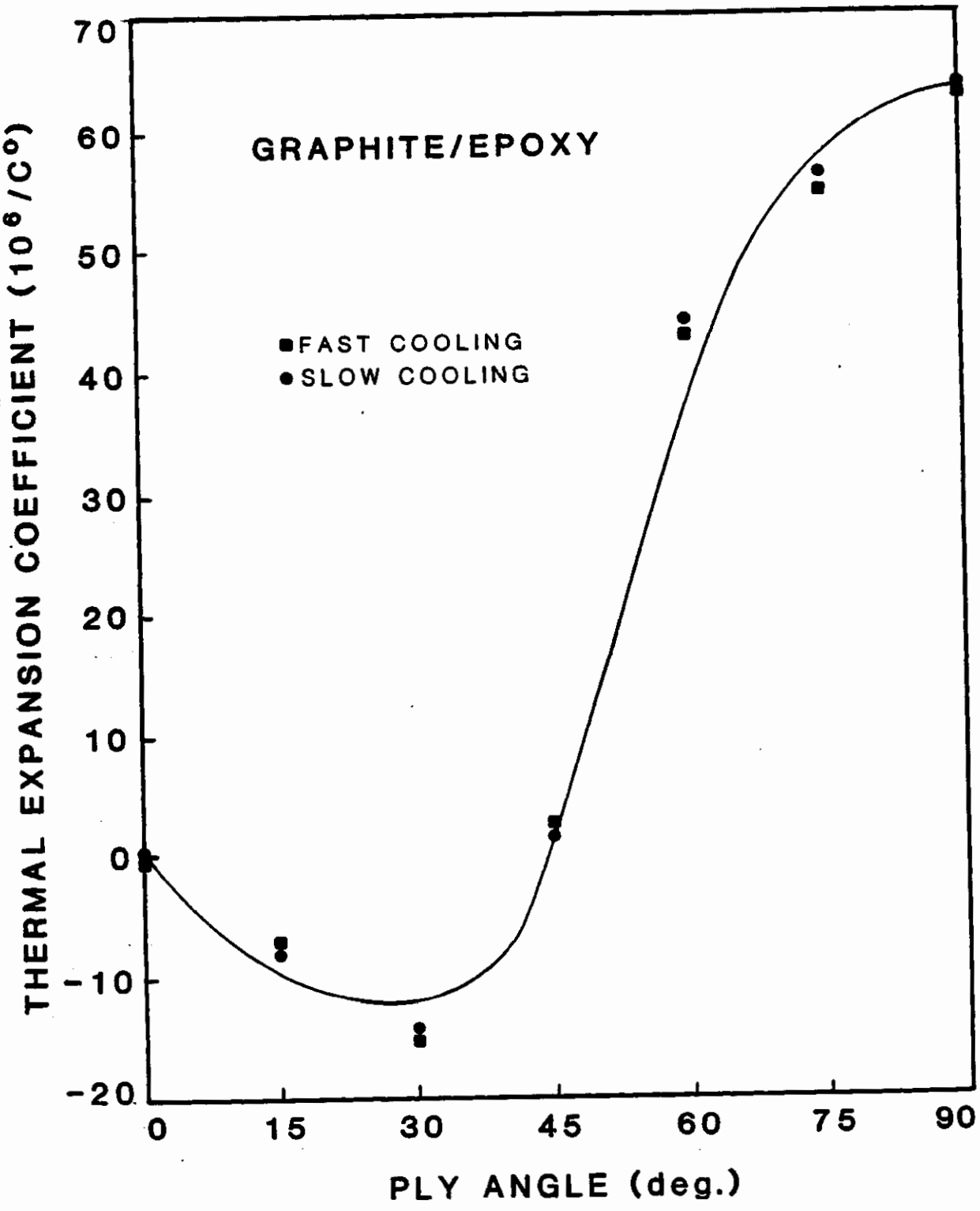

Figure 79. Coefficient of Thermal Expansion vs. Ply Angle for T300 Graphite/Rigidite 5209 Epoxy.

TABLE 80. THERMAL EXPANSION COEFFICIENTS OF GRAPHITE/EPOXY LAMINATES (x 10^{-6}/DEGREES CELSIUS)

PLY ANGLE	FAST COOL	SLOW COOL	CALCULATED
0	0.19	0.42	0.30 [1]
15	-3.87	-4.23	-3.15
30	-14.71 -4.20 [2] -30.09 [3]	-14.30 -4.07 [2] -27.77 [3]	-9.09
45	2.91	2.70	4.71
60	41.19 17.86 [2] 85.03 [3]	42.77 16.95 [2] 79.15 [3]	39.29
75	54.40 31.50 [2] 84.00 [3]	56.88 28.20 [2] 86.03 [3]	58.22
90	62.06	63.54	62.80 [1]
0/90	1.7	2.35	4.71 [4]

[1] These are experimental values of longitudinal and transverse coefficients used for calculating laminate coefficients.

[2] Slope was determined between 30 and 80 degrees Celsius.

[3] Slope was determined between 100 and 130 degrees Celsius--all other values were measured between 30 and 130 degrees Celsius.

[4] Same as for plus or minus 45 degree laminate.

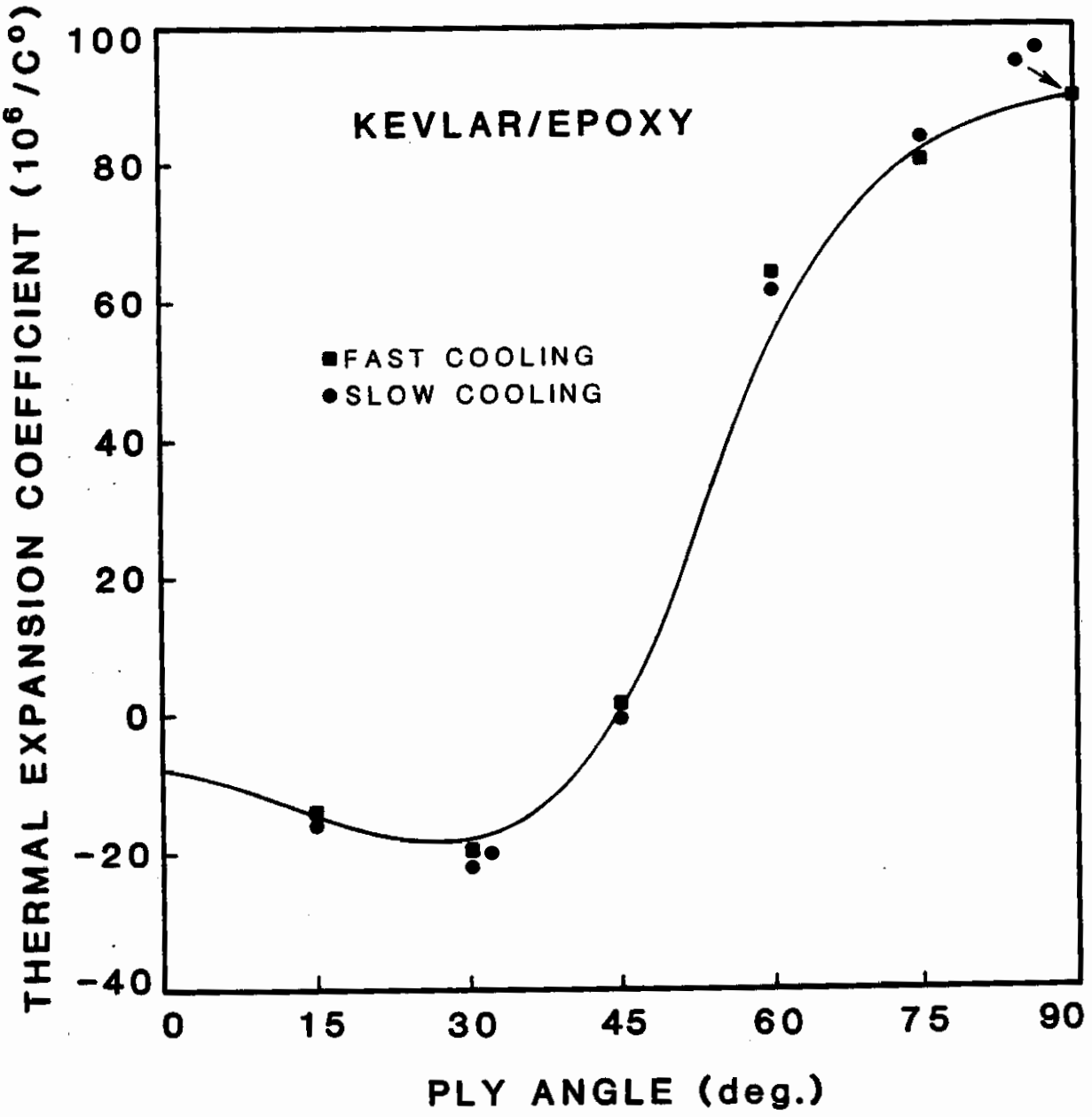

Figure 80. Coefficient of Thermal Expansion vs. Ply Angle for Kevlar 49C/Rigidite 5216 Epoxy.

TABLE 81. THERMAL EXPANSION COEFFICIENTS OF KEVLAR-EPOXY LAMINATES
($\times 10^{-6}$/DEGREE CELSIUS)

PLY ANGLE	FAST COOL	SLOW COOL	CALCULATED
0	-4.69	-3.71	-4.20 [1]
15	-9.09	-9.79	-9.43
30	-23.18	-23.83	-18.76
45	2.99	1.61	2.50
60	63.91 43.67 [2] 90.84 [3]	62.03 46.34 [2] 92.62 [3]	55.63
75	81.62	86.44	83.14
90	89.59	89.41	89.50 [1]
0/90	0.68 3.38 [2] -2.95 [3]	0.73 3.30 [2] -2.48 [3]	2.50 [4]

[1] These are experimental values of longitudinal and transverse coefficients used for calculating laminate coefficients.

[2] Slope was determined between 30 and 80 degrees Celsius.

[3] Slope was determined between 100 and 130 degrees Celsius--all other values were measured between 30 and 130 degrees Celsius.

[4] Same as for plus or minus 45 degree laminate.

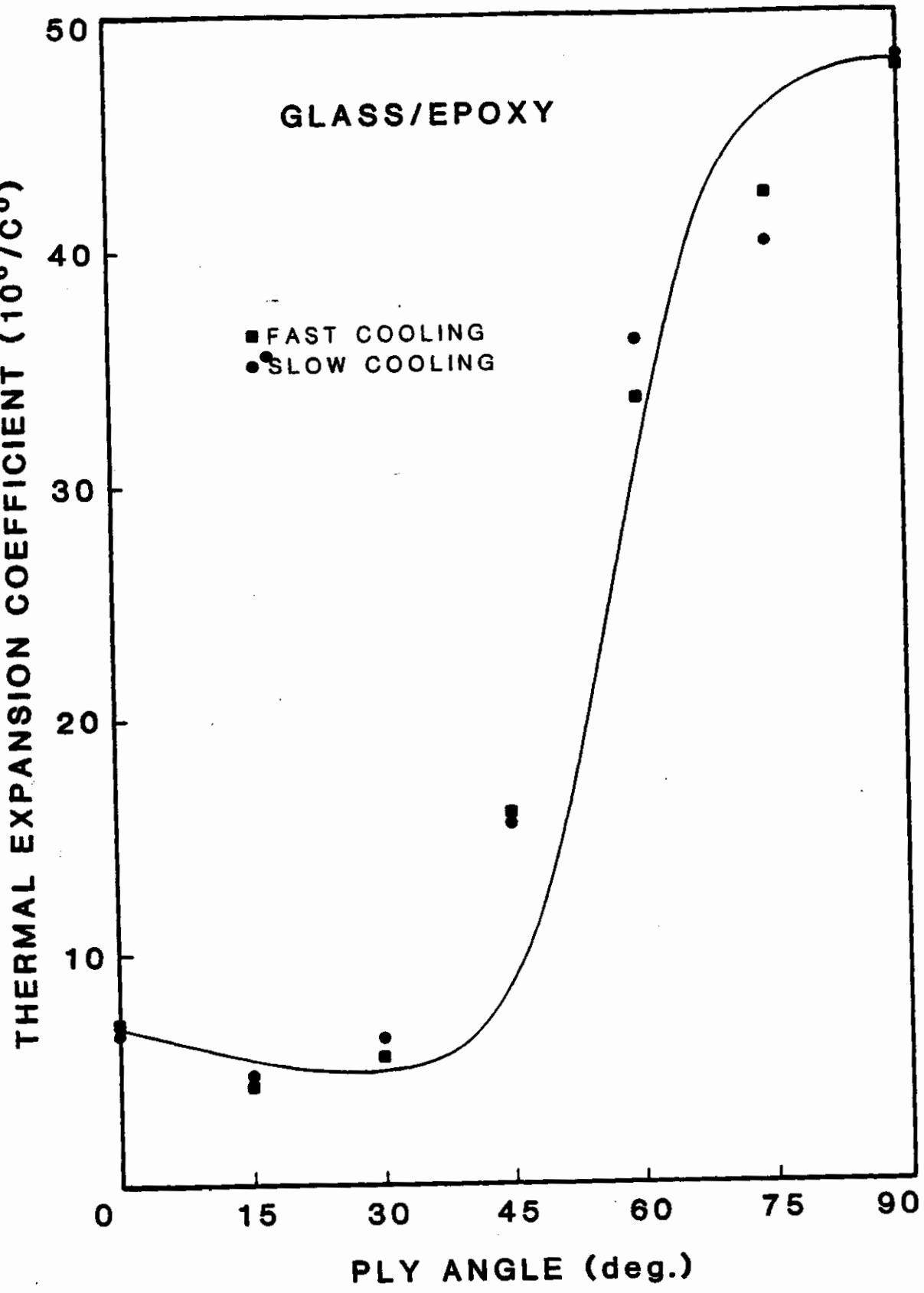

Figure 81. Coefficient of Thermal Expansion vs. Ply Angle for E-Glass/Rigidite 5216 Epoxy.

TABLE 82. THERMAL EXPANSION COEFFICIENTS OF GLASS/EPOXY LAMINATES
($\times 10^{-6}$/DEGREE CELSIUS)

PLY ANGLE	FAST COOL	SLOW COOL	CALCULATED
0	7.09	6.71	6.90 [1]
15	4.92	5.04	5.31
30	1.84 5.84 [2] -15.75 [3]	1.51 6.73 [2] -14.63 [3]	3.16
45	15.27	15.12	17.39
60	33.54 16.52 [2] 60.36 [3]	35.71 16.75 [2] 69.04 [3]	40.78
75	42.71	40.30	47.09
90	47.67	47.93	47.80 [1]
0/90	14.74	14.50	17.39 [4]

[1] These are experimental values of longitudinal and transverse coefficients used for calculating laminate coefficients.

[2] Slope was determined between 30 and 80 degrees Celsius.

[3] Slope was determined between 100 and 130 degrees Celsius--all other values were measured between 30 and 130 degrees Celsius.

[4] Same as for plus or minus 45 degree laminate.

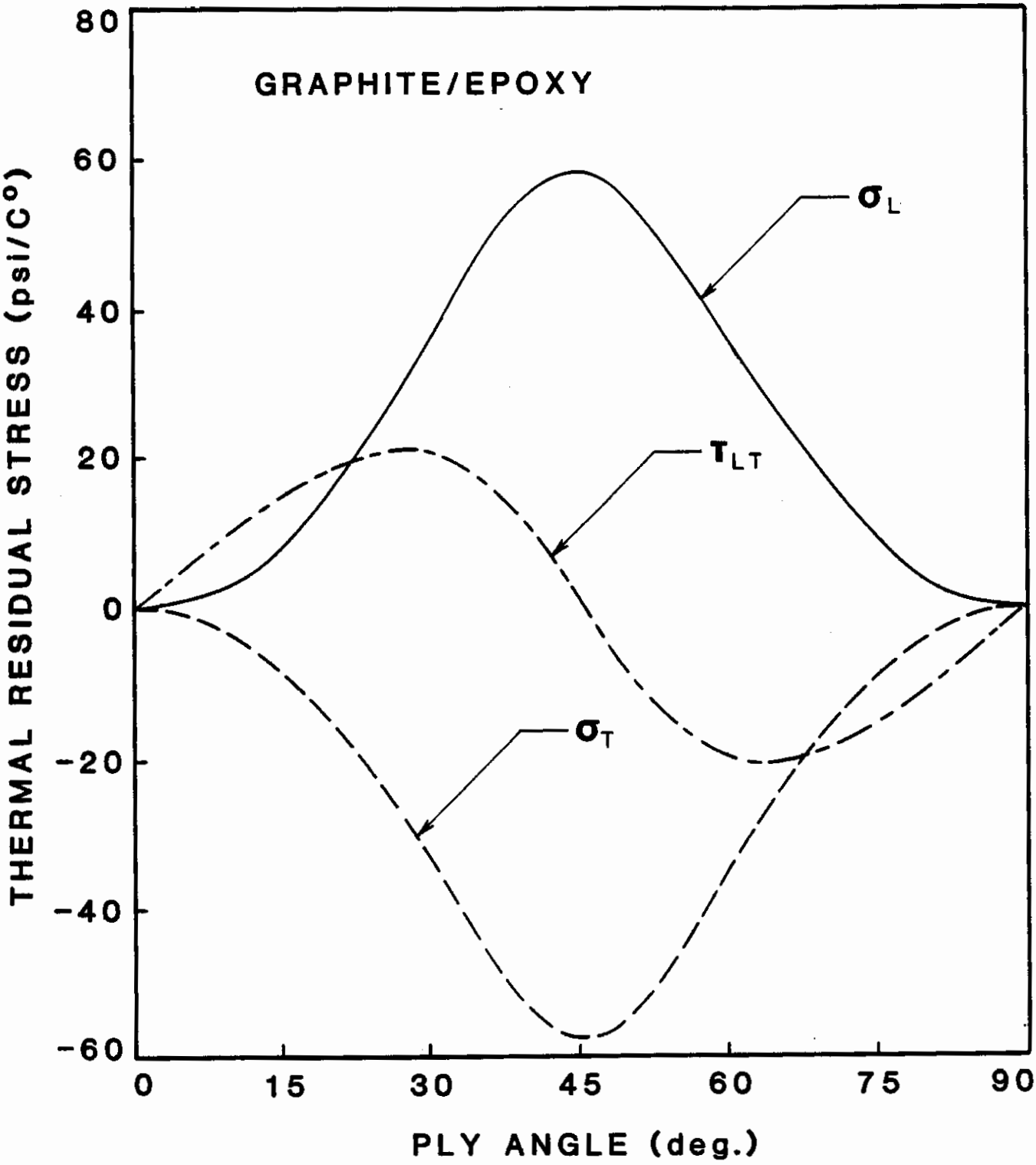

Figure 82. Residual Stress vs. Ply Angle for T300 Graphite/ Rigidite 5209 Epoxy.

TABLE 83. THERMAL EXPANSION COEFFICIENTS OF HYBRIDS

TYPE	FAST	SLOW
T1-15(KGK)	-1.28	-1.73
T1-15(GKG)	-0.62	-1.25
T2-15	-1.16	-1.37
T1-45(KGK)	7.18	6.29
T1-45(GKG)	6.90	7.02
T2-45	7.76	7.61

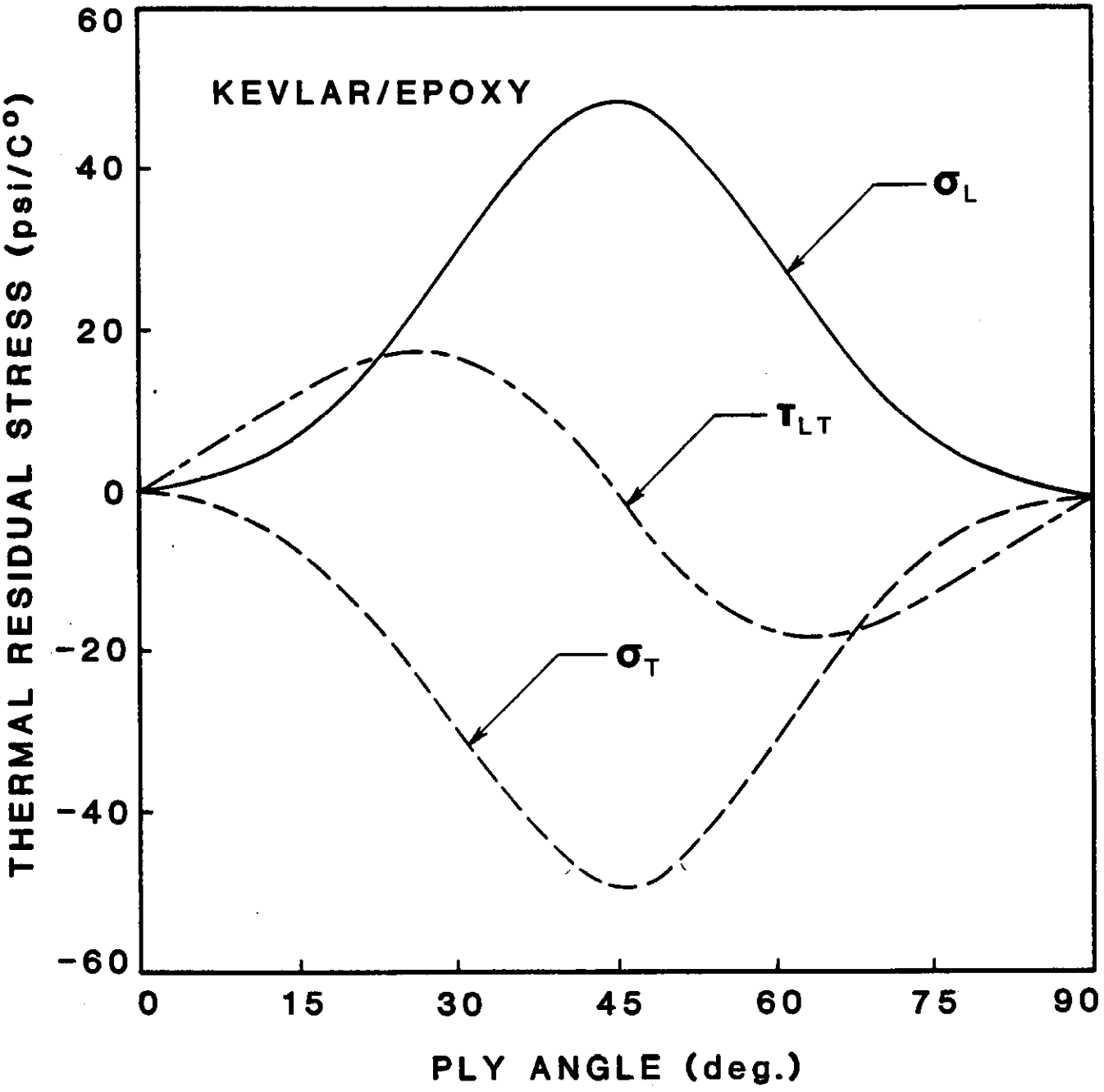

Figure 83. Residual Stress vs. Ply Angle for Kevlar 49C/ Rigidite 5216 Epoxy.

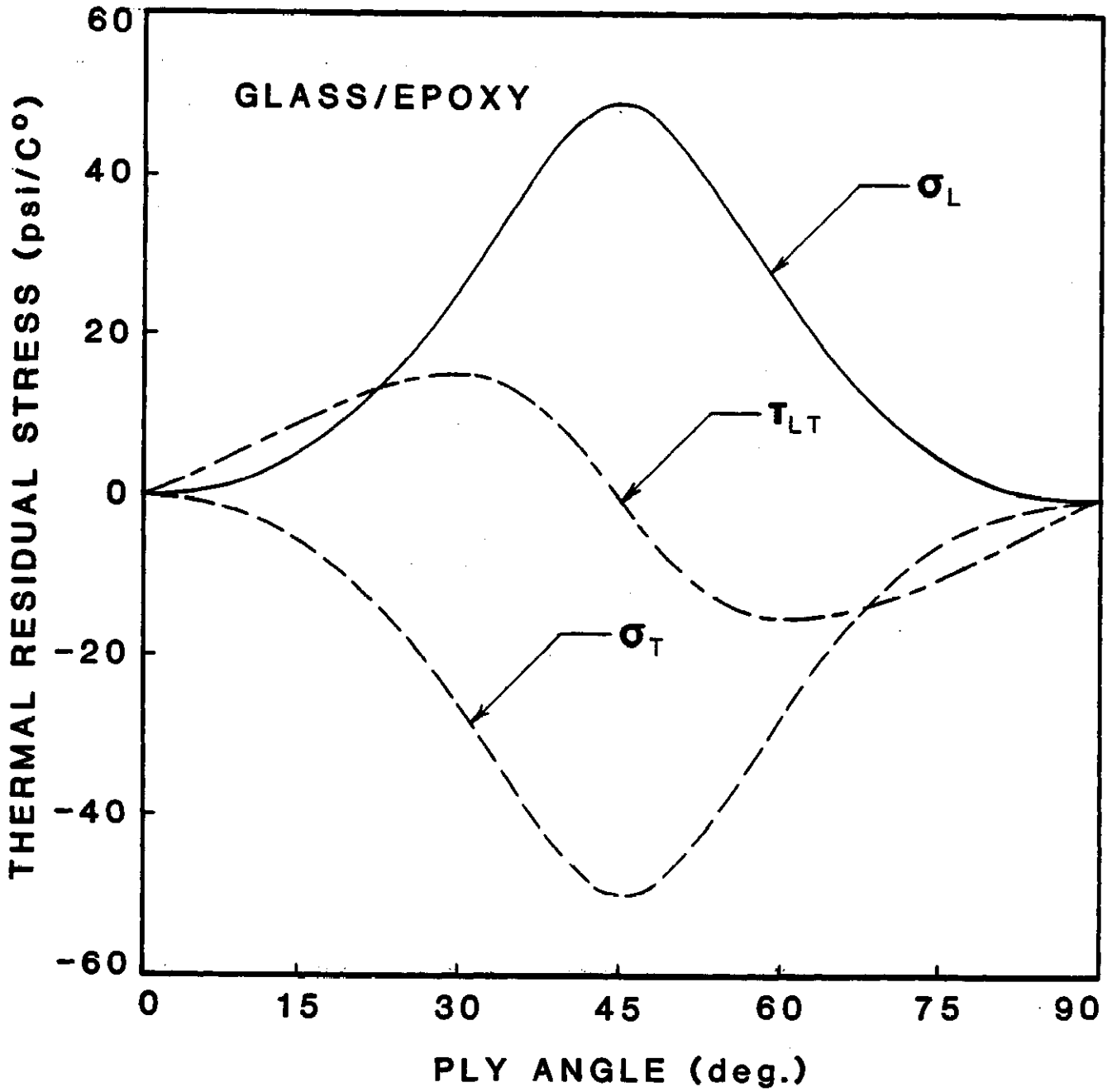

Figure 84. Residual Stress vs. Ply Angle for E-Glass/ Rigidite 5216 Epoxy.

DISTRIBUTION LIST

No. of Copies	To
1	Office of the Under Secretary of Defense for Research Engineering, The Pentagon, Washington, D.C. 20301
12	Commander, Defense Technical Information Center, Cameron Station, Building 5, 5010 Duke Street, Alexandria, Virginia 22314
1	Metals and Ceramics Information Center, Battelle Columbus Laboratories, 505 King Avenue, Columbus, Ohio 43201
	Deputy Chief of Staff, Research, Development, and Acquisition, Headquarters, Department of the Army, Washington, D.C. 20310
1	ATTN: DAMA-ARZ
2	Dr. J. I. Bryant
	Commander, Army Research Office, P.O. Box 12211, Research Triangle Park, North Carolina 27709
1	ATTN: Information Processing Office
2	Dr. J. Hurt
1	Dr. G. Mayer
1	Dr. D. Squire
	Commander, U.S. Army Materiel Development and Readiness Command, 5001 Eisenhower Avenue, Alexandria, Virginia 22333
1	ATTN: DRCLDC
	Commander, U.S. Army Armament Research and Development Command, Dover, New Jersey 07801
1	ATTN: Mr. H. Pebly, PLASTEC
1	Mr. A. Slobodzinski, PLASTEC
1	Mr. W. Tanner
	Commander, U.S. Army Natick Research and Development Command, Natick, Massachusetts 01760
1	ATTN: Technical Library
	Commander, U.S. Army Aviation Research and Development Command, P.O. Box 209, St. Louis, Missouri 63166
1	ATTN: Mr. R. Vollmer
	Commander, Harry Diamond Laboratories, 2800 Powder Mill Road, Adelphi, Maryland 20783
1	ATTN: Technical Information Office
	Commander, U.S. Army Foreign Science and Technology Center, 220 7th Street, N.E., Charlottesville, Virginia 22901
1	ATTN: Military Tech, Mr. Marley

No. of Copies	To
	Director, Eustis Directorate, U.S. Army Air Mobility Research and Development Laboratory, Fort Eustis, Virginia 23604
2	ATTN: Mr. H. Reddick
	Chief of Naval Research, Arlington, Virginia 22217
1	ATTN: Code 471
	Office of Naval Research, Boston Branch, 495 Summer Street, Boston, Massachusetts 02210
1	ATTN: Dr. L. H. Peebles
	Naval Research Laboratory, Washington, D.C. 20375
2	ATTN: Dr. W. B. Moniz, Code 6120
2	Dr. I. Woloch, Code 8433
2	Dr. L. B. Lockhart, Jr., Code 6120
	Commander, Naval Air Systems Command, Washington, D.C. 20361
2	ATTN: M. Stander
	Commander, Naval Surface Weapons Center, White Oak, Silver Spring, Maryland 20
1	ATTN: Dr. J. M. Augl
	Air Force Office of Scientific Research (NC), Building 410, Bolling Air Force Base, Washington, D.C. 20332
1	ATTN: Dr. D. R. Ulrich
	Commander, U.S. Air Force Wright Aeronautical Laboratories, Wright-Patterson Ai Force Base, Ohio 45433
1	ATTN: Dr. S. W. Tsai
1	Dr. N. J. Pagano
1	Dr. H. T. Hahn
1	Dr. C. E. Browning
	Air Force Flight Dynamics Laboratory, Wright-Patterson Air Force Base, Ohio 454
1	ATTN: Dr. G. P. Sendeckyj
	National Aeronautics and Space Administration, Lewis Research Center, 21000 Brookpark Road, Cleveland, Ohio 44135
2	ATTN: Dr. T. T. Serafini (49-1)
1	Dr. C. C. Chamis
1	Professor D. F. Adams, Department of Mechanical Engineering, University of Wyoming, Laramie, Wyoming 82070
1	Professor F. J. McGarry, MIT, Cambridge, Massachusetts 02139
1	Professor K. H. G. Ashbee, University of Bristol, H. H. Wills Physics Lab., Bristol, England BS81TL
1	Professor O. Ishai, Department of Mechanics, Technicon - Israel Institute of Technology, Haifa, Israel

No. of Copies	To
1	Dr. D. H. Kaelble, Science Center, Rockwell International, Thousand Oaks, California 91360
1	Dr. B. W. Rosen, Materials Science Corporation, Blue Bell, Pennsylvania 19422
1	Mr. R. J. Zentner, EAI Corporation, 198 Thomas Johnson Drive, Suite 16, Frederick, Maryland 21701
	Defense Research Establishment Office, Sheelay Bay, Ottawa, Ontario KIA 024
1	ATTN: Mr. H. L. Nash
	Defence Standard Laboratories, Department of Supply, P.O. Box 50, Ascot Vale 3032, Victoria, Australia
1	ATTN: Dr. D. Pinkerton
1	Dr. G. George
	Director, Army Materials and Mechanics Research Center, Watertown, Massachusetts 02172
2	ATTN: DRXMR-PL
1	DRXMR-PR
1	DRXMR-K
1	DRXMR-FD
3	DRXMR-OC, Dr. Halpin